

Politecnico di Torino

Corso di Laurea Magistrale in  
Ingegneria Energetica e Nucleare

**Study of eigenvalue formulations in the  $P_N$  approximation  
of the neutron transport equation**



*Supervisor:*

Sandra Dulla

*Co-supervisors:*

Piero Ravetto

Paolo Saracco (INFN)

*Author:*

Miriam Burrone

Torino, December 2018

# Abstract

Transport processes of particles and physical quantities through matter constitute a physical fundamental occurring in an extremely broad range of applications. The original Boltzmann conservation equation, derived in study through a statistical approach of the transport of molecules in a medium, it is nowadays properly declined for the study of the transport of several different types of particles, from the spreading of cancer cells in human bodies, to the photons transport through matter and neutrons throughout a nuclear reactor core. As regards the case of neutrons, an accurate knowledge of the neutrons population distribution, consequence of the transport processes involving these particles and the nuclei of the background matter, constitutes a crucial basic for any assessments concerning reactor physics analysis, as design and safety analysis computations. Specifically, a peculiar issue is establishing whether the neutron population throughout the reactor core is independent of time, decreases or increases with it, through the different operating stages of the nuclear device. This task is referred to as the criticality problem, commonly intended as the research of the combination of material composition and reactor geometrical configuration, which allows the nuclear device to achieve a stationary energy production. In criticality analysis, the study of the time-dependent behaviour of a neutron population is treated as an eigenvalue problem, representing a fundamental field of interest both for the description of deviations from the reactor stationary configuration, and for the use of the higher eigenvalue modes as a valid tool for the characterization of localized phenomena and the study of nuclear reactor kinetics. The most widely inspected eigenvalue is the effective multiplication factor  $k$ , together with the time-eigenvalue  $\alpha$ , particularly exploited for subcritical systems analysis. Though, other eigenvalue types, as the effective multiplication factor per collision  $\gamma$  and the most unexplored effective density factor  $\delta$ , may constitute an interesting field of investigation for physical interpretation of eigenvalue problems. Scope of this work consists in the study of the solution of the Boltzmann equation applied to the transport of neutrons in an infinite-slab geometry reactor core, in the most simplified case of a homogeneous medium, through the application of the spherical harmonics method to a mono-energetic model. Hence, the  $P_N$  approximation is applied to the different eigenvalue formulations of the neutron transport equation in order to investigate its time-independent solution for simplified models, in attempting to promote

a deeper knowledge about the relations occurring in solving with different eigenvalue forms the transport equation, at diverse orders of approximation accuracy. The first three chapters are devoted to the outline of the theoretical physics foundations of the present work. The successive one is dedicated to the description of the numerical algorithm implemented by the author in MATLAB environment, to solve the time-independent neutron transport equation in the specific eigenvalue form through PN approximation. The last part is finally devoted to the examination of the results obtained by the algorithm solutions, with the appropriate comparisons between both different eigenvalue forms and approximation orders of accuracy, to the conclusions report and the proposal of future application fields.

# Contents

<b>Abstract</b>	<b>1</b>
<b>Introduction</b>	<b>4</b>
<b>1 The Neutron Transport Equation</b>	<b>7</b>
1.1 The integro-differential neutron transport equation . . . . .	8
1.1.1 The general model . . . . .	8
1.1.2 Boundary and initial conditions . . . . .	13
1.1.3 Mono-energetic model . . . . .	13
1.1.4 Plane geometry model . . . . .	14
<b>2 The Criticality Problem</b>	<b>16</b>
2.1 The $k$ eigenvalue . . . . .	19
2.2 The $\alpha$ eigenvalue . . . . .	22
2.3 The $\gamma$ eigenvalue . . . . .	25
2.4 The $\delta$ eigenvalue . . . . .	26
<b>3 The Spherical Harmonics Method</b>	<b>29</b>
3.1 Spherical harmonics method in general geometry . . . . .	30
3.2 Spherical harmonics method in plane geometry . . . . .	34
3.2.1 Boundary Conditions . . . . .	38
3.2.2 The $P_1$ and $P_3$ system of equations . . . . .	40
3.2.3 Application to the eigenvalue forms of the neutron transport equation	42
<b>4 Numerical code implementation</b>	<b>45</b>
4.1 On the necessity of a staggered mesh in the spatial discretization . . . . .	45
4.2 Spatial staggered grid for higher-order $P_N$ approximations . . . . .	52
4.3 Boundary condition imposition . . . . .	55
4.4 Outline of the code: $k$ -eigenvalue case . . . . .	57
4.4.1 Matrix formulation . . . . .	58

4.4.2	$P_N$ global matrices automation . . . . .	60
4.4.3	Boundary conditions evaluation and imposition . . . . .	62
4.4.4	Eigenvalues and eigenvectors calculation . . . . .	65
<b>5</b>	<b>Numerical results</b>	<b>66</b>
5.1	Grid independence study . . . . .	66
5.2	Comparison to benchmark criticality results . . . . .	68
5.3	Odd- and even-order $P_N$ approximations comparison . . . . .	76
5.3.1	Fundamental eigenvalue convergence . . . . .	76
5.3.2	Higher-order modes convergence . . . . .	84
5.3.3	Associated eigenvectors . . . . .	90
5.3.4	Parametric studies . . . . .	92
<b>6</b>	<b>Conclusions</b>	<b>96</b>
	<b>Bibliography</b>	<b>98</b>

# Introduction

Climate change represents one of the greater and challenging issues which contemporary society has to address. In this contest, energy production technologies performed a crucial role in possible solution strategies [1]. It is by now widely recognized among the scientific community, that the exploitation of a mix of low-carbon and alternative energy sources constitutes the current most effective and feasible strategy in facing the greenhouse-gas worldwide emissions. As part of the alternative energy supply, nuclear power can provide a critical contribution to a sustainable future energy production [2]. Nevertheless, due to the peculiarities of such a technology, important issues concerning safety of nuclear power reactors, resilience to nuclear weapons proliferation and public acceptance arise in the discussion about nuclear power development.

In the last decades extremely great enhancement in these issues have been achieved, results of both theoretical and technological efforts. In particular, the improvements in computing technologies allow to handle more accurate and sophisticated models in the simulation of physical phenomena occurring in nuclear energy production, returning always more precise results which permit a deeper and more robust knowledge in safety issue.

It is in this specific contest, safety and design assessments in nuclear power reactor, which the scope of the present work lies. Drive for this master thesis has been indeed the interest in the investigation of a crucial aspect of design and safety analysis, and more in general, reactor physics analysis, constituted by the *criticality problem*. Specifically, in criticality analysis the study of the time-dependent behavior of a neutron population in a nuclear reactor is addressed as an eigenvalue problem, a pseudo-stationary model for the description of slight changes in reactor temporal behavior [3]. Criticality computations have indeed an important role in the description of the deviation of a reactor from the stationary configuration which allow a stationary energy production, and in the use of the higher eigenvalue modes as an adequate tool for the study of localized phenomena behaviour and nuclear reactor kinetics.

In literature, four different eigenvalue formulations of the neutron transport equation, the governing equation of particles transport processes in a medium, have been presented. Having in mind that new generations of nuclear reactors are under constructions or object of research and development efforts, a deeper knowledge of the difference which arise in the diverse

neutron transport eigenvalue formulation may give a contribution in the investigation of some new reactor design aspects. Indeed, while the most widely inspected eigenvalue of neutron transport equation is the effective multiplication factor  $k$ , together with the time eigenvalue  $\alpha$ , other eigenvalue types, as the effective multiplication factor per collision  $\gamma$  and the most unexplored effective density factor  $\delta$ , represent a possibility in criticality computations.

Hence, scope of this work consists in the study of the solution of the linear Boltzmann equation applied to the transport of neutrons in an infinite-slab geometry reactor core, in the most simplified case of a homogeneous medium, by means of the application of the spherical harmonics method to the case of a mono-energetic model. In particular, the  $P_N$  approximation is applied to the different eigenvalue formulations in order to investigate the eigenvalues and eigenvectors solution to the generalized eigenvalue problem, at diverse orders of approximation accuracy. In particular, both odd- and even-orders of the  $P_N$  approximation have been taken into consideration.

The first chapter is thus devoted to the introduction of the theoretical physics foundations of the present work, specifically, the integro-differential form of the neutron transport equation. Then, the criticality problem definition for the different eigenvalue types analyzed is outlined in Chapter 2. The following chapter is instead dedicated to the spherical harmonics method presentation, both for a general geometry configuration and the simplified plane geometry employed for the present work numerical calculations. A brief outline of the computational code implemented by the author in order to investigate some numerical criticality results is performed in Chapter 4. Finally, in chapter 5 numerical results obtained referring to the eigenvalue spectrum and eigenvectors solutions of the generalized eigenvalue problems, with different orders of  $P_N$  approximation and different boundary conditions imposition, are reported.

# Chapter 1

## The Neutron Transport Equation

The aim of this introductory chapter is to present the foundation equation of the study conducted in this thesis: the neutron transport equation. This equation draws its origin from the classical Boltzmann equation, of which it constitutes a linear version. The Boltzmann equation, derived by Ludwig Boltzmann in 1872, represents a non-linear integro-differential equation which describes, through a statistical approach, the behavior of thermodynamic systems not in equilibrium. It was derived as a conservation model for the transport of molecules in a medium, constituting the base of the kinetic theory of gas [4]. Thus, this fundamental tool used for the study of transport of particles in a fluid, can be exploited, in a more general sense, for the study of the transport of any type of particles, among which neutrons or photons, or even physical quantities such as heat or charge.

In case of neutrons, the governing equation describing transport processes in a medium was derived from the original Boltzmann equation with some essential assumptions, among which: neutrons are considered as point particles<sup>1</sup> moving along straight trajectories between subsequent collisions, which might occur only between neutrons and nuclei of the medium, meaning that neutron-neutron interactions are neglected<sup>2</sup>. Hence, the general neutron transport equation is reported in order to present the main physical quantities involved in the work discussion, with proper definitions. Among its several possible formulations, it is here presented in the integro-differential version, since this is the form that constitutes the starting point for the application of the spherical harmonics method, to which Chapter 3 is devoted. In Section 1.1.1 the integro-differential transport equation is derived for the most general case of a three-dimensions space domain, time and energy dependent system. Then, the mono-energetic model is reported in Section 1.1.2, whereas the last section of the chapter is dedicated to the presentation of the most simplified case of the one-dimensional, steady-state, mono-energetic model.

---

<sup>1</sup>A point-particle description implies that neutrons may be completely described by their positions and velocities. [5]

<sup>2</sup>For the complete list of the 7 assumptions the transport theory for neutrons is based upon, refer to [6]

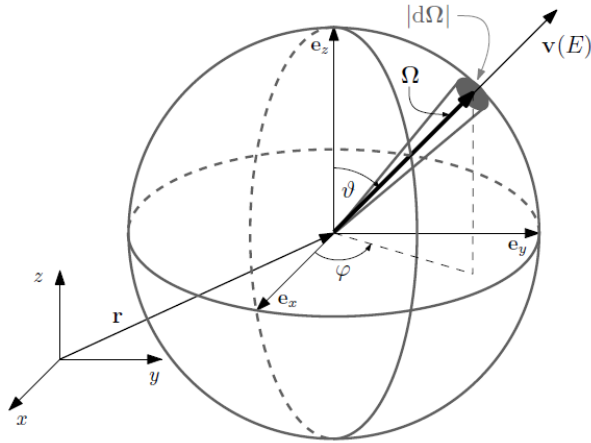


Figure 1.1: Neutrons phase space[7]

## 1.1 The integro-differential neutron transport equation

### 1.1.1 The general model

The neutron transport equation is the mathematical expression of the balance in time of the expected number of neutrons<sup>3</sup> in an element of the phase space. The balance is built by considering the different mechanisms which could alter the number of neutrons initially contained within the elemental volume  $d\mathbf{r}$  around position  $\mathbf{r}$ , with kinetic energy  $E$  within  $dE$  and direction of motion  $\Omega$  within the solid angle  $d\Omega$ . Thus, this package of neutrons is observed in its modifications with an approach similar to the Lagrangian approach of fluid dynamic.

Due to their free motion through the medium, neutrons could enter or leave the volume  $d\mathbf{r}$ , passing through its boundaries, collisions could cause a change in energy or direction of motion of neutrons and finally, neutrons could be introduced in the observed volume with the energy and direction of interest by neutron sources.

The phase space volume under study consists in a 6 dimensions space defined by the position  $\mathbf{r}$ , the energy  $E$  and the direction along which particles travel  $\Omega$ .

Alternatively to the energy  $E$  within  $dE$ , the neutron velocity vector may be defined as  $\mathbf{v} = v\Omega$ , where  $v$  is the magnitude of the velocity and  $\Omega$  a unit vector in the direction of motion [6].

Hence, the neutron population is generally described by the quantity called *neutron angular density*, function of the independent variables defining the phase space. This quantity appears,

<sup>3</sup>The expression *expected (or probable) number of neutrons* refers to the fact that the average behavior of the neutron population is under study, and possible fluctuation are generally not taken into account, as well highlighted in [5].

in symbols [5]:

$$\begin{aligned}
 n(\mathbf{r}, E, \boldsymbol{\Omega}, t) &\equiv \text{probable numbers of neutrons at position } \mathbf{r}, \\
 &\text{with energy } E, \text{ direction } \boldsymbol{\Omega} \text{ at time } t \\
 &\text{per unit volume per unit energy and per unit solid angle.}
 \end{aligned} \tag{1.1}$$

Generally, it is measured in  $\text{n}/(\text{cm}^3 \text{MeV sr})$ .

The *neutron angular flux* is then defined as:

$$\phi(\mathbf{r}, E, \boldsymbol{\Omega}, t) \equiv v n(\mathbf{r}, E, \boldsymbol{\Omega}, t) \tag{1.2}$$

where  $v$  is the neutron speed, while term *angular* appearing in its definition emphasizes the dependence on the direction of motion. The angular flux  $\phi$  thus represents the total path length traveled per unit time by the neutrons defined by (1.1) [8]. Its integration over all the possible directions is referred to as the *total flux*, or the *scalar flux*, whose definition is, in symbols:

$$\Phi(\mathbf{r}, E, t) \equiv \oint d\boldsymbol{\Omega} \phi(\mathbf{r}, E, \boldsymbol{\Omega}, t). \tag{1.3}$$

Furthermore, the *neutron current* consists in:

$$\mathbf{J}(\mathbf{r}, E, t) \equiv \oint d\boldsymbol{\Omega} \boldsymbol{\Omega} \phi(\mathbf{r}, E, \boldsymbol{\Omega}, t) \tag{1.4}$$

representing the net number of neutrons at position  $\mathbf{r}$ , with energy  $E$  and direction  $\boldsymbol{\Omega}$  at time  $t$ , crossing the unit area perpendicular to such a direction per unit energy and unit time [5].

In order to characterize the different probabilities of interaction, based on the different interaction types which neutrons may experience in the transport through the medium, a set of macroscopic cross-sections are defined. These are, respectively: the total cross-section  $\Sigma_t$ , which quantifies the probability per unit path of any type of interaction; the absorption cross-section  $\Sigma_a$ , characteristic of the absorption events; the scattering cross-section  $\Sigma_s$ , for both elastic and inelastic scattering collisions and finally, the fission cross-section  $\Sigma_f$ , for fission reactions. Therefore, cross-sections are defined as the probability per unit path travelled by a neutron to experience a specific interaction with the nuclei of matter. Their unit of measure is the reciprocal of a length and the reciprocal of a macroscopical cross-section corresponds to the *neutron mean free path*.

In this presentation cross-sections are considered as functions of space and particle energy only. In most cases in nuclear engineering, isotropic materials are used and, as a consequence, the dependence on the direction  $\boldsymbol{\Omega}$  of the macroscopic cross-sections could be neglected. Furthermore, concerning the dependence on time  $t$ , it becomes relevant in few cases if one

considers the different timescale characterizing the variation of  $\Sigma$  with respect to the average lifetime of a neutron [5].

Thus, taking into account the different physical mechanisms involved in the neutron transport equation, the balance in time of the number of neutrons in the elemental volume  $d\mathbf{r}$ , characterized by energy  $E$  and direction of motion  $\Omega$  may be outlined as:

$$\begin{aligned}
\text{variation in time of neutrons number} = & - \text{Leakage rate due to streaming} \\
& - \text{Leakage rate due to collisions} \\
& (\text{ absorptions + scattering out}) \\
& + \text{Gain rate due to scattering in} \\
& + \text{Gain rate due to independent sources}
\end{aligned}$$

where *scattering out* losses identify those neutrons having the energy and direction of interest which suffer a scattering collision that causes a modification in energy and direction; as a consequence, they are treated as a loss from the package of neutrons under investigation. In the same way, *scattering in* identifies those neutrons with energy and direction different from the ones of interest which, suffering a scattering event, emerge with energy  $E$  and direction  $\Omega$ , representing a gain from the point of view of the neutron balance.

Hence, in terms of angular flux  $\phi$  (1.2), the mathematical expression of the neutron transport equation in its integro-differential form reads:

$$\begin{aligned}
& \frac{1}{v(E)} \frac{\partial \phi(\mathbf{r}, E, \Omega, t)}{\partial t} + \Omega \cdot \nabla \phi(\mathbf{r}, E, \Omega, t) + \Sigma_t(\mathbf{r}, E) \phi(\mathbf{r}, E, \Omega, t) \\
& = \int dE' \oint d\Omega' \Sigma_s(\mathbf{r}, E') \phi(\mathbf{r}, E', \Omega', t) f_s(\mathbf{r}, E' \rightarrow E, \Omega' \rightarrow \Omega) + S(\mathbf{r}, E, \Omega, t) \quad (1.5)
\end{aligned}$$

where the angular flux  $\phi(\mathbf{r}, E, \Omega, t)$  constitutes the unknown of the equation.

On the left-hand side, the first term appearing in (1.5) represents the variation in time of the angular flux, origin of the differential nature of the equation. Then, the second is generally called the *streaming term* and constitutes the net variation of neutrons traveling in and out the space volume through its boundaries. Eventually, the last term concerns the probable number of neutrons lost due to an absorption event or a scattering interaction involving neutrons with the energy and direction of interest before the collision, which experience a change either in their energy or direction caused by the interaction: the scattering out contribution. This last term consists of the total cross-section  $\Sigma_t$ , which represents the probability per unit path for a neutron of energy  $E$  at the position  $\mathbf{r}$ , to undergo a collision. In this case in which the absorption and scattering out contribution are combined,  $\Sigma_t$  is equal to the summation of the

absorption and the scattering partial cross-sections [8]:

$$\Sigma_t = \Sigma_a + \Sigma_s. \quad (1.6)$$

Then, on the right-hand side of Eq. (1.5) the former term deals with neutrons of every energy and direction of motion which, undergoing a scattering collision, emerge in the investigated package with the energy and direction of interest, respectively  $E$  and  $\Omega$ : it consists in the scattering in contribution. In order to comprise neutrons of all the possible energies, coming from all the possible directions, integrals over the energies  $E'$  and the directions  $\Omega'$  before the scattering event are performed. Thus, this term is the one responsible of the integral nature of the equation. The probability per unit path for a neutron of energy  $E'$  in the volume  $d\mathbf{r}$  about  $\mathbf{r}$  to undergo a scattering interaction with a nucleus of the background medium is expressed by the scattering cross-section  $\Sigma_s$ . Instead, the probability that a neutron with the initial energy  $E'$  and direction  $\Omega'$  will emerge from the collision in the volume  $d\mathbf{r}$  about  $\mathbf{r}$ , with the energy  $dE$  about  $E$  and direction  $\Omega$  within the solid angle  $d\Omega$  is given by the *scattering probability function*  $f_s(\mathbf{r}, E' \rightarrow E, \Omega' \rightarrow \Omega)$ . Thus, the scattering kernel  $f_s$  is defined as a probability density function which may be conveniently normalized through the integration over the energy range and over all the directions as:

$$\oint d\Omega' \int_0^\infty dE' f_s(\mathbf{r}, E' \rightarrow E, \Omega' \rightarrow \Omega) = 1. \quad (1.7)$$

Besides, it is useful to note that, generally, the scattering function  $f_s$  may be assumed as dependent only on the angle between the direction of motion of the particle before the scattering event,  $\Omega'$ , and the one after the interaction,  $\Omega$ , which is referred to as the *scattering angle*  $\theta_0$ . Defining the cosine of the scattering angle as:

$$\cos \theta_0 \equiv \mu_0 = \Omega' \cdot \Omega \quad (1.8)$$

then the dependence of the scattering function  $f_s$  may be rewritten as [8]:

$$f_s(\mathbf{r}, E' \rightarrow E, \Omega' \rightarrow \Omega) = f_s(\mathbf{r}, E' \rightarrow E, \Omega' \cdot \Omega) \quad (1.9)$$

Finally, the latter term appearing in the right-hand side of Eq. (1.5) consists in the source term, which accounts for neutrons injected in the volume  $d\mathbf{r}$  around position  $\mathbf{r}$ , with energy  $E$  within  $dE$ , direction  $\Omega$  within  $d\Omega$  at time  $t$  [5].

Hence, substituting the simplified notation adopted for the scattering kernel  $f_s$  (1.9) in the scattering integral, the neutron transport equation for a three-dimensional, time and energy

dependent system yields<sup>4</sup>:

$$\begin{aligned} & \frac{1}{v(E)} \frac{\partial \phi(\mathbf{r}, E, \boldsymbol{\Omega}, t)}{\partial t} + \boldsymbol{\Omega} \cdot \nabla \phi(\mathbf{r}, E, \boldsymbol{\Omega}, t) + \Sigma_t(\mathbf{r}, E) \phi(\mathbf{r}, E, \boldsymbol{\Omega}, t) = \\ & = \int dE' \oint d\boldsymbol{\Omega}' \Sigma_s(\mathbf{r}, E') \phi(\mathbf{r}, E', \boldsymbol{\Omega}', t) f_s(\mathbf{r}, E' \rightarrow E, \boldsymbol{\Omega}' \cdot \boldsymbol{\Omega}) + S(\mathbf{r}, E, \boldsymbol{\Omega}, t). \end{aligned} \quad (1.10)$$

Moreover, to considered also the case of fundamental interest in nuclear reactor engineering of fissionable material, a further term accounting for neutrons emerging from fission reactions in the package of interest, that is with energy  $E$  and direction  $\boldsymbol{\Omega}$  in the volume  $d\mathbf{r}$ , should be included in the transport equation (1.10). As for the scattering term, the fission term is built starting from the fission partial cross-section  $\Sigma_f$  and the fission probability density function  $\chi(\mathbf{r}, E)$ , which refers to the probability that from a fission reaction between neutrons transported in the medium and the nuclei constituting of it, will emerge a neutron at the position  $\mathbf{r}$ , with energy  $E$ . The simplification with respect to the case of scattering concerns the fact that fission may be considered in a good approximation as an isotropic phenomenon, meaning that all directions are equally likely for the fission neutrons emission. Thus the additional term to be inserted in Eq. (1.10) results in:

$$\frac{\chi(\mathbf{r}, E)}{4\pi} \int dE' \oint d\boldsymbol{\Omega}' \nu(E') \Sigma_f(\mathbf{r}, E') \phi(\mathbf{r}, E', \boldsymbol{\Omega}', t) \quad (1.11)$$

where  $\nu(E')$  is defined as the average number of fission neutrons emitted at the position  $\mathbf{r}$  due to the fission reaction of a nucleus induced by a neutron of energy  $E'$ . Hence, the time-dependent neutron transport equation in presence of fission reactions and external source  $S$  reads:

$$\begin{aligned} & \frac{1}{v(E)} \frac{\partial \phi(\mathbf{r}, E, \boldsymbol{\Omega}, t)}{\partial t} + \boldsymbol{\Omega} \cdot \nabla \phi(\mathbf{r}, E, \boldsymbol{\Omega}, t) + \Sigma(\mathbf{r}, E) \phi(\mathbf{r}, E, \boldsymbol{\Omega}, t) \\ & = \int dE' \oint d\boldsymbol{\Omega}' \Sigma_s(\mathbf{r}, E') \phi(\mathbf{r}, E', \boldsymbol{\Omega}', t) f_s(\mathbf{r}, E' \rightarrow E, \boldsymbol{\Omega}' \cdot \boldsymbol{\Omega}) \\ & + \frac{\chi(\mathbf{r}, E)}{4\pi} \int dE' \oint d\boldsymbol{\Omega}' \nu(E') \Sigma_f(\mathbf{r}, E') \phi(\mathbf{r}, E', \boldsymbol{\Omega}', t) + S(\mathbf{r}, E, \boldsymbol{\Omega}, t). \end{aligned} \quad (1.12)$$

Finally, if a stationary system has to be considered, the term characterized by the derivative with respect to time is cancelled and the time variable is deleted from any quantity appearing in the equation governing the particles transport.

---

<sup>4</sup>For the overall derivation the interested lecturer could refer to any transport theory or reactor analysis book, such as yet cited [6] or [5].

### 1.1.2 Boundary and initial conditions

From the mathematical point of view, the neutron transport equation requires initial and boundary conditions to be solved. About the latter, different types of conditions may be imposed based on the specific case of interest. As concerns the initial condition instead, the integro-differential neutron transport equation is characterized by a first derivative with respect to time, meaning that it is necessary to provide the initial value of the neutron angular density or angular flux, as [9]:

$$\phi(\mathbf{r}, E, \boldsymbol{\Omega}, t = 0) = \phi_0(\mathbf{r}, E, \boldsymbol{\Omega}). \quad (1.13)$$

Conversely, the boundary conditions imply different possible options. Some of the most common choices are the *free surface*, *reflecting* or *albedo* conditions, and *periodic* boundary conditions [9].

In the present work, only the free surface type is examined and employed in the developed mathematical discussion. These conditions are also denoted as *vacuum boundary conditions* and interest those regions which are simply connected, meaning non-reentrant bodies. According to this type of conditions, neutrons which leave the region are supposed unable to return in it and in addition, it is assumed that no neutrons can enter the region from outside. Defining the outward normal direction vector  $\hat{\mathbf{n}}$  with respect to the surface  $\partial V$  delimiting the domain  $V$  at the position  $\mathbf{r}_s$ , the free surface boundary conditions are then expressed as [5]:

$$\phi(\mathbf{r}_s, E, \boldsymbol{\Omega}_{\text{inc}}, t) = 0 \quad \text{for } \boldsymbol{\Omega}_{\text{inc}} \cdot \hat{\mathbf{n}} < 0. \quad (1.14)$$

### 1.1.3 Mono-energetic model

The *mono-energetic model*, also denoted as *one-velocity model* or *one-group theory* [5], represents a simplified model of the general neutron transport equation in which the description of the distribution of neutrons in the energy space is not treated. However, even though it constitutes a restricted description of the neutron population transported in a medium, the mono-energetic model may reveal itself extremely useful in several occasions in reactor analysis [6].

The model may be derived from the integration over the energy range of the energy-dependent neutron transport equation in the form (1.10). Holding true that cross-sections are independent on energy, generally a reasonable assumption in case of thermal neutrons [5],

the neutron transport equation becomes:

$$\begin{aligned} \frac{1}{v} \frac{\partial \phi(\mathbf{r}, \boldsymbol{\Omega}, t)}{\partial t} + \boldsymbol{\Omega} \cdot \nabla \phi(\mathbf{r}, \boldsymbol{\Omega}, t) + \Sigma_t(\mathbf{r}) \phi(\mathbf{r}, \boldsymbol{\Omega}, t) \\ = \oint d\boldsymbol{\Omega}' \Sigma_s(\mathbf{r}) \phi(\mathbf{r}, \boldsymbol{\Omega}', t) f_s(\mathbf{r}, \boldsymbol{\Omega}' \cdot \boldsymbol{\Omega}) + S(\mathbf{r}, \boldsymbol{\Omega}, t). \end{aligned} \quad (1.15)$$

### 1.1.4 Plane geometry model

A simplified but useful approximation which may be derived about the neutron transport equation is the one-dimensional mono-energetic model for homogeneous media. Despite its several simplifications with respect to the most general neutron transport problem (1.10), this model may be effective in different applications of transport theory calculations. The following model is indeed the one employed in the description of the behavior of a neutron population transported in a slab, which is the geometrical configuration considered in the present thesis.

The fundamental assumption in plane geometry consists in the fact that the neutron angular flux, or in general the neutron angular density, depends on a unique spatial coordinate, for instance the  $x$  coordinate [9]. Then, as concerns the direction  $\boldsymbol{\Omega}$ , the angular flux depends only on the angle formed by the direction with the  $x$ -axis or alternatively, on the cosine of this angle, generally denoted as  $\mu$  (see Figure). Besides, as a consequence of the plane symmetry assumption, the angular flux is independent of the azimuthal angle  $\varphi$ , taking the polar coordinate as coincident with the  $x$ -axis of Cartesian reference system.

In Cartesian coordinates, the expression of the unit direction vector  $\boldsymbol{\Omega}$  as function of the the co-latitude angle  $\theta$  and the azimuthal angle  $\varphi$  is:

$$\boldsymbol{\Omega} = \cos \theta \hat{\mathbf{e}}_x + \sin \theta \cos \varphi \hat{\mathbf{e}}_y + \sin \theta \sin \varphi \hat{\mathbf{e}}_z. \quad (1.16)$$

Defining  $\mu = \cos \theta$ , the formulation becomes:

$$\boldsymbol{\Omega} = \mu \hat{\mathbf{e}}_x + \sqrt{1 - \mu^2} \cos \varphi \hat{\mathbf{e}}_y + \sqrt{1 - \mu^2} \sin \varphi \hat{\mathbf{e}}_z. \quad (1.17)$$

Then, taking as reference the mono-energetic version of the neutron transport equation (1.15), the streaming term appearing in the left-hand side reduces in plane geometry to [9]:

$$\boldsymbol{\Omega} \cdot \nabla \phi(x, \boldsymbol{\Omega}, t) = \Omega_x \frac{\partial}{\partial x} \phi(x, \Omega_x, t) \quad (1.18)$$

where the  $x$ -component of the direction vector  $\boldsymbol{\Omega}$ , namely  $\Omega_x$ , corresponds to  $\mu$  as evident from (1.17). Hence, the one-dimensional form of the mono-energetic neutron transport

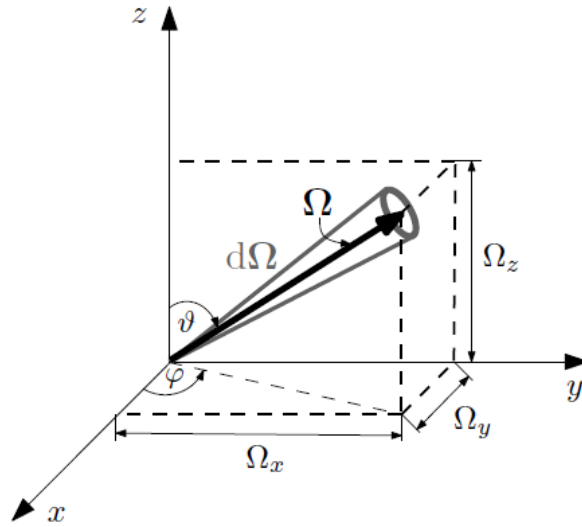


Figure 1.2: Cartesian coordinate reference system[7]

equation yields:

$$\frac{1}{v} \frac{\partial \phi(x, \mu, t)}{\partial t} + \mu \frac{\partial \phi(x, \mu, t)}{\partial x} + \Sigma_t \phi(x, \mu, t) = \int_{-1}^1 d\mu \Sigma_s \phi(x, \mu', t) f_s(x, \mu \mu') + S(x, \mu, t). \quad (1.19)$$

in which it may be noted how the range of integration over  $d\mu$ , between  $-1$  and  $1$ , corresponds to the variation of the polar angle  $\theta$  between  $0$  and  $\pi$  [9].

## Chapter 2

# The Criticality Problem

A crucial issue in nuclear reactor theory is establishing whether the neutron population throughout the reactor core is independent on time, decreases or increases with it, through the different operating stages of the nuclear device. As a consequence, one has to establish whether the fission chain reaction involving the fissile or fissionable nuclei of the reactor fuel, can be maintained stationary and controlled [10]

In particular, for fission chain reaction is intended the process in which neutrons produced by fission reactions of heavy nuclides, as  $U^{235}$  or  $U^{238}$ , interacting with others of these nuclides are able to induce further fission events and so on. Hence, it is said *nuclear reactor* that specific device able to maintain a self-sustainable and controlled fission chain reaction [11].

In order to ensure a stationary energy production from the fission reactions taking place in the reactor core, an exact balance between neutrons produced by fission events and those lost due to absorption or leakages out of the boundary of the system has to occurred. In the case in which such a balance is verified, it is then possible to have a neutron population throughout the reactor that is independent of time, with fission as unique neutron source term. A reactor in such a condition is said a *critical* reactor, characterized by a stationary fission chain reaction. Whether instead the number of neutrons released in fission events involving the nuclear fuel is smaller than the neutrons lost due to absorption or leakage out of outer surface, in absence of an external neutron source <sup>1</sup>, the chain reaction will die out over time and the reactor is said *subcritical*. On the contrary, whether the number of neutrons produced by fission reactions overcomes the number of those which are lost, the number of neutrons in the system is destined to increase from generation to generation and the reactor is defined *supercritical* [12].

Therefore, primary interest of the nuclear engineer is to design a power reactor able to accomplish and maintain the critical state [13]. The two design aspects which play major roles in relation to criticality are the material composition and the geometrical configuration.

---

<sup>1</sup>In general, a source different from fission is intended.

The *criticality problem* is indeed commonly intended as the research of the right combination of these two aspects that allows the reactor to achieve a critical state. Generally, nuclear power reactors are designed in such a way that their condition, among critical, super- or sub-critical, can be modified as needed. The modification and control of the critical state of a nuclear reactor is indeed an extremely delicate and fundamental aspect of nuclear reactor analysis, commonly known as *nuclear reactor control* [13]. Several physical phenomena participate in altering the reactor criticality over its different operating stages. Some phenomena, as the fuel depletion or the accumulation of fission products in the core as the chain reaction develops, contribute to decrease the number of neutrons in the neutron balance, making the system tend to a subcritical condition. The increment of the amount of plutonium instead induces an increase in the number of neutrons and, as a consequence, it contributes to make the system supercritical [14]. From the engineering point of view, several different countermeasures are foreseen in the reactor design in order to compensate for departure from the critical and stationary state of the device. To name a few, the insertion or withdrawing of control rods, the use of soluble poisons or the buildup of xenon are some of the strategies available [14], [15].

Mathematically, the criticality problem is approached as an eigenvalue problem. This means that a non-trivial and non-negative solution to the homogeneous form of the stationary neutron transport equation, meaning in absence of external sources, is searched, under appropriate boundary conditions.

Bearing to mind the physical meaning of critical state in the reactor core, a perfect balance between the number of neutrons produced by fission reactions and the number of neutrons lost for absorption and leakage out of the system, the time-independent transport equation expression of such a balance reads:

$$\begin{aligned} & \boldsymbol{\Omega} \cdot \nabla \phi(\mathbf{r}, E, \boldsymbol{\Omega}) + \Sigma_t(\mathbf{r}, E) \phi(\mathbf{r}, E, \boldsymbol{\Omega}) \\ &= \oint d\boldsymbol{\Omega}' \int dE' \Sigma_s(\mathbf{r}, E') \phi(\mathbf{r}, E', \boldsymbol{\Omega}') f_s(\mathbf{r}, E' \rightarrow E, \boldsymbol{\Omega}' \cdot \boldsymbol{\Omega}) \\ & \quad + \frac{\chi(\mathbf{r}, E)}{4\pi} \oint d\boldsymbol{\Omega}' \int dE' \nu(E') \Sigma_f(\mathbf{r}, E') \phi(\mathbf{r}, E', \boldsymbol{\Omega}') \quad (2.1) \end{aligned}$$

for which vacuum boundary conditions are considered. However, due to the use of approximations in numerical calculations and uncertainties in nuclear data, there are cases in which, even if the reactor is actually critical, when computed, it may result deviated from criticality [3]. Thus, in order to apply the steady-state Eq. (2.1) also to those systems that result slightly not critical, and hence requiring a time-dependent model for the description of their behavior, neutron transport equation is transformed in an eigenvalue problem by inserting a constant, characteristic of the case to be analysed [15].

Mathematically, an eigenvalue equation is an expression which reads:

$$\hat{\mathbf{A}} \varphi = \lambda \varphi \quad (2.2)$$

where  $\hat{\mathbf{A}}$  is a square matrix  $\in C^{n \times n}$ ,  $\lambda$  is a scalar, real or complex, and  $\varphi$  is a non-null vector such that the expression (2.2) is verified. Thus, any  $\lambda$  satisfying Eq. (2.2) is called an *eigenvalue* of the matrix  $\hat{\mathbf{A}}$  and the corresponding solution vector  $\varphi$  is the associated *eigenvector* [16]. This two, combined together, are named *eigenpair*. In summary,  $\hat{\mathbf{A}}$  consists in an operator which, when applied to  $\varphi$ , behaves like the operator "multiplication times a constant", where the constant is the eigenvalue of the problem [10].

Concerning the neutron transport equation, four different eigenvalue equations may be formulated in relation to, respectively, the eigenvalues:  $k$ , the *effective multiplication factor*,  $\alpha$ , the *fundamental multiplication rate*,  $\gamma$ , the *multiplication factor per collision* and lastly  $\delta$ , the *effective density factor*. The eigenfunctions corresponding to the various eigenvalues, constituting the neutron population distribution solution of the eigenvalue equations, differ except in case of a critical systems [3].

Generally, it is useful in the treatment of eigenvalue problems the use of the operator notation. Thus, referring to the steady-state homogeneous version of the integro-differential form of the neutron transport equation (2.1), the following operators are defined:

$$\begin{aligned} \mathbf{L} &= \boldsymbol{\Omega} \cdot \nabla && \text{Leakage operator} \\ \mathbf{R} &= \Sigma_t(\mathbf{r}, E) && \text{Removal operator} \\ \mathbf{S} &= \oint d\boldsymbol{\Omega}' \int dE' \Sigma_s(\mathbf{r}, E') f_s(\mathbf{r}, E' \rightarrow E, \boldsymbol{\Omega}' \cdot \boldsymbol{\Omega}) && \text{Scattering operator} \\ \mathbf{F} &= \frac{\chi(\mathbf{r}, E)}{4\pi} \oint d\boldsymbol{\Omega}' \int dE' \nu(E') \Sigma_f(\mathbf{r}, E') && \text{Fission operator} \end{aligned}$$

In addition, the combination of the  $\mathbf{L}$  and  $\mathbf{R}$  operator is defined as the *transport operator*  $\mathbf{T} = \mathbf{L} + \mathbf{R}$ . The transport equation (2.1) in operator form then yields:

$$\mathbf{L}\phi(\mathbf{r}, E, \boldsymbol{\Omega}) + \mathbf{R}\phi(\mathbf{r}, E, \boldsymbol{\Omega}) = \mathbf{S}\phi(\mathbf{r}, E, \boldsymbol{\Omega}) + \mathbf{F}\phi(\mathbf{r}, E, \boldsymbol{\Omega}).$$

The four different eigenvalue types are inserted in the neutron balance equation as modification of its specific terms, peculiar of each possible type of eigenvalue. They constitute an identifier of the amount of the system deviation from criticality.

Referring to each type of eigenvalue equation, the set of eigenvalues solution of the equation is denoted as the *eigenvalue spectrum*, or *eigenspectrum*. The eigenfunctions associated to the values of the spectrum are then called *modes*, or *harmonics*. The characteristic spectrum of a specific operator can be continuous, discrete or can have the two natures combined.

Furthermore, the eigenvalues may be real or complex, single or multiple [17]. Supposing a discrete spectrum and organizing its eigenvalues in a descending order of modulus, it is possible to individuate the eigenvalue with the largest modulus generally denoted as the *spectral radius*, or the *fundamental eigenvalue*. The associated eigenfunction is then referred to as the fundamental solution or the fundamental mode which, in case of the neutron transport equation, consists in the unique solution of the eigenvalue problem of physical significance. It is indeed the only one of constant sign over all the domain [18], [16]. The solutions associated to the other values of the spectrum are lastly denoted as higher-modes.

## 2.1 The $k$ eigenvalue

In literature, the most widely inspected eigenvalue is the *effective multiplication factor*  $k$ . The denomination comes from the fact that it is inserted in the homogeneous transport equation as a modification to the fission source term. Specifically, it divides the fission contribution of the time-independent neutron transport equation as follows:

$$\begin{aligned} & \boldsymbol{\Omega} \cdot \nabla \phi(\mathbf{r}, E, \boldsymbol{\Omega}) + \Sigma_t(\mathbf{r}, E) \phi(\mathbf{r}, E, \boldsymbol{\Omega}) \\ &= \oint d\boldsymbol{\Omega}' \int dE' \Sigma_s(\mathbf{r}, E') f_s(\mathbf{r}, E' \rightarrow E, \boldsymbol{\Omega}' \cdot \boldsymbol{\Omega}) \phi(\mathbf{r}, E', \boldsymbol{\Omega}') \\ & \quad + \frac{1}{k} \frac{\chi(\mathbf{r}, E)}{4\pi} \oint d\boldsymbol{\Omega}' \int dE' \nu(E') \Sigma_f(\mathbf{r}, E') \phi(\mathbf{r}, E, \boldsymbol{\Omega}). \end{aligned} \quad (2.3)$$

In operator notation the transport equation with the  $k$  eigenvalue (2.3) reads:

$$\mathbf{L}\phi + \mathbf{R}\phi = \mathbf{S}\phi + \frac{1}{k}\mathbf{F}\phi. \quad (2.4)$$

Thus, the effective multiplication factor  $k$  intervenes, in terms of neutron balance, as a modification of the gain term with respect to the losses, allowing to alter the number of neutrons emitted by fission reactions in order to make the system critical [17]. A first definition hence denotes  $k$  as the ratio of the number of neutrons present in the core in two successive fission generations [13]:

$$k = \frac{\text{Number of neutrons in one generation}}{\text{Number of neutrons in preceding generation}}$$

Moreover, based on this definition, the  $k$  eigenvalue can be also found as the *effective neutron multiplication factor per neutron generation* [15].

In reference to the  $k$ -eigenvalue spectrum, the set of  $k$  values for which a non-trivial solution  $\phi$  of Eq. (2.4) exists, the eigenvalue with the algebraically largest real part is denoted

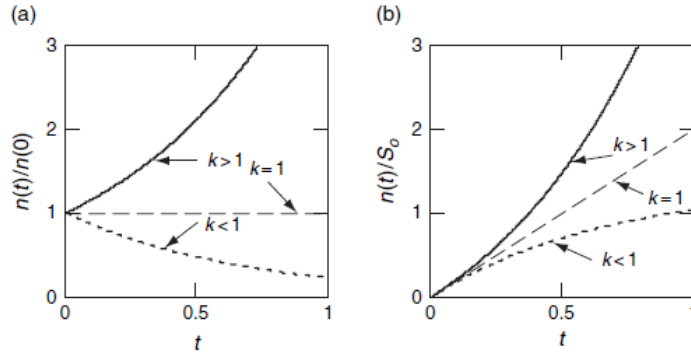


Figure 2.1: Neutron population density time behaviour in case of a sub-critical, critical and super-critical system without external sources and  $n(0) = 1$  (on the left), with the presence of an external source and  $n(0) = 0$  (on the right). [12]

as the fundamental  $k$ -eigenvalue, generally indicated as  $k_0$  or  $k_{\text{eff}}$ . As mentioned above, the solution associated to this eigenvalue is the fundamental  $k$ -mode, the unique solution for the neutron population distribution with a physical meaning because positive over all the domain. Then, it may be noted that if  $k_0 = 1$ , the number of neutrons in the reactor core does not vary from a generation to the successive one. Hence, in this case the chain reaction is independent on time and the reactor is referred to as *critical*. If  $k_0 < 1$ , the reactor constitutes instead a *subcritical* system, characterized by a chain reaction destined to die out. Finally, if  $k_0 > 1$  the system is *supercritical*, with the number of neutrons which increase from generation to generation and consequently, the chain reaction does too.

Schematically:

$$\begin{cases} k_0 > 1 & \text{supercritical reactor} \\ k_0 = 1 & \text{critical reactor} \\ k_0 < 1 & \text{subcritical reactor} \end{cases}$$

Furthermore, alternatively to the definition of the multiplication factor  $k$  in terms of neutron generations, the  $k$  factor may be also referred to as the ratio between the fission production rate and the loss rate due to both absorption and leakage [13]. A graphical representation of the different behavior of the neutron population with respect to time in a system that is, respectively, critical, sub- or super-critical, is reported in Figure 2.1.

Looking to Figure 2.1, it interesting to notice how even for extremely small deviations of the multiplication factor from unity, correspond substantial changes in neutron population evolution with respect to time. The main cause of such a change is the small extent of neutron lifetime, whose values are included between  $10^{-8}$  and  $10^{-4}$  s. However, the nuclear reactor control is made possible by the presence of the *delayed neutrons*, those neutrons which are not released immediately after the fission event. Delayed neutrons are indeed emitted in the

decay process of some fission products called the *delayed neutron precursors*. The delay with respect to those particles emitted almost instantaneously with the fission reaction, indicated as *prompt neutrons*, ranges from values of the order of milliseconds up to seconds, nearly a minute, in relation to the different half-live values of neutron precursors. Therefore, the substantial difference in timescales between prompt and delayed neutrons emission constitutes the crucial feature that permits the reactor control [12].

In the present work, delayed neutrons are not included in the mathematical and physical discussion of the neutron transport in the reactor core. For steady-state problems and criticality evaluations this is a reasonable assumption, but their fundamental role in nuclear reactor kinetics is worth the citation.

### 1D mono-energetic model with $k$ eigenvalue

With respect to the eigenvalue formalism of the neutron transport equation in its most general model (2.3), object of the entire presentation consists in its simplified 1D mono-energetic version, for a slab geometry reactor with isotropic scattering. Then, the equation the work is concerned with, here presented specifically for the case with the  $k$  eigenvalue, reads:

$$\mu \frac{\partial \phi(x, \mu)}{\partial x} + \Sigma_t \phi(x, \mu) = \left( \frac{\Sigma_s}{2} + \frac{1}{k} \frac{\nu \Sigma_f}{2} \right) \int d\mu' \phi(x, \mu') \quad (2.5)$$

where, as yet introduced in Sect. 1.1.4,  $\phi(x, \mu)$  is the neutron angular flux for geometrical configuration implying plane symmetry. Furthermore, cross-sections are assumed as independent of space and direction. Hence, in operator notation Eq. (2.5) results in:

$$\mathbf{L} \phi + \mathbf{R} \phi = \left( \mathbf{S} + \frac{1}{k} \mathbf{F} \right) \phi \quad (2.6)$$

constituting the base for the application of the  $P_N$  approximation to which Sect.3.2.3 is devoted. Therefore, in this form Eq. (2.6) represents a generalized eigenvalue equation which may be transformed in the standard form (Eq. (2.2)), by manipulating the left-hand side as [17]:

$$(\mathbf{L} + \mathbf{R} - \mathbf{S}) \phi = \hat{\mathbf{L}} \phi = \frac{1}{k} \mathbf{F} \phi. \quad (2.7)$$

Since the  $\mathbf{F}$  operator could be singular, that is it does not admit the inverse, the inversion is applied to the  $\mathbf{L}$  operator which is not singular. Finally, the multiplication factor is taken on the other side of the equation and the problem yields:

$$\hat{\mathbf{L}}^{-1} \mathbf{F} \phi = k \phi. \quad (2.8)$$

Thus, the problem consists in determining the discrete eigenvalues  $k_i$  of the global matrix  $\hat{\mathbf{L}}^{-1}\mathbf{F}$  and their associated eigenfunctions  $\phi_i$  [17].

## 2.2 The $\alpha$ eigenvalue

The  $\alpha$  eigenvalue may be found in literature as the *fundamental multiplication rate eigenvalue* [15], the *decay constant* [19] or the *time eigenvalue* [20], based on the different contexts in which such an eigenvalue may have a role.

Nearly all these denominations emphasize the relation between this eigenvalue type and the description of the time-dependent behavior of a neutron population in a nuclear reactor, representing a fundamental field of interest in nuclear reactor kinetic. In particular, in criticality analysis the  $\alpha$  eigenvalue equations constitute a valid tool for the study of subcritical systems, for which an adequate description of the temporal behavior of the neutron population requires the fundamental solution as well as a relevant number of higher modes [21].

The starting point to formulate the  $\alpha$  eigenvalue problem is represented by the homogeneous version of the time-dependent neutron transport equation in its integro-differential form:

$$\begin{aligned} \frac{1}{v} \frac{\partial \phi(\mathbf{r}, E, \boldsymbol{\Omega}, t)}{\partial t} + \boldsymbol{\Omega} \cdot \nabla \phi(\mathbf{r}, E, \boldsymbol{\Omega}, t) + \Sigma_t \phi(\mathbf{r}, E, \boldsymbol{\Omega}, t) \\ = \oint d\boldsymbol{\Omega}' \int dE' \Sigma_s \phi(\mathbf{r}, E', \boldsymbol{\Omega}', t) f_s(\mathbf{r}, E' \rightarrow E, \boldsymbol{\Omega}' \cdot \boldsymbol{\Omega}) \\ + \frac{\nu \chi(\mathbf{r}, E)}{4\pi} \oint d\boldsymbol{\Omega}' \int dE' \Sigma_f \phi(\mathbf{r}, E', \boldsymbol{\Omega}', t). \end{aligned} \quad (2.9)$$

This equation, with proper boundary conditions applied, such as vacuum boundary conditions (1.14), defines an initial value problem. If the initial condition for the neutron population distribution,  $\phi(\mathbf{r}, E, \boldsymbol{\Omega}, t = 0)$ , is provided, the neutron angular flux may be found at any time  $t > 0$ , as solution of Eq. (2.9), which has been demonstrated by many authors to exist and to be unique under some mathematical constraints about cross-sections and the source term [5].

Assuming boundary conditions as constant in time, solutions to Eq. (2.9) of the following form are considered:

$$\phi(\mathbf{r}, E, \boldsymbol{\Omega}, t) = \phi(\mathbf{r}, E, \boldsymbol{\Omega}) e^{\alpha t} \quad (2.10)$$

where  $\alpha$  may assume all the values that generate a non-trivial solution of the homogeneous time-independent neutron transport equation. The corresponding solutions constitute the eigenfunctions of the problem, exponentials which are referred to as  $\alpha$ -modes [22].

Hence, by inserting the function (2.10) and the corresponding derivative with respect to time into Eq. (2.9), one obtains:

$$\begin{aligned} & \frac{\alpha}{v} \phi(\mathbf{r}, E, \boldsymbol{\Omega}) e^{\alpha t} + \boldsymbol{\Omega} \cdot \nabla \phi(\mathbf{r}, E, \boldsymbol{\Omega}) e^{\alpha t} + \Sigma_t \phi(\mathbf{r}, E, \boldsymbol{\Omega}) e^{\alpha t} \\ &= \oint d\boldsymbol{\Omega}' \int dE' \Sigma_s \phi(\mathbf{r}, E', \boldsymbol{\Omega}') e^{\alpha t} f_s(\mathbf{r}, E' \rightarrow E, \boldsymbol{\Omega}' \cdot \boldsymbol{\Omega}) \\ & \quad + \frac{\nu \chi(\mathbf{r}, E)}{4\pi} \oint d\boldsymbol{\Omega}' \int dE' \Sigma_f \phi(\mathbf{r}, E', \boldsymbol{\Omega}') e^{\alpha t}. \end{aligned}$$

Then, canceling out the exponential from the above equation, the  $\alpha$  eigenvalue problem is obtained as [5]:

$$\begin{aligned} & \boldsymbol{\Omega} \cdot \nabla \phi(\mathbf{r}, E, \boldsymbol{\Omega}) + \left(\Sigma_t + \frac{\alpha}{v}\right) \phi(\mathbf{r}, E, \boldsymbol{\Omega}) \\ &= \int dE' \oint d\boldsymbol{\Omega}' \Sigma_s \phi(\mathbf{r}, E', \boldsymbol{\Omega}') f_s(\mathbf{r}, E' \rightarrow E, \boldsymbol{\Omega}' \cdot \boldsymbol{\Omega}) \\ & \quad + \frac{\chi(\mathbf{r}, E)}{4\pi} \int dE' \oint d\boldsymbol{\Omega}' \Sigma_f \nu \phi(\mathbf{r}, E', \boldsymbol{\Omega}') \quad (2.11) \end{aligned}$$

which may be also reached by applying Laplace transforms to Eq. 2.10.

In operator formalism Eq. (2.11) reads:

$$\left(\mathbf{T} + \frac{\alpha}{v}\right) \phi = (\mathbf{S} + \mathbf{F}) \phi. \quad (2.12)$$

Thus, the criticality problem with  $\alpha$  eigenvalue is approached with an increment of the total macroscopic cross-section  $\Sigma_t$  by a factor  $\alpha/v$ , which may be referred to as *fictitious capture* [6] or *time-absorption* term [23]. With  $v$ , the neutron speed is denoted. The absorption term of the neutron transport equation may be varied through the  $\alpha$  eigenvalue, until the system critical state is reached.

The  $\alpha$  eigenvalue, differently from the other eigenvalue types, has a unit of measure corresponding to the inverse of time. The set of  $\alpha$  eigenvalues for which Eq. (2.12) is verified, is referred to as the  $\alpha$ -eigenvalue spectrum. Among these, the  $\alpha$  which presents the largest real part in absolute value is called the fundamental eigenvalue and it is generally denoted as  $\alpha_0$ . The corresponding solution, an exponential with  $\alpha_0$  as characteristic constant, represents the asymptotic behavior of a neutron population described by Eq. (2.12). Indeed, being  $\alpha_0$  the eigenvalue with the largest real part, at late times the corresponding solution will be the only one to survive with respect to the higher exponential modes [5].

Thus, the criticality problem reduces to determine the sign of  $\alpha_0$ . It follows indeed that for  $\alpha_0 < 0$  the system neutron population will decay over time following an exponential behavior and, as a consequence, the system is subcritical; on the contrary, for  $\alpha_0 > 0$  the neutron

population will diverge over time and the system results supercritical, whereas for  $\alpha_0 = 0$  the system is critical.

To summarize:

$$\begin{cases} \alpha_0 > 0 & \text{supercritical reactor} \\ \alpha_0 = 0 & \text{critical reactor} \\ \alpha_0 < 0 & \text{subcritical reactor} \end{cases}$$

Finally, in reference to this type of eigenvalue many studies concerning the nature of the eigenvalue spectrum in different geometries with diverse boundary conditions applied and different scattering features, have been conducted. In particular, it has been demonstrated that for unbounded geometries a discrete eigenvalue spectrum could be not always found. As regards for instance the case of a mono-energetic model applied to an infinite slab geometry, it has been proved that the  $\alpha$ -eigenvalue spectrum consists of both a finite set of real and discrete eigenvalues and of a continuous part. The respective composition in terms of number and location of the eigenvalues is based upon the extent of the eigenvalue real part in relation to the value of the product between the total macroscopic cross-section and neutron speed considered, named the Corngold limit [5], [24].

### 1D mono-energetic model with $\alpha$ eigenvalue

As reported for the  $k$  eigenvalue, the eigenvalue formalism of the neutron transport equation for a slab geometry with isotropic scattering, with  $\alpha$  as eigenvalue reads:

$$\mu \frac{\partial \phi(x, \mu)}{\partial x} + (\Sigma_t + \frac{\alpha}{v}) \phi(x, \mu) = \frac{c \Sigma_t}{2} \int d\mu' \phi(x, \mu') \quad (2.13)$$

where  $c$  is defined as the average number of secondary neutrons, the mean number of particles that one has to expect from a collision event.

In operator formalism Eq. (2.13) results in:

$$\mathbf{L}\phi + (\mathbf{R} + \frac{\alpha}{v})\phi = (\mathbf{S} + \mathbf{F})\phi \quad (2.14)$$

basis for the application of the  $P_N$  approximation reported in Sect. 3.2.3. Eq. (2.14) consists in a generalized eigenvalue equation which, transformed in its standard form, yields:

$$v\mathbf{B}\phi = \alpha\phi \quad (2.15)$$

with  $\mathbf{B} = [(\mathbf{L} + \mathbf{R}) - (\mathbf{S} + \mathbf{F})]$ . In these terms, the problem is therefore reduced to determine the  $\alpha$ -eigenvalue spectrum and the associated eigenfunctions  $\phi$ , solutions of the equation [17].

## 2.3 The $\gamma$ eigenvalue

The  $\gamma$  eigenvalue was suggested by Davison [6] as a direct eigenvalue of the integro-differential neutron transport equation. In literature it may be found as the *effective multiplication factor per collision* or with the same physical meaning of the number of secondary neutrons per collision, generally denoted as  $c$  [15], [24].

As its denomination indicates, the  $\gamma$  eigenvalue is inserted in the integro-differential neutron transport equation as a modification of the number of neutrons per collision, which may be altered until the criticality condition is achieved [17]. In particular, this type of eigenvalue is inserted as constant factor by which, both the scattering in and the fission source term in the neutron balance, are divided.

Hence, the  $\gamma$ -eigenvalue formalism of the homogeneous time-independent neutron transport equation reads:

$$\begin{aligned} \Omega \cdot \nabla \phi(\mathbf{r}, E, \Omega) + \Sigma_t \phi(\mathbf{r}, E, \Omega) \\ = \frac{1}{\gamma} \left( \oint d\Omega' \int dE' \Sigma_s \phi(\mathbf{r}, E', \Omega') f_s(E' \rightarrow E, \Omega' \cdot \Omega) \right. \\ \left. + \frac{\nu \chi(\mathbf{r}, E)}{4\pi} \oint d\Omega' \int dE' \Sigma_f \phi(\mathbf{r}, E', \Omega') \right) \end{aligned} \quad (2.16)$$

which, written in operator formalism Eq. (2.16) yields:

$$(\mathbf{L} + \mathbf{R}) \phi = \frac{1}{\gamma} (\mathbf{S} + \mathbf{F}) \phi. \quad (2.17)$$

Likewise the previous eigenvalue types, the set of  $\gamma$  values for which Eq. (2.17) is verified, is referred to as the  $\gamma$ -eigenvalue spectrum, whereas the corresponding eigenfunctions  $\phi$  are denoted as  $\gamma$ -modes [17]. Among the possible  $\gamma$ , the one with the largest real part in absolute value is named the fundamental eigenvalue and it is generally indicated as  $\gamma_0$ . The corresponding eigenfunction  $\phi$  is the fundamental solution, the unique with a physical meaning. The higher modes are oscillating functions which may assume negative values [18].

From a physical standpoint, the eigenvalue  $\gamma_0$  is interpreted as the ratio between the number of neutrons produced by the scattering in and the fission source term, and the number of those lost due to collisions and leakage through the system boundary [17]. According to this approach, this type of eigenvalue is named the *effective multiplication factor per collision*.

Concerning the criticality condition discussion, a system is referred to as critical if  $\gamma_0 = 1$ , as subcritical if  $\gamma_0 < 1$  and finally as supercritical if  $\gamma_0 > 1$ .

Schematically:

$$\begin{cases} \gamma_0 > 1 & \text{supercritical reactor} \\ \gamma_0 = 1 & \text{critical reactor} \\ \gamma_0 < 1 & \text{subcritical reactor} \end{cases}$$

### 1D mono-energetic model with $\gamma$ eigenvalue

The  $\gamma$ -eigenvalue formalism of the neutron transport equation for a slab geometry with isotropic scattering reads:

$$\mu \frac{\partial \phi(x, \mu)}{\partial x} + \Sigma_t \phi(x, \mu) = \frac{1}{\gamma} \frac{c \Sigma_t}{2} \int d\mu' \phi(x, \mu') \quad (2.18)$$

with  $c$  number of secondaries per collision or critical parameter. Eq. (2.18) may be written in operator form as:

$$\mathbf{T} \phi = \frac{1}{\gamma} \mathbf{H} \phi \quad (2.19)$$

where the operator  $\mathbf{H}$  is given by the union of the scattering integral and the fission one.

In Sect.3.2.3 the application of the  $P_N$  approximation to this equation (2.19) is reported.

Eq. (2.19) represents a generalized eigenvalue equation which may be transformed in its standard form through the inversion of the left-hand side operator  $\mathbf{T}$ , mentioned above equals to  $\mathbf{L} + \mathbf{R}$ :

$$\mathbf{T}^{-1} \mathbf{H} \phi = \gamma \phi. \quad (2.20)$$

Hence, the problem is reduced to determine the  $\gamma$  eigenvalues and the associated eigenfunctions  $\phi$  [17].

## 2.4 The $\delta$ eigenvalue

The  $\delta$  eigenvalue, named the *effective density factor* [3], is certainly the more obscure eigenvalue type, rarely present in literature. As its denomination indicates, it is inserted in the neutron transport equation as a modification of the nuclides densities in such a way that the reactor criticality condition may be reached by altering the neutron leakage rate or the nuclear densities [17].

Specifically, the  $\delta$ -eigenvalue form of the homogeneous stationary neutron transport equation reads:

$$\begin{aligned} \boldsymbol{\Omega} \cdot \nabla \phi(\mathbf{r}, E, \boldsymbol{\Omega}) + \frac{1}{\delta} \Sigma_t \phi(\mathbf{r}, E, \boldsymbol{\Omega}) \\ = \frac{1}{\delta} \left( \oint d\boldsymbol{\Omega}' \int dE' \Sigma_s \phi(\mathbf{r}, E', \boldsymbol{\Omega}') f_s(E' \rightarrow E, \boldsymbol{\Omega}' \cdot \boldsymbol{\Omega}) \right. \\ \left. + \frac{\nu \chi(\mathbf{r}, E)}{4\pi} \oint d\boldsymbol{\Omega}' \int dE' \Sigma_f \phi(\mathbf{r}, E', \boldsymbol{\Omega}') \right). \end{aligned} \quad (2.21)$$

In operator formalism Eq.(2.21) yields:

$$\mathbf{L}\phi + \frac{1}{\delta} \mathbf{R}\phi = \frac{1}{\delta} (\mathbf{S} + \mathbf{F})\phi \quad (2.22)$$

where it is made evident how the  $\delta$  eigenvalue intervenes both on the removal term that on the source terms of the neutron balance, constituted by the scattering in and the fission contribution.

As for the previously presented eigenvalue types, the different values which  $\delta$  may assume to make Eq. (2.22) verified, are referred to as the  $\delta$ -eigenvalue spectrum. The corresponding eigenfunctions  $\phi$  are denoted as  $\delta$ -modes instead. From the physical point of view, the solution of interest is the one denominated as the fundamental solution eigenfunction, corresponding to the  $\delta_0$  eigenvalue, the one characterized by the algebraically largest real part among the discrete  $\delta$ -eigenvalue spectrum.

Furthermore,  $\delta_0$  represents the ratio between the difference of the fission and absorption rate, and the leakage rate [17].

Based on this definition, the criticality condition in a nuclear system is characterized by  $\delta_0 = 1$ , a subcritical system is a reactor such that  $\delta_0 < 1$  and, as a consequence, a supercritical system is characterized by  $\delta_0 > 1$ .

Schematically:

$$\begin{cases} \delta_0 < 1 & \text{subcritical reactor} \\ \delta_0 = 1 & \text{critical reactor} \\ \delta_0 > 1 & \text{supercritical reactor.} \end{cases}$$

### 1D mono-energetic model with $\delta$ eigenvalue

The  $\delta$ -eigenvalue formalism of the one-dimensional neutron transport equation for a slab geometry with isotropic scattering yields:

$$\mu \frac{\partial \phi(x, \mu)}{\partial x} + \frac{1}{\delta} \Sigma_t \phi(x, \mu) = \frac{1}{\delta} \frac{c \Sigma_t}{2} \int d\mu' \phi(x, \mu'). \quad (2.23)$$

In operator form Eq. (2.23) then reads:

$$\mathbf{L} \phi + \frac{1}{\delta} \mathbf{R} \phi = \frac{1}{\delta} (\mathbf{S} + \mathbf{F}) \phi, \quad (2.24)$$

constituting the base upon which the  $P_N$  approximation is applied in Sect. 3.2.3.

The standard form of the generalized eigenvalue equation (2.24) is then obtained through:

$$\mathbf{L}^{-1} (\mathbf{R} - (\mathbf{S} + \mathbf{F})) \phi = \delta \phi \quad (2.25)$$

and the problem is reduced to determine the  $\delta$  eigenvalues and the associated eigenvectors [17].

# Chapter 3

## The Spherical Harmonics Method

A complete description of a neutron population in phase space should involve information regarding the distribution in space, energy, time and travel direction of the population itself [8]. The solution of equations including contemporary all these dependencies requires extremely great efforts, feasible only for simplified models.

Several methods have been developed in order to provide a description of the angular distribution of a neutron population, among which the spherical harmonics method, the discrete ordinates method and the method of the characteristics. Other methods, devoted to the study of the distribution in the energy space of the population, are based on the discretization of the energy domain. For the solution of the energy dependent problems *multigroup methods* are generally applied [5].

In the present work, only the angular distribution of neutrons moving in a medium is inspected, with the fundamental assumption of isotropic and homogeneous media. The description of the neutron population distribution is limited to its spatial and angular dependency, thus a mono-energetic model of the transport equation is adopted for the discussion. Among the different approximations suitable for the study of the angular properties of the neutron motion through a medium, the spherical harmonics method is the one explored in this presentation. Thus, the derivation of the method applied to the neutron transport equation in a general geometry is briefly outlined<sup>1</sup> in Sect. 3.1, and the application of the method to the simplified case of a plane geometry model is then developed in Sect. 3.2. Eventually, the application of the spherical harmonics method to the different eigenvalue equations, to which the entire work is devoted, is reported in Sect. 3.2.3.

In general, the starting point of the spherical harmonics method is the Boltzmann transport equation in its integro-differential form. The angular dependency of the neutron flux is treated through the use of an expansion in terms of spherical harmonics, which leads to an infinite set of coupled differential equations in the various moments of the neutron flux. The

---

<sup>1</sup>For a rigorous derivation of the method one may refer to [8].

resulting infinite set is then reduced to a finite system of differential equations by truncating the series expansion of the neutron flux at an arbitrary high order of accuracy  $N$ , acquiring the so-called  $P_N$  approximation.

### 3.1 Spherical harmonics method in general geometry

Starting from the transport integro-differential formulation for a mono-energetic model, a series representation of the functions involved in the equation is developed. The expansions are carried out through the use of an orthonormal set of functions, the spherical harmonics[8]. The time-dependent neutron transport equation for the considered model reads:

$$\begin{aligned} \frac{1}{v} \frac{\partial \phi(\mathbf{r}, \boldsymbol{\Omega}, t)}{\partial t} + \boldsymbol{\Omega} \cdot \nabla \phi(\mathbf{r}, \boldsymbol{\Omega}, t) + \Sigma_t \phi(\mathbf{r}, \boldsymbol{\Omega}, t) = \\ = \oint d\boldsymbol{\Omega}' \Sigma_s \phi(\mathbf{r}, \boldsymbol{\Omega}', t) f_s(\boldsymbol{\Omega}' \cdot \boldsymbol{\Omega}) + S(\mathbf{r}, \boldsymbol{\Omega}, t). \end{aligned} \quad (3.1)$$

First, the probability density function for scattering collisions  $f_s(\boldsymbol{\Omega}' \cdot \boldsymbol{\Omega})$  is inspected. As a consequence of the isotropic and homogeneous medium assumption, the scattering function results to be a function only of the scattering angle  $\theta_0$  between the direction of motion  $\boldsymbol{\Omega}'$ , before the scattering event, and the particle direction after the scattering interaction  $\boldsymbol{\Omega}$ . Generally, the cosine of the scattering angle is defined, as previously reported:

$$\mu_0 \equiv \cos \theta_0 = \boldsymbol{\Omega}' \cdot \boldsymbol{\Omega}.$$

Thus, the scattering function  $f_s(\boldsymbol{\Omega}' \cdot \boldsymbol{\Omega})$  may be expanded in a series of Legendre polynomials  $P_n(\mu)$ , which constitute a complete set of orthogonal polynomials defined on the interval  $-1 \leq \mu \leq 1$  [5].

The expansion yields:

$$f_s(\boldsymbol{\Omega}' \cdot \boldsymbol{\Omega}) \equiv f_s(\mu_0) \equiv \sum_{n=0}^{\infty} \frac{(2n+1)}{2} f_n P_n(\boldsymbol{\Omega}' \cdot \boldsymbol{\Omega}). \quad (3.2)$$

By making use of the orthogonality properties of the Legendre polynomials, through the multiplication by the Legendre polynomial  $P_m(\mu_0)$  and the integration over  $d\mu_0$  one acquires:

$$\int_{-1}^1 d\mu_0 f_s(\mu_0) P_m(\mu_0) = \sum_{n=0}^{\infty} \frac{(2n+1)}{2} f_n \int_{-1}^1 d\mu_0 P_n(\mu_0) P_m(\mu_0) = f_m^{-L} \quad (3.3)$$

where  $f_m$  are referred to as the *moments of the scattering function*, whereas  $L$  denotes the *order of scattering anisotropy*.

The first moment of the scattering function  $f_s$  corresponds to the average value of the cosine of the scattering angle  $\bar{\mu}_0$ .

Inserting (3.2) in the scattering integral of integro-differential equation (3.1), and considering that  $d\Omega' = d\mu' d\varphi'$ , yield the expression:

$$\begin{aligned} \oint d\Omega' \Sigma_s \phi(\mathbf{r}, \Omega', t) f_s(\Omega' \cdot \Omega) &= \\ &= \oint d\Omega' \Sigma_s \phi(\mathbf{r}, \Omega', t) \sum_{n=0}^{\infty} \frac{(2n+1)}{2} f_n P_n(\Omega' \cdot \Omega) = \\ &= \int_{-1}^1 d\mu' \int_0^{2\pi} d\varphi' \Sigma_s \phi(\mathbf{r}, \Omega', t) \sum_{n=0}^{\infty} \frac{(2n+1)}{2} f_n P_n(\Omega' \cdot \Omega). \end{aligned} \quad (3.4)$$

The complicated dependency upon  $\Omega' \cdot \Omega$  of the Legendre polynomial  $P_n(\Omega' \cdot \Omega)$  appearing in the scattering integral could be rewritten in terms of the components of the directions  $\Omega'$  and  $\Omega$ , respectively  $\mu'$ ,  $\varphi'$ ,  $\mu$  and  $\varphi$ , through the use of the addition theorem:

$$P_n(\Omega' \cdot \Omega) = \sum_{\beta=-n}^n \frac{(n-\beta)!}{(n+\beta)!} P_n^\beta(\mu) P_n^\beta(\mu') e^{i\beta(\varphi-\varphi')} \quad (3.5)$$

where  $P_n^\beta$  are the *associated Legendre functions*, whose definition is:

$$P_n^\beta(\mu) = (\sin \theta)^\beta \frac{d^\beta}{d\mu^\beta} P_n(\mu). \quad (3.6)$$

If  $\beta$  is even, the function  $P_n^\beta$  is a polynomial [25]. The associated functions appear applied for  $n \geq 0$  and  $-n \leq \beta \leq n$ . Then, the following relations may be noted:

$$P_n^0(\mu) = P_n(\mu) \quad (3.7)$$

$$P_n^\beta(\mu) = 0 \quad \text{for } \beta > n. \quad (3.8)$$

Exploiting the addition theorem (3.5), rearranging the terms and by the multiplication and division by  $2\pi$ , the scattering integral appears as:

$$\begin{aligned} \int_{-1}^1 d\mu' \int_0^{2\pi} d\varphi' \Sigma_s \phi(\mathbf{r}, \Omega', t) \sum_{n=0}^{\infty} \frac{2\pi}{2\pi} \frac{(2n+1)}{2} f_n \sum_{\beta=-n}^n \frac{(n-\beta)!}{(n+\beta)!} P_n^\beta(\mu) P_n^\beta(\mu') e^{i\beta(\varphi-\varphi')} &= \\ = \Sigma_s \sum_{n,\beta} \frac{(n-\beta)!}{(n+\beta)!} \frac{2n+1}{4\pi} 2\pi f_n P_n^\beta(\mu) e^{i\beta\varphi} \int_{-1}^1 d\mu' \int_0^{2\pi} d\varphi' \phi(\mathbf{r}, \Omega', t) P_n^\beta(\mu') e^{-i\beta\varphi'} \end{aligned} \quad (3.9)$$

where the following term may be defined as the coefficient  $H_n^\beta$ :

$$\sqrt{\frac{(n-\beta)! 2n+1}{(n+\beta)! 4\pi}} \equiv H_n^\beta. \quad (3.10)$$

The spherical harmonics, representing a complete orthonormal set of functions suitable for the expansion in series of any functions sufficiently smooth on a sphere, are defined as [8]:

$$Y_n^\beta(\Omega) \equiv Y_n^\beta(\mu, \varphi) \equiv H_n^\beta P_n^\beta(\mu) e^{i\beta\varphi} \quad (3.11)$$

where  $Y_n^\beta$  is the spherical harmonic function of degree  $n$  and order  $\beta$ , with  $n = 0, 1, \dots$  and  $-n \leq \beta \leq n$ . The complex conjugate of the spherical harmonic  $Y_n^\beta$  is defined as [8]:

$$Y_n^{\beta*}(\Omega) \equiv (-1)^\beta Y_n^{-\beta} \equiv H_n^\beta P_n^\beta(\mu) e^{-i\beta\varphi} \quad (3.12)$$

The orthogonality property of the spherical harmonics is expressed as:

$$\int Y_n^\beta(\Omega) Y_m^{\alpha*}(\Omega) d\Omega = \delta_{nm} \delta_{\beta\alpha} \quad (3.13)$$

where the notation  $\delta_{ij}$  denotes the Kronecker delta.

The expansion in spherical harmonics of the scattering function appearing in the scattering integral, thus yields:

$$\Sigma_s \sum_n \sum_\beta 2\pi f_n Y_n^\beta(\Omega) \oint d\Omega' \phi(\mathbf{r}, \Omega', t) Y_n^{\beta*}(\Omega') \quad (3.14)$$

The expansion in series in terms of spherical harmonics may be applied also to the neutron flux  $\phi(\mathbf{r}, \Omega, t)$  and to the source term  $S(\mathbf{r}, \Omega, t)$ , respectively:

$$\phi(\mathbf{r}, \Omega, t) \equiv \sum_{n=0}^{\infty} \sum_{\beta=-n}^n \phi_n^\beta(\mathbf{r}, t) Y_n^\beta(\Omega) \quad (3.15)$$

$$S(\mathbf{r}, \Omega, t) \equiv \sum_{n=0}^{\infty} \sum_{\beta=-n}^n S_n^\beta(\mathbf{r}, t) Y_n^\beta(\Omega) \quad (3.16)$$

The coefficients  $\phi_n^\beta(\mathbf{r}, t)$ , defined as the *moments of the angular flux*, and  $S_n^\beta(\mathbf{r}, t)$ , the *moments of the source function*, can be obtained with the same procedure exploited for the moments of the scattering function, by means of the orthogonality properties of spherical

harmonics:

$$\phi_n^\beta(\mathbf{r}, t) \equiv \int \phi(\mathbf{r}, \boldsymbol{\Omega}, t) Y_m^{\alpha*}(\boldsymbol{\Omega}) d\boldsymbol{\Omega} \quad (3.17)$$

$$S_n^\beta(\mathbf{r}, t) \equiv \int S(\mathbf{r}, \boldsymbol{\Omega}, t) Y_m^{\alpha*}(\boldsymbol{\Omega}) d\boldsymbol{\Omega} \quad (3.18)$$

The integral nature of the integro-differential form of the neutron transport equation could be hidden by the reformulation of the scattering integral in terms of moments of the neutron flux. The scattering term as function of angular flux moments reads:

$$\Sigma_s \sum_{n,\beta} \eta_n \phi_n^\beta(\mathbf{r}, t) Y_n^\beta(\boldsymbol{\Omega}) \quad (3.19)$$

where the coefficients  $\eta_n$  are related to the moments of the scattering function through  $\eta_n = 2\pi f_n$ .

Thus, referring to the original formulation of the transport equation (3.1), expressing each member constituting of it in terms of spherical harmonics expansion, the neutron transport equation figures as:

$$\begin{aligned} \frac{1}{v} \frac{\partial}{\partial t} \sum_{n,\beta} \phi_n^\beta(\mathbf{r}, t) Y_n^\beta(\boldsymbol{\Omega}) + \boldsymbol{\Omega} \cdot \nabla \sum_{n,\beta} \phi_n^\beta(\mathbf{r}, t) Y_n^\beta(\boldsymbol{\Omega}) + \Sigma_t \sum_{n,\beta} \phi_n^\beta(\mathbf{r}, t) Y_n^\beta(\boldsymbol{\Omega}) = \\ = \Sigma_s \sum_{n,\beta} \eta_n \phi_n^\beta(\mathbf{r}, t) Y_n^\beta(\boldsymbol{\Omega}) + \sum_{n,\beta} S_n^\beta(\mathbf{r}, t) Y_n^\beta(\boldsymbol{\Omega}). \end{aligned} \quad (3.20)$$

By multiplying each term by  $Y_m^{\alpha*}(\boldsymbol{\Omega})$ , integrating over all the possible directions of motion  $\boldsymbol{\Omega}$  and exploiting the orthogonality property of spherical harmonics functions, the neutron transport equation terms that are immediately obtainable read:

$$\frac{1}{v} \frac{\partial}{\partial t} \sum_{n,\beta} \phi_n^\beta(\mathbf{r}, t) \oint d\boldsymbol{\Omega} Y_n^\beta(\boldsymbol{\Omega}) Y_m^{\alpha*}(\boldsymbol{\Omega}) = \frac{1}{v} \frac{\partial}{\partial t} \phi_m^\alpha(\mathbf{r}, t) \quad (3.21)$$

$$\Sigma_t \sum_{n,\beta} \phi_n^\beta(\mathbf{r}, t) \oint d\boldsymbol{\Omega} Y_n^\beta(\boldsymbol{\Omega}) Y_m^{\alpha*}(\boldsymbol{\Omega}) = \Sigma_t \phi_m^\alpha(\mathbf{r}, t) \quad (3.22)$$

$$\Sigma_s \sum_{n,\beta} \eta_n \phi_n^\beta(\mathbf{r}, t) \oint d\boldsymbol{\Omega} Y_n^\beta(\boldsymbol{\Omega}) Y_m^{\alpha*}(\boldsymbol{\Omega}) = \Sigma_s \eta_m \phi_m^\alpha(\mathbf{r}, t) \quad (3.23)$$

$$\sum_{n,\beta} S_n^\beta(\mathbf{r}, t) \oint d\boldsymbol{\Omega} Y_n^\beta(\boldsymbol{\Omega}) Y_m^{\alpha*}(\boldsymbol{\Omega}) = S_m^\alpha(\mathbf{r}, t) \quad (3.24)$$

In order to obtain the leakage term, the expansion of the operator  $\boldsymbol{\Omega} \cdot \nabla$  is necessary:

$$\boldsymbol{\Omega} \cdot \nabla = \mu \frac{\partial}{\partial x} + \sin \theta \cos \varphi \frac{\partial}{\partial y} + \sin \theta \sin \varphi \frac{\partial}{\partial z} \quad (3.25)$$

In this case, the spherical harmonics expansion of the term involves different orders and degrees with respect to the ones characterizing the remaining members of the neutron transport equation <sup>2</sup>. Conceptually, the result of the expansion in spherical harmonics of the leakage term could be seen as:

$$\nabla \cdot \phi_{\{near(m,\alpha)\}} \quad (3.26)$$

where the notation  $near(m,\alpha)$  denotes the involvement of spherical harmonics of orders near  $\alpha$ , specifically  $\alpha - 1$  and  $\alpha + 1$ , and degrees near  $m$ , respectively  $m - 1$  and  $m + 1$  <sup>3</sup>.

By the combination of the terms (3.21), (3.26), (3.22), (3.23) and (3.24), one obtains:

$$\frac{1}{v} \frac{\partial}{\partial t} \phi_m^\alpha(\mathbf{r}, t) + \nabla \cdot \phi_{near(m,\alpha)}(\mathbf{r}, t) + \Sigma_t \phi_m^\alpha(\mathbf{r}, t) = \Sigma_s \eta_m \phi_m^\alpha(\mathbf{r}, t) + S_m^\alpha(\mathbf{r}, t). \quad (3.27)$$

The resulting system of equations is thus an infinite set of coupled partial differential equations. For practical computation calculations, the expansion in terms of spherical harmonics of the terms of the transport equation have to be truncated at the order  $N$ , obtaining the so-called  $P_N$  approximation.

## 3.2 Spherical harmonics method in plane geometry

In plane geometry the neutron flux depends only on a single Cartesian coordinate, for instance the  $x$  coordinate, and on the single angle  $\theta$  which the neutrons direction of motion  $\Omega$  forms with the adopted Cartesian axis, the  $x$  axis. Defining  $\mu \equiv \cos \theta$ , in symbols the neutron flux figures as:

$$\phi_{1D} = \phi(x, \mu, t) \quad (3.28)$$

Hence, the derivation of the spherical harmonics method applied for a problem with general geometry greatly simplifies in case of a plane geometry model, thanks to the system azimuthal symmetry [8]. In a one dimensional system spherical harmonics reduce to Legendre polynomials, as evident from (3.11) considering  $\beta = 0$ .

Thus, for functions dependent only on the  $x$ -component of the direction  $\Omega$ , spherical harmonics are not necessary and Legendre polynomials are sufficient.

As yet reported, Legendre polynomials  $P_n(\mu)$  constitute an orthogonal set of functions defined for  $-1 \leq \mu \leq 1$ . They represent a suitable type of functions for the expansion in series of sufficiently regular functions of the angular component  $\mu$ . The application of the spherical harmonics method in case of plane geometry is outlined following the same procedure adopted in the more complicated case of general geometry, and the consequent simplifications are properly highlighted when occurring.

<sup>2</sup>The development of this term involves recursion relations [8]

<sup>3</sup>The formula containing all the terms explicitly expressed may be found in [8].

The starting equation of the discussion this section deals with, is the neutron transport equation for a one-dimensional, mono-energetic, time-dependent system. The assumption of isotropic and homogeneous medium is made. The equation in the analyzed case reads:

$$\begin{aligned} \frac{1}{v} \frac{\partial}{\partial t} \phi(x, \mu, t) + \mu \frac{\partial}{\partial x} \phi(x, \mu, t) + \Sigma_t \phi(x, \mu, t) \\ = \oint d\Omega' \Sigma_s \phi(x, \mu', t) f_s(x, \Omega' \cdot \Omega) + S(x, \mu, t). \end{aligned} \quad (3.29)$$

The scattering function  $f_s$ , function of the cosine of the scattering angle only, could be expanded in series of Legendre polynomials as yet developed in (3.2) and here reported again for clarity in the exposition:

$$f_s(x, \Omega' \cdot \Omega) \equiv \sum_{n=0}^{\infty} \frac{(2n+1)}{2} f_n(x) P_n(\Omega' \cdot \Omega).$$

where  $f_n(x)$  are the expansion coefficients obtainable through the use of the orthogonality property of Legendre polynomials. This is stated as:

$$\int_{-1}^1 d\mu P_n(\mu) P_m(\mu) = \frac{2}{2n+1} \delta_{nm} \quad (3.30)$$

where  $\delta_{nm}$  denotes the Kronecker delta. The expansion (3.2) could be inserted in the scattering integral of (3.29) as it follows:

$$\oint d\Omega' \Sigma_s \phi(x, \mu', t) \sum_{n=0}^{\infty} f_n P_n(\Omega' \cdot \Omega). \quad (3.31)$$

The dependency upon  $\Omega' \cdot \Omega$  of the Legendre polynomial  $P_n$  is treated through the use of the addition theorem (3.5) which involves the associated Legendre functions  $P_n^\beta(\mu)$ . In case of functions not depending on the angular coordinate  $\varphi$ ,  $\beta$  is equal to 0 and one obtains for the corresponding associated Legendre polynomials:

$$P_n^\beta(\mu) = P_n(\mu) \quad \text{for } \beta = 0.$$

Considering that  $d\Omega' = d\mu' d\varphi'$ , inserting the addition theorem (3.5) and rearranging the terms, the scattering integral results in:

$$\begin{aligned} & \Sigma_s(x) \sum_{n=0}^{\infty} \sum_{\beta=-n}^n \oint d\Omega' \phi(x, \mu', t) \frac{2n+1}{2} f_n(x) \frac{(n-\beta)!}{(n+\beta)!} P_n^\beta(\mu) P_n^\beta(\mu') e^{i\beta(\varphi-\varphi')} = \\ & \Sigma_s(x) \sum_{n,\beta} \frac{2n+1}{2} \frac{(n-\beta)!}{(n+\beta)!} f_n(x) P_n^\beta(\mu) \int_{-1}^1 d\mu' \phi(x, \mu', t) P_n^\beta(\mu') \int_0^{2\pi} d\varphi' e^{i\beta(\varphi-\varphi')}. \end{aligned} \quad (3.32)$$

With  $\beta = 0$ , the integral over  $d\varphi'$  of the exponential, the unique part of the term depending on  $\varphi'$ , results in  $2\pi$ . Furthermore, taking into account (3.2) and denoting  $2\pi f_s(x) = \eta_n(x)$  one obtains:

$$\Sigma_s(x) \sum_{n=0}^{\infty} \frac{2n+1}{2} \eta_n(x) P_n(\mu) \int_{-1}^1 d\mu' \phi(x, \mu', t) P_n(\mu'). \quad (3.33)$$

Eventually, also the angular flux  $\phi(x, \mu, t)$  and the source term  $S(x, \mu, t)$  may be expressed as series of Legendre polynomials through:

$$\phi(x, \mu, t) = \sum_{n=0}^{\infty} \frac{2n+1}{2} \phi_n(x, t) P_n(\mu) \quad (3.34)$$

$$S(x, \mu, t) = \sum_{n=0}^{\infty} \frac{2n+1}{2} S_n(x, t) P_n(\mu) \quad (3.35)$$

where the expansion coefficients  $\phi_n(x, t)$  and  $S_n(x, t)$  may be computed exploiting the orthogonality properties of the polynomials  $P_n(\mu)$ , respectively:

$$\phi_n(x, t) = \int_{-1}^1 d\mu' \phi(x, \mu', t) P_n(\mu') \quad (3.36)$$

$$S_n(x, t) = \int_{-1}^1 d\mu' S(x, \mu', t) P_n(\mu'). \quad (3.37)$$

One of the advantage of the expansion in terms of Legendre functions for the angular flux concerns the fact that the first two terms of it have a fundamental physical meaning [5]. Let us consider that:

$$\begin{cases} P_n(\mu) = 1 & \text{for } n = 0; \\ P_n(\mu) = \mu & \text{for } n = 1. \end{cases} \quad (3.38)$$

The insertion of these results in the definition of the angular flux moments (3.36) yields, for the first moment:

$$\phi_0(x, t) = \int_{-1}^1 d\mu' \phi(x, \mu', t) \quad (3.39)$$

which represents the *total flux* evaluated at  $x$ . The second moment instead reads:

$$\phi_1(x, t) = \int_{-1}^1 d\mu' \mu' \phi(x, \mu', t) \quad (3.40)$$

which constitutes the current in the  $x$  direction, generally denoted as  $J(x, t)$ . Inserting the angular flux expansion (3.34) and the source expansion (3.35) in the original transport equation (3.29), one obtains:

$$\begin{aligned} & \frac{1}{v} \frac{\partial}{\partial t} \sum_{n=0}^{\infty} \frac{2n+1}{2} \phi_n(x, t) P_n(\mu) \\ & + \mu \frac{\partial}{\partial x} \sum_{n=0}^{\infty} \frac{2n+1}{2} \phi_n(x, t) P_n(\mu) + \Sigma_t(x) \sum_{n=0}^{\infty} \frac{2n+1}{2} \phi_n(x, t) P_n(\mu) \\ & = \Sigma_s(x) \sum_{n=0}^{\infty} \frac{2n+1}{2} \eta_n(x) \phi_n(x, t) P_n(\mu) + \sum_{n=0}^{\infty} \frac{2n+1}{2} S_n(x, t) P_n(\mu). \end{aligned} \quad (3.41)$$

In order to expressed each member of the equation in terms of angular flux moments, the orthogonality of Legendre polynomials is exploited through the multiplication by  $P_m(\mu)$  and the integration over  $d\mu$  of each terms. The ones immediately evaluable are:

$$\frac{1}{v} \frac{\partial}{\partial t} \sum_{n=0}^{\infty} \frac{2n+1}{2} \phi_n(x, t) \int_{-1}^1 P_n(\mu) P_m(\mu) d\mu = \frac{1}{v} \frac{\partial}{\partial t} \phi_m(x, t) \quad (3.42)$$

$$\Sigma_t(x) \sum_{n=0}^{\infty} \frac{2n+1}{2} \phi_n(x, t) \int_{-1}^1 d\mu P_n(\mu) P_m(\mu) = \Sigma_t(x) \phi_m(x, t) \quad (3.43)$$

$$\Sigma_s(x) \sum_{n=0}^{\infty} \frac{2n+1}{2} \eta_n(x) \phi_n(x, t) \int_{-1}^1 d\mu P_n(\mu) P_m(\mu) = \Sigma_s(x) \eta_m(x) \phi_m(x, t) \quad (3.44)$$

$$\sum_{n=0}^{\infty} \frac{2n+1}{2} S_n(x, t) \int_{-1}^1 d\mu P_n(\mu) P_m(\mu) = S_m(x, t). \quad (3.45)$$

The leakage term instead requires in its development the recurrence relation given by:

$$\mu P_n(\mu) = \frac{(n+1)P_{n+1}(\mu) + nP_{n-1}(\mu)}{2n+1}. \quad (3.46)$$

Thus, substituting this relation in the second term of (3.41), with the multiplication by  $P_m(\mu)$  and the integration over  $d\mu$  one obtains:

$$\begin{aligned} \frac{\partial}{\partial x} \sum_{n=0}^{\infty} \frac{2n+1}{2} \phi_n(x, t) \int_{-1}^1 \frac{(n+1)P_{n+1}(\mu) + nP_{n-1}(\mu)}{2n+1} P_m(\mu) \\ = \frac{m}{2m+1} \frac{\partial}{\partial x} \phi_{m-1}(x, t) + \frac{m+1}{2m+1} \frac{\partial}{\partial x} \phi_{m+1}(x, t) \end{aligned} \quad (3.47)$$

Recombining together all the terms previously evaluated, the *spherical harmonics equation*, or *equation for the moments* is finally obtained:

$$\begin{aligned} \frac{1}{v} \frac{\partial}{\partial t} \phi_m(x, t) + \frac{m}{2m+1} \frac{\partial}{\partial x} \phi_{m-1}(x, t) + \frac{m+1}{2m+1} \frac{\partial}{\partial x} \phi_{m+1}(x, t) + \Sigma_t(x) \phi_m(x, t) \\ = \Sigma_s(x) \eta_m \phi_m(x, t) + S_m(x, t) \quad m = 0, 1, 2, \dots \end{aligned} \quad (3.48)$$

The Eq. (3.48) represents an infinite set of coupled partial differential equations, whose infinite number of unknowns is constituted by the moments of the angular flux. Due to its dimension, the exact solution of this system of equations is, of course, not possible [6]. However, its size may be reduced to a finite dimension which allows an approximated solution of the problem, by the introduction of a truncation in the angular flux expansion, based upon the assumption:

$$\phi_{N+1}(x, t) = 0 \quad (3.49)$$

which lead to the  $P_N$  approximation. Finally, the time-independent form of the equation for the moments of the angular flux in plane geometry consists in:

$$\begin{aligned} \frac{m}{2m+1} \frac{d}{dx} \phi_{m-1}(x) + \frac{m+1}{2m+1} \frac{d}{dx} \phi_{m+1}(x) + \Sigma_t(x) \phi_m(x) \\ = \Sigma_s(x) \eta_m \phi_m(x) + S_m(x) \quad m = 0, 1, 2, \dots, N. \end{aligned} \quad (3.50)$$

### 3.2.1 Boundary Conditions

Considering an infinite slab geometry, vacuum boundary conditions are developed to be imposed to the set of first-order differential equations deriving from the application of the  $P_N$  approximation to the one-dimensional, steady-state, mono-energetic form of the neutron transport equation, as presented in Sect. 3.2. Due to the approximate nature of the developed model, also the boundary conditions may be not rigorously satisfied at the boundary [8]. Concerning the vacuum boundary conditions, different set of conditions may be exploited and in particular, in the present work Mark and Marshak boundary conditions are taken into consideration.

The analytical expression of the free-surface boundary conditions as they have been presented in Sect. 1.1.2, it is here declined for the case of plane geometry:

$$\begin{aligned}\phi(0, \mu) &= 0 & \mu < 0 \\ \phi(a, \mu) &= 0 & \mu > 0\end{aligned}\tag{3.51}$$

where the boundaries have been located at the generic positions  $x = 0$  and  $x = a$ . Thus, this type of conditions corresponds to the statement of a neutron *incoming* flux equals to zero, as from vacuum nothing can come.

### Mark boundary conditions

In Mark boundary conditions physical interpretation, the proposed conditions are equivalent to those for the case in which vacuum is replaced by a purely absorbing medium [5]. The conditions to be imposed are:

$$\begin{aligned}\phi(0, \mu_i) &= 0 & \mu_i = 1, 2, 3, \dots, \frac{N+1}{2} \\ \phi(a, -\mu_i) &= 0 & \mu_i = 1, 2, 3, \dots, \frac{N+1}{2}\end{aligned}\tag{3.52}$$

where, being  $N + 1$  the number of first-order differential equations expected by the  $P_N$  approximation, as many conditions must be provided. Thus, assuming  $N$  as odd, even though in the numerical computation also even orders of accuracy are treated,  $(N+1)/2$  positive values  $\mu_i$  are chosen for the slab left-boundary, whereas the corresponding negative directions, identified by  $-\mu_i$ , are individuated for the application to the right-boundary. The positive  $\mu_i$  consists in the positive roots of equation [5]:

$$P_{N+1}(\mu) = 0,\tag{3.53}$$

where  $P_{N+1}(\mu)$  represents the Legendre polynomial of order  $N + 1$ .

### Marshak boundary conditions

The approach suggested by Marshak for the free-surface boundary conditions provides for the verification of the following relations at the boundary:

$$\begin{aligned}\int_0^1 \phi(0, \mu) P_m(\mu) d\mu &= 0 \\ \int_{-1}^0 \phi(a, \mu) P_m(\mu) d\mu &= 0 & m = 1, 3, 5, \dots, \frac{(N+1)}{2}\end{aligned}\tag{3.54}$$

The result consists in  $(N + 1)/2$  equations at each boundary with all the moments of the flux coupled. Furthermore, solving such relations (3.54) for  $m = 1$  leads to set the conditions of partial positive and partial negative incoming current respectively, equal to zero at each boundary. Indeed:

$$\begin{aligned} \int_0^1 \mu \phi(0, \mu) d\mu &= J_+(0) = 0 \\ \int_{-1}^0 \mu \phi(a, \mu) d\mu &= J_-(a) = 0. \end{aligned} \tag{3.55}$$

Thus, these relations express the zero incoming current condition, generally exploited in diffusion theory [5].

Moreover, by the application of the  $P_1$  approximation to a slab geometry reactor with Marshak boundary conditions, it may be noted that the extrapolation distance which may be derived is coincident with the one from diffusion theory, hence representing a better approximation with respect to the one assessed with Mark boundary conditions. Such a consideration may suggest an higher accuracy of Marshak conditions, nevertheless even Mark conditions are commonly exploited [5].

### 3.2.2 The $P_1$ and $P_3$ system of equations

By way of example, the system of differential equations characterizing the  $P_1$  and  $P_3$  approximation are here reported for the case of a slab geometry with isotropic scattering and isotropic source, in a mono-energetic and time-independent system.

#### The $P_1$ approximation

In the  $P_1$  approximation the expression of the angular flux  $\phi$  reads:

$$\phi(x, \mu) \approx \sum_{n=0}^1 \frac{2n+1}{2} \phi_n(x) P_n(\mu) = \frac{1}{2} \phi_0(x) + \frac{3}{2} \mu \phi_1(x) \tag{3.56}$$

where, recalling the physical meaning of the first and second order moment of the angular flux,  $\phi_0(x)$  represents the total flux  $\Phi(x)$ , whereas  $\phi_1(x)$  is the neutron current  $J(x)$ . Further, by this expression it may be noted that the angular flux in the  $P_1$  approximation is linearly dependent on the cosine of the direction  $\mu$ .

Then, referring to the time-independent version of the set of equations (3.48), the system characteristic of the  $P_1$  approximation deriving from it consists in:

$$\begin{aligned} \frac{d\phi_1(x)}{dx} + \Sigma_t \phi_0(x) &= \eta_0 \Sigma_s \phi_0(x) + S_0(x) \quad \mathbf{n=0} \\ \frac{1}{3} \frac{d\phi_0(x)}{dx} + \frac{2}{3} \frac{d\phi_2(x)}{dx} + \Sigma_t \phi_1(x) &= \eta_1 \Sigma_s \phi_1(x) + S_1(x) \quad \mathbf{n=1} \end{aligned}$$

to which the assumption that  $\phi_2(x) = 0$  is imposed as a closure requirement for the set of differential equations. Then, considering the appearing moments of the scattering function, respectively  $\eta_0$  and  $\eta_1$ , it may be noted that:

$$\eta_0 = \int_{-1}^1 \eta(\mu_0) P_0(\mu_0) d\mu_0 = 1 \quad (3.57)$$

$$\eta_1 = \int_{-1}^1 \eta(\mu_0) P_1(\mu_0) d\mu_0 = 0 \quad \text{if scattering is isotropic.} \quad (3.58)$$

Lastly, the assumption of an isotropic source  $S(x, \mu)$  yields:

$$S_1(x) = \int_{-1}^1 S(x) P_1(\mu) d\mu = 0. \quad (3.59)$$

Thus, the system (3.2.2) may be rewritten as:

$$\frac{d\phi_1(x)}{dx} + \Sigma_t \phi_0(x) = \Sigma_s \phi_0(x) + S_0(x) \quad (3.60)$$

$$\frac{1}{3} \frac{d\phi_0(x)}{dx} + \Sigma_t \phi_1(x) = 0 \quad (3.61)$$

to which appropriate boundary conditions have to be imposed.

### The $P_3$ approximation

In the  $P_3$  approximation, being  $N = 3$ , the angular flux is expressed through:

$$\begin{aligned} \phi(x, \mu) &\approx \sum_{n=0}^3 \frac{2n+1}{2} \phi_n(x) P_n(\mu) \\ &= \frac{1}{2} P_0(\mu) \phi_0(x) + \frac{3}{2} P_1(\mu) \phi_1(x) + \frac{5}{2} P_2(\mu) \phi_2(x) + \frac{7}{2} P_3(\mu) \phi_3(x). \end{aligned} \quad (3.62)$$

As for the  $P_1$  approximation, the time-independent version of the equation for the moments (3.48) is reduced to the system of differential equations characterized by  $0 \leq n \leq 3$ .

Thus, based on the assumption that  $\phi_4(x) = 0$ , the system reads:

$$\frac{d\phi_1(x)}{dx} + \Sigma_t \phi_0(x) = \eta_0 \Sigma_s \phi_0(x) + S_0(x) \quad (3.63)$$

$$\frac{1}{3} \frac{d\phi_0(x)}{dx} + \frac{2}{3} \frac{d\phi_2(x)}{dx} + \Sigma_t \phi_1(x) = 0 \quad (3.64)$$

$$\frac{2}{5} \frac{d\phi_1(x)}{dx} + \frac{3}{5} \frac{d\phi_3(x)}{dx} + \Sigma_t \phi_2(x) = 0 \quad (3.65)$$

$$\frac{3}{7} \frac{d\phi_2(x)}{dx} + \Sigma_t \phi_3(x) = 0 \quad (3.66)$$

where, as a consequence of the isotropic assumption for the scattering and the source term, the scattering function moments  $\eta_n$  and the source function ones  $S_n$  with  $n \geq 0$  have been neglected. Finally, appropriate boundary conditions have to be applied to solve the system of equations.

### 3.2.3 Application to the eigenvalue forms of the neutron transport equation

This section is devoted to the introduction of the neutron transport models basis of the study conducted in the present work. The different eigenvalue forms of the neutron transport equation, associated to the four different eigenvalue types presented in the previous chapter 2, have been solved in their one-dimensional, monoenergetic and time-independent model by means of the  $P_N$  approximation.

The steady-state, mono-energetic model of the neutron transport equation for a plane geometry, declined in its possible eigenvalue forms, has been yet reported in Sect. (??). Here, the associated equations for the moments of the angular flux, results of the application of the  $P_N$  approximation, are listed. The assumption of homogeneous medium and isotropic scattering is made. The equations are all derived following the method exposed in Sect. ?? for the general model of plane geometry.

#### Moments equation with $k$ eigenvalue

The  $k$ -eigenvalue form of the equation for the moments of the angular flux for a steady-state, monoenergetic, one-dimensional system yields:

$$\begin{aligned} \frac{m+1}{2m+1} \frac{d}{dx} \phi_{m+1}(x) + \frac{m}{2m+1} \frac{d}{dx} \phi_{m-1}(x) + \Sigma_t \phi_m(x) \\ = \frac{\Sigma_s}{\phi_0}(x) \delta_{m0} + \frac{1}{k} \frac{\nu \Sigma_f}{\phi_0}(x) \delta_{m0} \quad m = 0, 1, 2, \dots, N \end{aligned} \quad (3.67)$$

where  $\delta_{m0}$  denotes the Kroenecker delta. Thus, the neutron transport equation appears in its homogeous version with isotropic scattering. As a consequence of the isotropic assumption for the scattering interactions, generally feasible also for fission phenomenon, both these terms appear only in relation to the first-order moment.

The  $k$  eigenvalue is then inserted as a modification of the fission source term, as characteristic for this type of eigenvalue.

By way of example, the  $P_1$  system of equations for the  $k$ -eigenvalue form of the transport equation is reported:

$$\begin{cases} \frac{d\phi_1(x)}{dx} + \Sigma_t\phi_0(x) = \frac{\Sigma_s}{\phi_0}(x) + \frac{1}{k}\frac{\nu\Sigma_f}{\phi_0}(x) & m = 0 \\ \frac{1}{3}\frac{d\phi_0(x)}{dx} + \Sigma_t\phi_0(x) = 0 & m = 1 \end{cases} \quad (3.68)$$

### Moments equation with $\alpha$ eigenvalue

The  $\alpha$ -eigenvalue form of the equation for the moments of the angular flux reads:

$$\frac{m+1}{2m+1}\frac{d}{dx}\phi_{m+1}(x) + \frac{m}{2m+1}\frac{d}{dx}\phi_{m-1}(x) + (\Sigma_t + \frac{\alpha}{v})\phi_m(x) = \frac{c\Sigma_t}{\phi_0}(x)\delta_{m0} \quad m = 0, 1, 2, \dots, N \quad (3.69)$$

where the scattering and the fission terms are gathered in unique member constituting of the right-hand side of the equation, by means of the introduction of the criticality parameter  $c$ .

The  $\alpha$  eigenvalue is introduced as an increment to the total cross section appearing in the left-hand side of Eq. (3.69).

As reported for the previous eigenvalue type, the  $P_1$  system of equations is developed for the  $\alpha$  eigenvalue case:

$$\begin{cases} \frac{d\phi_1(x)}{dx} + (\Sigma_t + \frac{\alpha}{v})\phi_0(x) = \frac{c\Sigma_t}{\phi_0}(x) & m = 0 \\ \frac{1}{3}\frac{d\phi_0(x)}{dx} + (\Sigma_t + \frac{\alpha}{v})\phi_0(x) = 0 & m = 1. \end{cases} \quad (3.70)$$

### Moments equation with $\gamma$ eigenvalue

The neutron transport equation in the  $\gamma$  eigenvalue version reads:

$$\frac{m+1}{2m+1}\frac{d}{dx}\phi_{m+1}(x) + \frac{m}{2m+1}\frac{d}{dx}\phi_{m-1}(x) + \Sigma_t\phi_m(x) = \frac{1}{\gamma}\frac{c\Sigma_t}{\phi_0}(x)\delta_{m0} \quad m = 0, 1, 2, \dots, N \quad (3.71)$$

where the eigenvalue originally suggested by Davison is inserted as a modification of the collisional part constituted by both the scattering and the fission contribution.

The first-order approximation for the  $\gamma$  eigenvalue case of the neutron transport equation yields:

$$\begin{cases} \frac{d\phi_1(x)}{dx} + \Sigma_t \phi_0(x) = \frac{1}{\gamma} \frac{c\Sigma_t}{\phi_0}(x) & m = 0 \\ \frac{1}{3} \frac{d\phi_0(x)}{dx} + \Sigma_t \phi_0(x) = 0 & m = 1. \end{cases} \quad (3.72)$$

### Moments equation with $\delta$ eigenvalue

As a last instance, the  $\delta$  eigenvalue version of the neutron transport equation is reported:

$$\frac{m+1}{2m+1} \frac{d}{dx} \phi_{m+1}(x) + \frac{m}{2m+1} \frac{d}{dx} \phi_{m-1}(x) + \frac{1}{\delta} \Sigma_t \phi_m(x) = \frac{1}{\delta} \frac{c\Sigma_t}{\phi_0}(x) \delta_{m0} \quad m = 0, 1, 2, \dots, N. \quad (3.73)$$

The  $P_1$  for the  $\delta$  eigenvalue case consists in:

$$\begin{cases} \frac{d\phi_1(x)}{dx} + \frac{1}{\delta} \Sigma_t \phi_0(x) = \frac{1}{\delta} \frac{c\Sigma_t}{2} \phi_0(x) & m = 0 \\ \frac{1}{3} \frac{d\phi_0(x)}{dx} + \Sigma_t \phi_0(x) = 0 & m = 1. \end{cases} \quad (3.74)$$

# Chapter 4

## Numerical code implementation

Neutron transport computations comprise two possible approaches for the prediction of the neutron distribution in phase space: the deterministic approach, which foresees the discretization of the variables on which the neutron transport equation depends upon, and the stochastic method, commonly referred to as the Monte Carlo method, which consists in a numerical method involving statistical theory. The Monte Carlo method is indeed able to simulate the random movement of a particle in a medium taking advantage of the probability density distributions characteristic of the phenomenon. By performing the simulation a large number of times the method is then able to mimic physical experiments from which is possible to retrieve averaged quantities of interest. Deterministic methods start instead from the mathematical equations describing the physical phenomenon under investigation, the neutron transport equation in this case, to which discretization of the phase space variables is applied in order to accomplish an approximate solution by means of numerical calculations [4].

In the present work a deterministic method has been adopted, starting from the integro-differential neutron transport equation in the  $P_N$  approximation, to evaluate the eigenvalues and the associated eigenfunctions of its eigenvalue formalisms, in the simplified case of a mono-energetic, time-independent model for an infinite-slab reactor core.

### 4.1 On the necessity of a staggered mesh in the spatial discretization

The following section is devoted to the demonstration that an equivalence between the diffusion equation for a one-dimensional, steady-state, mono-energetic model and the  $P_1$  approximation in the continuous world is not straightforwardly verified passing to discrete. In fact although in continuous is simple to demonstrate how the  $P_1$  approximation under relative general assumptions corresponds to the diffusion approximation, the same procedure

developed for discretized models reveal some tricky aspects. Hence, here it is reported the logical path that has been followed for the implementation of the computational code which has been developed for the solution of the  $P_N$  model applied to the different eigenvalue forms of the neutron transport equation, to which the entire work is devoted.

Starting from the diffusion approximation for a one-dimensional, mono-energetic and steady-state model, in the case of non-multiplying medium, the equivalence between this model and the  $P_1$  approximation is derived. The diffusion equation for the considered case thus reads:

$$-\frac{d}{dx}D(x)\frac{d}{dx}\Phi(x) + \Sigma_a(x)\Phi(x) = S(x) \quad (4.1)$$

where  $D(x)$  represents the *diffusion coefficient*, peculiar of the governing equation of the migration of particles in medium [12].

The differential equations characteristic of the  $P_1$  approximation are instead derived starting from the equation for the moments of the angular flux in case of plane geometry which is, as yet reported in Sect.3.2 for the time-dependent case:

$$\frac{m}{2m+1}\frac{d}{dx}\phi_{m+1}(x) + \frac{m+1}{2m+1}\frac{d}{dx}\phi_{m-1}(x) + \Sigma_t(x)\phi_m(x) = \eta_m \Sigma_s(x)\phi_m(x) + S_m(x) \quad m = 0, \dots, N$$

where  $\Sigma$  denotes the total macroscopic cross section  $\Sigma_t$ . The relative equations, respectively corresponding to  $m = 0$  and  $m = 1$ , are:

$$\begin{aligned} \frac{d\phi_1(x)}{dx} + \Sigma(x)\phi_0(x) &= \eta_0 \Sigma_s(x)\phi_0(x) + S_0(x) \\ \frac{1}{3}\frac{d\phi_0(x)}{dx} + \Sigma(x)\phi_1(x) &= \eta_1 \Sigma_s(x)\phi_1(x) + S_1(x) \end{aligned} \quad (4.2)$$

to which the closure requirement of the  $P_1$  approximation,  $\phi_2(x) = 0$ , is applied. Focusing on the former of the two equations presented, and recalling the physical significance attributed to the zeroth and first order moment of the angular flux, the equation can be rewritten as:

$$\frac{dJ(x)}{dx} + \Sigma_a(x)\Phi(x) = S_0(x) \quad (4.3)$$

where  $\phi_0(x)$ , which constitutes the total flux, is denoted with the usual notation  $\Phi(x)$  whereas  $\phi_1(x)$ , the current, is denoted as  $J(x)$ . The equation thus represents a *continuity equation*, which combined with the Fick's law of diffusion theory, leads to the diffusion equation. Therefore, an isotropic neutron emission is assumed, leading to  $S_1(x) = 0$ , and an isotropic scattering is stated through  $\eta_1 = 0$ . As a consequence, the right-hand side of the equation for  $m = 1$  becomes null and the equation is rewritten, with the same notation introduced for the

former one, as:

$$\frac{1}{3} \frac{d\Phi(x)}{dx} + \Sigma(x) J(x) = 0. \quad (4.4)$$

From this equation, the Fick's law of diffusion is merely derived as:

$$J(x) = -\frac{1}{3\Sigma(x)} \frac{d\Phi(x)}{dx} = -D(x) \frac{d\Phi(x)}{dx}. \quad (4.5)$$

Lastly, substituting this result (4.5) in the continuity equation (4.3), the diffusion equation is obtained:

$$-\frac{d}{dx} D(x) \frac{d}{dx} \Phi(x) + \Sigma_a(x) \Phi(x) = S(x). \quad (4.6)$$

Thus, an equivalence between the two models under the assumption of isotropic emission, may be easily derived in continuous. Passing to discrete, the equivalence between the linear system of equations corresponding to the spatial discretization of the one-dimensional diffusion equation, and the result of the combination of the two differential equations involved by the  $P_1$  approximation properly discretized over the space coordinate, is not immediately clear.

Supposing a infinite-slab domain of width  $a$  in the  $x$ -coordinate, the diffusion equation (4.1) should be satisfied at any generic location  $x_i$  in the interval  $(0, a)$ , yielding:

$$-D \frac{d^2\Phi(x_i)}{dx^2} + \Sigma_a \Phi(x_i) = S(x_i) \quad \text{with } i = 2, \dots, N-1 \quad (4.7)$$

where the left-side boundary corresponding to the position  $x = 0$  is supposed individuated by the node  $i = 1$ , whereas the right-side boundary at  $x = a$  is denoted by the node  $i = N$ . Diffusion vacuum boundary conditions are then assumed at the slab boundaries, stated as:

$$\Phi(x_1) = 0, \quad \Phi(x_N) = 0. \quad (4.8)$$

For simplicity, the hypothesis of homogeneous medium, and hence, diffusion length and cross-sections independent of space, have been introduced.

The set of equations (4.7) is then approximated at any nodes  $x_i$  of the discretized domain by means of the *centered finite difference* formula. The formula is applied in sequence by considering the second-order derivative of the total flux evaluated at  $x_i$  as a first-order derivative of the first derivative of the total flux, centered in the  $x_i$  node and involving two neighboring nodes distant  $\Delta x/2$  from  $x_i$ , with  $\Delta x$  the constant space discretization step of

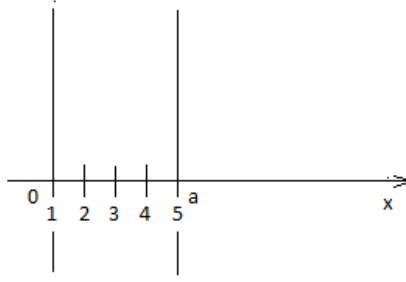


Figure 4.1: Spatial discretization slab in an example with 5 nodes.

the considered domain [16]. The procedure thus reads:

$$\begin{aligned} \frac{d^2}{dx^2}\Phi(x_i) &= \frac{d}{dx}\left(\frac{d}{dx}\Phi x_i\right) \approx \frac{\frac{d\Phi}{dx}\big|_{i+1/2} - \frac{d\Phi}{dx}\big|_{i-1/2}}{2\frac{\Delta x}{2}} \\ &= \frac{\Phi_{i+1} - 2\Phi_i + \Phi_{i-1}}{\Delta x^2} \end{aligned}$$

where the abbreviated notation  $\Phi_i$  denotes  $\Phi(x_i)$ .

The system of algebraic equations result of the spatial discretization of the diffusion equation hence is:

$$-D \frac{\Phi_{i+1} - 2\Phi_i + \Phi_{i-1}}{\Delta x^2} + \Sigma_a \Phi_i = S_i \quad \text{with } i = 2, \dots, N-1 \quad (4.9)$$

with Eq. (4.8) as boundary conditions imposed at  $x_1$  and  $x_N$ . As an example, the resulting system of equations for a slab domain discretized by a total of 5 nodes yields (see Fig. 4.1:

$$\begin{aligned} -D \frac{\Phi_3 - 2\Phi_2 + \Phi_1}{\Delta x^2} + \Sigma_a \Phi_2 &= S_2 & i = 2 \\ -D \frac{\Phi_4 - 2\Phi_3 + \Phi_2}{\Delta x^2} + \Sigma_a \Phi_3 &= S_3 & i = 3 \\ -D \frac{\Phi_5 - 2\Phi_4 + \Phi_3}{\Delta x^2} + \Sigma_a \Phi_4 &= S_4 & i = 4 \end{aligned} \quad (4.10)$$

setting aside the equations at the boundary nodes. Once the discretization of the diffusion equation has been obtained, the  $P_1$  differential equations are taken into account. The purpose is to apply the same procedure adopted in continuous to reach diffusion starting from  $P_1$ , but with discretized equations. Thus, the centered difference formula exploited for the diffusion laplacian approximation is here applied to the first derivatives involved in the differential equations of  $P_1$ , with a space discretization step equal to  $\Delta x/2$ . The approximation of the

equations evaluated at the generic location  $x_i$  then reads:

$$\begin{aligned} \frac{J_{i+1/2} - J_{i-1/2}}{\Delta x/2} + \Sigma_a \Phi_i &= S_i \\ \frac{1}{3} \frac{\Phi_{i+1/2} - \Phi_{i-1/2}}{\Delta x/2} + \Sigma J_i &= 0 \end{aligned} \quad \text{with } i = 2, \dots, N-1 \quad (4.11)$$

where the same notation previously introduced is exploited to indicate the unknowns. The use of a *collocated* grid for the two equations of  $P_1$ , which are coupled equations, implies a discrepancy between the unknown referred to the current appearing in the second equation at the node  $x_i$  and the ones appearing in the first equation of the system (4.11), which are the current at the nodes  $x_{i+1/2}$  and  $x_{i-1/2}$ , respectively. This is due to the fact that the collocated derivative of the current in the latter equation, and the one of the total flux in the corresponding former equation ignores the quantity at  $x_i$  involved by the specific derivative.

As a consequence, the substitution of the discretized Fick's law derived from the second equation of the system (4.11) in the corresponding discrete continuity equation, constituted by the first discretized equation, can not be carried out. If instead a different spatial discretization step is chosen in such a way that half-integer nodes are not involved in the approximation of derivatives of  $P_1$ , making possible in discrete the substitution adopted in continuous, the resulting discretized diffusion equation system is still different from the one obtained at the beginning of this description (4.10). Indeed, assuming in this case a spatial discretization step equal to  $\Delta x$  instead of  $\Delta x/2$ , and applying the centered difference formula, the system obtained in reference to the generic point  $x_i$  for the  $P_1$  approximation is:

$$\begin{aligned} \frac{J_{i+1} - J_{i-1}}{\Delta x} + \Sigma_a \Phi_i &= S_i \\ \frac{1}{3} \frac{\Phi_{i+1} - \Phi_{i-1}}{\Delta x} + \Sigma J_i &= 0 \end{aligned} \quad \text{with } i = 2, \dots, N-1 \quad (4.12)$$

which, written explicitly for the originally defined 3 internal nodes of the slab mesh yields:

$$\frac{J_3 - J_1}{\Delta x/2} + \Sigma_a \Phi_2 = S_2 \quad (4.13a)$$

$$\frac{1}{3} \frac{\Phi_3 - \Phi_1}{\Delta x/2} + \Sigma J_2 = 0 \quad (4.13b)$$

$$\frac{J_4 - J_2}{\Delta x/2} + \Sigma_a \Phi_3 = S_3 \quad (4.14a)$$

$$\frac{1}{3} \frac{\Phi_4 - \Phi_2}{\Delta x/2} + \Sigma J_3 = 0 \quad (4.14b)$$

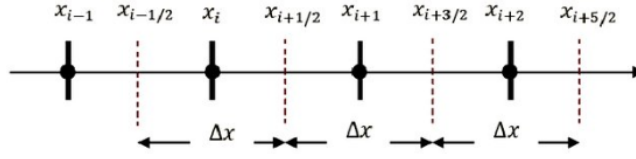


Figure 4.2: Staggered grid for the spatial discretization of the  $P_1$  approximations system of equations [26].

$$\frac{J_5 - J_3}{\Delta x/2} + \Sigma_a \Phi_4 = S_4 \quad (4.15a)$$

$$\frac{1}{3} \frac{\Phi_5 - \Phi_3}{\Delta x/2} + \Sigma J_4 = 0. \quad (4.15b)$$

Deriving the expression for  $J_2$  and  $J_4$  respectively from Eqs. (4.13b) and (4.15b), and substituting the results in Eq. (4.14b), it yields a diffusion equation which must be satisfied at the node  $i = 3$ , reading:

$$-D \frac{\Phi_5 - 2\Phi_3 + \Phi_1}{2\Delta x^2} + \Sigma_a \Phi_3 = S_3 \quad i = 3 \quad (4.16)$$

where it is made evident the fact that with a collocated grid for the spatial discretization of  $P_1$  equations, the resulting laplacian of the total flux in the obtained diffusion equation does not involved the immediate neighbors of the total flux at  $x_i$ , where in this case  $i = 3$ , as an example. This collocated discretization scheme leads to oscillations in the solution of the  $P_1$  system of equations.

A solution to address this problem consists in a different choice about the spatial grid adopted in reference to the discretization of the two equations involved by  $P_1$ . In particular, a staggered grid is exploited, shown in Fig. 4.2. The overall spatial staggered grid adopted for  $P_1$  system discretization is reported in the figure below.

The spatial step between the nodes is constant and equal to  $\Delta x/2$ . The first-order derivative involving the current in the first equation of  $P_1$  is approximated by means of the centered finite difference formula, centered in the integer nodes, yielding:

$$\left. \frac{dJ}{dx} \right|_i \approx \frac{J_{i+\frac{1}{2}} - J_{i-\frac{1}{2}}}{2 \frac{\Delta x}{2}} = \frac{J_{i+\frac{1}{2}} - J_{i-\frac{1}{2}}}{\Delta x} \quad (4.17)$$

The resulting systems of algebraic equations written at the generic integer node  $i$  of the first equation of  $P_1$  system is, exploiting (4.17):

$$\frac{J_{i+\frac{1}{2}} - J_{i-\frac{1}{2}}}{\Delta x} + \Sigma_a \Phi_i = S_i \quad \text{with } i = 2, \dots, N - 1. \quad (4.18)$$

The first-order derivative involving the total flux appearing in the second equation of  $P_1$  is approximated by means of a centered finite difference, centered in the half-integer nodes of the grid, yielding:

$$\begin{aligned} \frac{d\Phi}{dx} \Big|_{i+\frac{1}{2}} &\approx \frac{\Phi_i - \Phi_{i-1}}{2 \frac{\Delta x}{2}} \\ &= \frac{\Phi_i - \Phi_{i-1}}{\Delta x} \end{aligned} \quad (4.19)$$

which substituted in the second equation of  $P_1$  leads to the discretized system of equations:

$$\frac{1}{3} \frac{\Phi_i - \Phi_{i-1}}{\Delta x/2} + \Sigma J_{i+\frac{1}{2}} = 0 \quad \text{with } i = 2, \dots, N - 1. \quad (4.20)$$

As previously done for the diffusion equation, considering a slab domain described by a total of 5 integer nodes, Eq. (4.18) may be written explicitly for the 3 internal nodes as:

$$\frac{J_{2+\frac{1}{2}} - J_{1+\frac{1}{2}}}{\Delta x} + \Sigma_a \Phi_2 = S_2 \quad i = 2 \quad (4.21a)$$

$$\frac{J_{3+\frac{1}{2}} - J_{2+\frac{1}{2}}}{\Delta x} + \Sigma_a \Phi_3 = S_3 \quad i = 3 \quad (4.21b)$$

$$\frac{J_{4+\frac{1}{2}} - J_{3+\frac{1}{2}}}{\Delta x} + \Sigma_a \Phi_4 = S_4 \quad i = 4 \quad (4.21c)$$

where, as for diffusion equation, the discussion concerning the imposition of the boundary conditions is set aside for the moment and addressed later in this section.

The same procedure is then performed for the second equation of  $P_1$  system which, written explicitly becomes:

$$\begin{aligned} \frac{1}{3} \frac{\Phi_3 - \Phi_2}{\Delta x/2} + \Sigma J_{2+\frac{1}{2}} &= 0 & i = 2 + \frac{1}{2} \\ \frac{1}{3} \frac{\Phi_4 - \Phi_3}{\Delta x/2} + \Sigma J_{3+\frac{1}{2}} &= 0 & i = 3 + \frac{1}{2} \\ \frac{1}{3} \frac{\Phi_5 - \Phi_4}{\Delta x/2} + \Sigma J_{4+\frac{1}{2}} &= 0 & i = 4 + \frac{1}{2} \end{aligned} \quad (4.22)$$

Therefore, the discrete diffusion Fick's law written for the internal half-integer nodes is derived as:

$$\begin{aligned}
J_{2+\frac{1}{2}} &= -D \frac{\Phi_3 - \Phi_2}{\Delta x/2} & i &= 2 + \frac{1}{2} \\
J_{3+\frac{1}{2}} &= -D \frac{\Phi_4 - \Phi_3}{\Delta x/2} & i &= 3 + \frac{1}{2} \\
J_{4+\frac{1}{2}} &= -D \frac{\Phi_5 - \Phi_4}{\Delta x/2} & i &= 4 + \frac{1}{2}
\end{aligned} \tag{4.23}$$

which, substituted in the system of equations constituted by Eqs. (4.21), leads exactly to the algebraic system of equations outcome of the approximation of the diffusion equation by means of the centered finite difference formula based on an spatial grid in which all nodes are equidistant of an extent  $\Delta x$  one from the subsequent. The result of the substitutions is indeed:

$$\begin{aligned}
-D \frac{\Phi_3 - 2\Phi_2 + \Phi_1}{\Delta x^2} + \Sigma_a \Phi_2 &= S_2 & i &= 2 \\
-D \frac{\Phi_4 - 2\Phi_3 + \Phi_2}{\Delta x^2} + \Sigma_a \Phi_3 &= S_3 & i &= 3 \\
-D \frac{\Phi_5 - 2\Phi_4 + \Phi_3}{\Delta x^2} + \Sigma_a \Phi_4 &= S_4 & i &= 4
\end{aligned} \tag{4.24}$$

## 4.2 Spatial staggered grid for higher-order $P_N$ approximations

The centered finite difference formula seemed to be the more suitable approximation formula to be applied to the type of problem addressed in the entire work. In fact, the transport of neutrons through a homogeneous medium is studied by means of a plane geometry model, referred to a symmetric infinite-slab domain, in the case of a multiplying material in which fission constitutes the unique neutron source term. Being both the fission emission and the scattering one assumed as isotropic, no favored directions of motion are supposed to exist with respect to neutron motion through the medium. For this reason, a symmetric finite difference formula it seemed the more suitable choice for the discretization of the  $P_N$  approximation system of equations. Furthermore, from the standpoint of the model solution accuracy, this specific approximation of the derivative of a function is second-order accurate, representing a further advantage.

The necessity of a staggered spatial grid has been proved for the case of the  $P_1$  approximation. The same demonstration may be performed also for the case of higher orders of accuracy of the  $P_N$  approximation and in particular, it is here carried out for the case of the  $P_2$  approximation, in order to verified that the staggered grid adopted for  $P_1$  in the previous section is suitable also for higher approximations, both even and odd ones.

The same procedure exploited for the case of the diffusion equation and the  $P_1$  approximation is performed for the case of  $P_2$  approximation, which is still diffusion except for a slightly modified diffusion coefficient. Firstly, the modified diffusion equation referred to  $P_2$  is found starting from the  $P_N$  characteristic system of differential equation, and then, passing to discrete, the effectiveness of a staggered grid is proved with respect to the discretized diffusion equation of  $P_2$ .

Therefore, the  $P_2$  system of first-order differential equations is obtained starting from the equation for the moments of the angular flux written for  $m \leq 2$ , which yields:

$$\begin{aligned} \frac{d\phi_1(x)}{dx} + \Sigma \phi_0(x) &= \eta_0 \Sigma_s \phi_0(x) + S_0(x) \\ \frac{1}{3} \frac{d\phi_0(x)}{dx} + \frac{2}{3} \frac{d\phi_2(x)}{dx} + \Sigma \phi_1 &= \eta_1 \Sigma_s(x) \phi_1(x) + S_1(x) \\ \frac{2}{5} \frac{d\phi_1(x)}{dx} + \Sigma \phi_2(x) &= \eta_2 \Sigma_s \phi_2(x) + S_2(x) \end{aligned} \quad (4.25)$$

to which the closure requirement of  $P_3$  approximation,  $\phi_3(x) = 0$  is imposed.

To achieve diffusion, the first step consists in assuming isotropic scattering, meaning  $\eta_m = 0$  with  $m \geq 1$ , and isotropic source, that is  $S_m = 0$  with  $m \geq 1$ . Recalling that  $\Sigma - \Sigma_s = \Sigma_a$ , the system may be rewritten as:

$$\frac{d\phi_1(x)}{dx} + \Sigma_a \phi_0(x) = S_0(x) \quad (4.26a)$$

$$\frac{1}{3} \frac{d\phi_0(x)}{dx} + \frac{2}{3} \frac{d\phi_2(x)}{dx} + \Sigma \phi_1(x) = 0 \quad (4.26b)$$

$$\frac{2}{5} \frac{d\phi_1(x)}{dx} + \Sigma \phi_2(x) = 0. \quad (4.26c)$$

Thus, from Eq. (4.26c) the third-order moment  $\phi_2(x)$  is derived:

$$\phi_2(x) = -\frac{2}{5} \frac{1}{\Sigma} \frac{d\phi_1(x)}{dx}. \quad (4.27)$$

From Eq. (4.26a) the derivative of  $\phi_1(x)$  is derived as function of  $\phi_0(x)$ :

$$\frac{d\phi_1(x)}{dx} = -(\Sigma_a \phi_0(x) - S_0(x)). \quad (4.28)$$

Substituting Eq. (4.28) in Eq. (4.27), making the assumption of source constant in space, and substituting the result in Eq. (4.26b), one obtains the Fick's law for  $P_2$  approximation:

$$\phi_1(x) = -\left( \frac{1}{3\Sigma} + \frac{4\Sigma_a}{15\Sigma^2} \right) \frac{d\phi_0(x)}{dx}. \quad (4.29)$$

Lastly, by the combination of Fick's law and of the continuity equation constituted by Eq. (4.26a), with the assumption of constant source over space, diffusion equation for  $P_2$  is obtained:

$$-D_{P_2} \frac{d^2 \phi_0(x)}{dx^2} + \Sigma_a \phi_0(x) = S_0 \quad (4.30)$$

where the diffusion coefficient characteristic of  $P_2$  corresponds to:

$$D_{P_2} = \frac{1}{3\Sigma} + \frac{4\Sigma_a}{15\Sigma^2}. \quad (4.31)$$

Thus, defining a discrete domain individuated by the position of indexes  $i = 1, \dots, N$ , the discretization of the diffusion equation by means of a centered finite difference yields:

$$-D_{P_2} \frac{\phi_{0,i+1} - 2\phi_{0,i} + \phi_{0,i-1}}{\Delta x^2} + \Sigma_a \phi_{0,i} = S_0 \quad \text{with } i = 1, \dots, N. \quad (4.32)$$

Hence, the staggered spatial grid exploited in the previous section 4.2 is taken as a reference for the discretization of the first-order differential equations comprised by  $P_2$ . In particular, the first derivative of odd order moments are approximated with centered finite difference centered in the integer nodes of the grids, whereas derivatives of even moments are centered in the half-integer nodes. The resulting system of algebraic equations for the  $P_2$  approximation yields:

$$\frac{\phi_{1,i+\frac{1}{2}} - \phi_{1,i-\frac{1}{2}}}{\Delta x} + \Sigma_a \phi_{0,i} = S_0 \quad (4.33a)$$

$$\frac{1}{3} \frac{\phi_{0,i+1} - \phi_{0,i}}{\Delta x} + \frac{2}{3} \frac{\phi_{2,i+1} - \phi_{2,i}}{\Delta x} + \Sigma \phi_{1,i+\frac{1}{2}} = 0 \quad (4.33b)$$

$$\frac{2}{5} \frac{\phi_{1,i+\frac{1}{2}} - \phi_{1,i-\frac{1}{2}}}{\Delta x} + \Sigma \phi_{2,i} = 0. \quad (4.33c)$$

with  $i = 1, \dots, N$

If the same procedure adopted for the  $P_2$  in continuous is conducted between equations of (4.33), the discrete diffusion equation in the  $P_2$  approximation (4.32) is found, proof of the validity of the staggered grid represented in Fig.(Ref) as a choice for the discretization of the system of differential equations characteristic of the  $P_N$  approximation even for order  $N$  higher than 1.

Briefly, from Eq. (4.33c) the moment  $\phi_2$  at the node  $i$ , meaning  $\phi_{2,i}$  is derived as:

$$\phi_{2,i} = -\frac{2}{5} \frac{1}{\Sigma} \frac{\phi_{1,i+\frac{1}{2}} - \phi_{1,i-\frac{1}{2}}}{\Delta x} \quad (4.34)$$

and the corresponding relation for  $\phi_{2,i+1}$ , appearing as unknown in Eq. (4.26b), consists in:

$$\phi_{2,i+1} = -\frac{2}{5} \frac{1}{\Sigma} \frac{\phi_{1,i+\frac{3}{2}} - \phi_{1,i+\frac{1}{2}}}{\Delta x} \quad (4.35)$$

From Eq. (4.33a) the expression for the discretized derivative of  $\phi_1$  centered in  $i$  is derived and, with the corresponding relation for the derivative centered in  $i + 1$ , they yield, respectively:

$$\begin{aligned} \frac{\phi_{1,i+\frac{1}{2}} - \phi_{1,i-\frac{1}{2}}}{\Delta x} &= -(\Sigma_a \phi_{0,i} - S_0) \\ \frac{\phi_{1,i+\frac{3}{2}} - \phi_{1,i+\frac{1}{2}}}{\Delta x} &= -(\Sigma_a \phi_{0,i+1} - S_0). \end{aligned} \quad (4.36)$$

Eqs. (4.36) may be substituted in Eqs. (4.34) and (4.35) respectively, in order to find an expression for the third-order moment unknowns as function of  $\phi_{0,i}$  and  $\phi_{0,i+1}$ . Then, the resulting expressions are substituted in Eq. (4.33b) in order to find the last unknown not related to the moment  $\phi_0$ , which is  $\phi_{1,i+\frac{1}{2}}$ , as:

$$\phi_{1,i+\frac{1}{2}} = -\left(\frac{1}{3\Sigma} \frac{4\Sigma_a}{15\Sigma^2}\right) \frac{\phi_{0,i+1} - \phi_{0,i}}{\Delta x} \quad (4.37)$$

which constitutes the approximation by means of a centered finite difference of the Fick's law for  $P_2$ , previously found in continuous as Eq. (4.29). By considering the corresponding relation for  $\phi_1$  centered in  $i - \frac{1}{2}$  which yields:

$$\phi_{1,i-\frac{1}{2}} = -\left(\frac{1}{3\Sigma} \frac{4\Sigma_a}{15\Sigma^2}\right) \frac{\phi_{0,i} - \phi_{0,i-1}}{\Delta x} \quad (4.38)$$

and lastly, substituting Eqs. (4.37) and (4.38) in the discrete continuity equation (4.33a), the diffusion equation derived from the  $P_2$  system of discrete equations is obtained, presenting an expression mathematically equals to the one achieved by the discretization of the  $P_2$  diffusion equation in continuous (4.32). The result reads indeed:

$$-D_{P_2} \frac{\phi_{0,i+1} - 2\phi_{0,i} + \phi_{0,i-1}}{dx^2} + \Sigma_a \phi_{0,i} = S_0 \quad \text{with } i = 1, \dots, N. \quad (4.39)$$

### 4.3 Boundary condition imposition

In order to correctly pose the discretized  $P_N$  approximation system of equations, the imposition of the boundary conditions must be carried out. The  $P_1$  approximation case is here presented as an example of how such conditions have been prescribed. Both Mark's and Marshak's conditions have been considered.

As been reported in the previous section, a centered finite difference discretization scheme based upon a staggered mesh has been exploited for the spatial discretization of the  $P_N$  system of equations. The choice of the centered finite difference has been justified both from a sort of physical point of view, considering the expectations about the transport of particles in the configuration considered, and from a numerical approximation point of view as regards the higher order of accuracy provided by such a scheme with respect to the forward and backward finite difference schemes. Although, being the mesh staggered and the equations of the  $P_N$  approximation system, coupled equations, the equations involving the boundary nodes needed some further considerations.

In order to treat the boundary conditions indeed, a change in the approximation scheme for the first-derivative of the odd-order moments appearing in the system of equations has been carried out. Specifically, the first-derivatives of the odd-order moments are approximated at the boundaries by means of a first-order accuracy finite difference scheme, instead of the centered finite difference used for the equations characteristic of the internal nodes. Since the centered finite difference can not be applied at the boundary nodes [16], a backward and a forward finite difference scheme are exploited as derivative approximation at the boundaries. To clarify this application, the case of the  $P_1$  approximation system of equation discretized on a staggered grid of a total of 5 integer nodes and 4 half-integer nodes, is here presented. As considered in the previous section, the left and the right slab boundary are assumed individuated by the nodes  $i = 1$  and  $i = 5$ , respectively. The  $P_1$  system of equations for the case considered is one again reported for sake of exposition clarity.

$$\frac{d\phi_1}{dx} + \Sigma_a \phi_0 = S_0 \quad (4.40a)$$

$$\frac{1}{3} \frac{d\phi_0}{dx} + \Sigma \phi_1 = 0. \quad (4.40b)$$

As a consequence of the staggered grid 4.2, equation (4.40a) is discretized moving on the integer nodes of the mesh. At the node  $i = 1$ , corresponding to the left boundary of the discretized slab, the derivative of the moment  $\phi_{1,1}$  is approximated by means of a forward finite difference scheme, yielding:

$$\frac{\phi_{1,1+\frac{1}{2}} - \phi_{1,1}}{\Delta x/2} + \Sigma_a \phi_{0,1} = S_0. \quad (4.41)$$

On the right boundary, individuated by the node  $i = 5$  in the considered mesh, the equation (4.40a) is instead approximated by means of a backward difference scheme, reading:

$$\frac{\phi_{1,5} - \phi_{1,5-\frac{1}{2}}}{\Delta x/2} + \Sigma_a \phi_{0,5} = S_0. \quad (4.42)$$

Then, the expression for the introduced unknowns are derived from the relations provided by Mark's or Marshak's boundary conditions. In particular, with Mark's boundary conditions the relations for the angular flux at the boundary state, in case of  $P_1$  approximation:

$$\begin{aligned} P_0(\mu_1)\phi_0(x=0) + P_1(\mu_1)\phi_1(x=0) &= 0 \\ P_0(\mu_2)\phi_0(x=a) + P_1(\mu_2)\phi_1(x=a) &= 0 \end{aligned} \quad (4.43)$$

which, expressed with the notation exploited in the spatial discretization become:

$$\begin{aligned} P_0(\mu_1)\phi_{0,1} + P_1(\mu_1)\phi_{1,1} &= 0 \\ P_0(\mu_2)\phi_{0,5} + P_1(\mu_2)\phi_{1,5} &= 0. \end{aligned} \quad (4.44)$$

Hence, from these set of equations the unknowns  $\phi_{1,1}$  and  $\phi_{1,5}$  are derived as functions of  $\phi_{0,1}$  and  $\phi_{0,5}$  respectively, and substituted in the set of algebraic equations outcome of the spatial discretization of the  $P_1$  system of differential equations. If Marshak's boundary condition are considered, the relations involving the angular flux at the boundaries yield:

$$\begin{aligned} \frac{1}{2}\phi_{0,1} + \frac{1}{3}\phi_{1,1} &= 0 \\ \frac{1}{2}\phi_{0,5} - \frac{1}{3}\phi_{1,5} &= 0. \end{aligned} \quad (4.45)$$

to which the same procedure adopted in the case of Mark's boundary condition is applied for the imposition to the discretized  $P_1$  system of differential equations.

## 4.4 Outline of the code: $k$ -eigenvalue case

After the general drawings of the discretization and the boundary conditions treatment for a general  $P_N$  approximation system of equations, a brief outline of the code implemented to solve numerically the eigenvalue formulations of the neutron transport equation in the  $P_N$  approximation presented in Sect. 3.2.3 is here reported. The code, implemented in a MATLAB environment, consists in four modules, one for each eigenvalue-type, and it has been implemented with the aim to solve a generalized eigenvalue problem formulated in an arbitrary high order of the  $P_N$  approximation. Hence, the accent has been posed upon the automation to high orders of  $P_N$  approximation and as a consequence, future efforts are supposed to focus deeply on the optimization of the eigenvalues and eigenvectors calculation, also considering the attention which has been paid in recent year to more sophisticated algorithms for the eigenproblem numerical solution [27]. In the implemented code, eigenvalues and eigenvectors computation is accomplished by means of a subroutine of the linear algebra package ARPACK provided by MATLAB [28] the main details of which are provided below.

The code is here presented for the particular case of the  $k$ -eigenvalue formulation of the neutron transport equation, since the same procedure has been exploited for the implementation of the modules referring respectively to the  $\gamma$ ,  $\alpha$  and  $\delta$  eigenvalue formulation.

#### 4.4.1 Matrix formulation

The starting point for the implementation of the MATLAB code for the evaluation of the eigenvalues and the associated eigenvectors of the  $k$ -eigenvalue problem is the creation of the matrices characteristics of the specific  $P_N$  approximation considered, outcomes of the spatial discretization of the operators peculiar of the one-dimensional, time-independent, mono-energetic version of the neutron transport equation. As way of example, the problem global left- and right-hand matrix individuation for the case of  $P_1$  approximation is here reported. The moments equation of the  $k$ -eigenvalue formulation (3.67) illustrated in Chapter 3, reads:

$$\begin{aligned} \frac{m+1}{2m+1} \frac{d}{dx} \phi_{m+1}(x) + \frac{m}{2m+1} \frac{d}{dx} \phi_{m-1}(x) + \Sigma_t \phi_m(x) \\ = \Sigma_s \phi_0(x) \delta_{m0} + \frac{1}{k} \nu \Sigma_f \phi_0(x) \delta_{m0} \quad m = 0, 1, 2, \dots, N \end{aligned}$$

from which the  $P_1$  approximation system of equations is derived as:

$$\begin{aligned} \frac{d\phi_1}{dx} + \Sigma_a \phi_0 &= \frac{1}{k} \frac{\nu \Sigma_f}{\phi_0} \\ \frac{1}{3} \frac{d\phi_0}{dx} + \Sigma \phi_1 &= 0. \end{aligned} \quad (4.46)$$

In operators notation the system may be rewritten as:

$$\underbrace{\begin{bmatrix} \Sigma_a & \frac{d}{dx} \\ \frac{d}{dx} & \Sigma_t \end{bmatrix}}_{\mathbf{L}} \underbrace{\begin{bmatrix} \phi_0 \\ \phi_1 \end{bmatrix}}_{\boldsymbol{\varphi}} = \frac{1}{k} \underbrace{\begin{bmatrix} \nu \Sigma_f & 0 \\ 0 & 0 \end{bmatrix}}_{\mathbf{F}} \underbrace{\begin{bmatrix} \phi_0 \\ \phi_1 \end{bmatrix}}_{\boldsymbol{\varphi}} \quad (4.47)$$

where  $\boldsymbol{\varphi}$  is the unknowns vector whose components are the discretized zeroth order moment  $\phi_0$  and the discretized first order moment  $\phi_1$ . In case of higher order of  $P_N$  approximations, the unknown moments are still disposed in an ascendant order per moment order.

The unknowns vector  $\boldsymbol{\varphi}$ , the left-hand matrix and the right-hand one characteristic of the  $P_1$  approximation in the  $k$ -eigenvalue formulation are here reported referred to a slab discretized on a mesh of a total of 9 nodes, with indexes  $i = 1$  and  $i = 5$  identifiers of the

slab boundaries nodes. Thus, in the proposed case the  $\varphi$  vector yields:

$$\varphi = \begin{pmatrix} \phi_1^0 \\ \phi_2^0 \\ \phi_3^0 \\ \phi_4^0 \\ \phi_5^0 \\ \phi_{1.5}^1 \\ \phi_{2.5}^1 \\ \phi_{3.5}^1 \\ \phi_{4.5}^1 \end{pmatrix} \quad (4.48)$$

where the notation  $\phi_1^0$  denotes  $\phi_0(x_1) = \phi_0(x = 0)$ . As yet reported in previous sections, the even orders moments appearing as unknowns in the equations are evaluated at the integer-index nodes of the staggered grid, whereas the odd-orders moments are computed at the locations individuated by the half-integer indexes (see Fig. 4.2).

Then, the global left-hand matrix, outcome of the discretization of the  $\mathbf{L}$  operator applied to the unknowns vector  $\varphi$ , is created as a composition of sub-matrices deriving from the discretization of the specific operator applied to the respective unknown in each equation. The left-hand matrix  $\mathbf{L}$  characteristic of the  $P_1$  approximation is reported explicitly for the case considered, in order to make evident the alternative square and rectangular nature of the sub-matrices which gives as result a global left-hand square matrix. Thus, the  $\mathbf{L}$  matrix yields:

$$\mathbf{L} = \begin{bmatrix} \begin{bmatrix} \Sigma_a & 0 & 0 & 0 & 0 \\ 0 & \Sigma_a & 0 & 0 & 0 \\ 0 & 0 & \Sigma_a & 0 & 0 \\ 0 & 0 & 0 & \Sigma_a & 0 \\ 0 & 0 & 0 & 0 & \Sigma_a \end{bmatrix} & \begin{bmatrix} \frac{2}{\Delta x} & 0 & 0 & 0 \\ -\frac{1}{\Delta x} & \frac{1}{\Delta x} & 0 & 0 \\ 0 & -\frac{1}{\Delta x} & \frac{1}{\Delta x} & 0 \\ 0 & 0 & -\frac{1}{\Delta x} & \frac{1}{\Delta x} \\ 0 & 0 & 0 & -\frac{2}{\Delta x} \end{bmatrix} \\ \begin{bmatrix} -\frac{1}{3} \frac{1}{\Delta x} & \frac{1}{3} \frac{1}{\Delta x} & 0 & 0 & 0 \\ 0 & -\frac{1}{3} \frac{1}{\Delta x} & \frac{1}{3} \frac{1}{\Delta x} & 0 & 0 \\ 0 & 0 & -\frac{1}{3} \frac{1}{\Delta x} & \frac{1}{3} \frac{1}{\Delta x} & 0 \\ 0 & 0 & 0 & -\frac{1}{3} \frac{1}{\Delta x} & \frac{1}{3} \frac{1}{\Delta x} \end{bmatrix} & \begin{bmatrix} \Sigma & 0 & 0 & 0 \\ 0 & \Sigma & 0 & 0 \\ 0 & 0 & \Sigma & 0 \\ 0 & 0 & 0 & \Sigma \end{bmatrix} \end{bmatrix} \quad (4.49)$$

where in the sub-matrix corresponding to the spatial approximation of the derivative of  $\phi_1(x)$  it may be noted the terms referred to the use of a forward and a backward finite difference respectively, at the boundaries nodes.

Lastly, the right-hand matrix  $\mathbf{F}$  characterized by fission terms consists in:

$$\mathbf{F} = \begin{bmatrix} \begin{bmatrix} \nu\Sigma_f & 0 & 0 & 0 & 0 \\ 0 & \nu\Sigma_f & 0 & 0 & 0 \\ 0 & 0 & \nu\Sigma_f & 0 & 0 \\ 0 & 0 & 0 & \nu\Sigma_f & 0 \\ 0 & 0 & 0 & 0 & \nu\Sigma_f \end{bmatrix} & \begin{bmatrix} 0 & 0 & 0 & 0 \\ 0 & 0 & 0 & 0 \\ 0 & 0 & 0 & 0 \\ 0 & 0 & 0 & 0 \\ 0 & 0 & 0 & 0 \end{bmatrix} \\ \begin{bmatrix} 0 & 0 & 0 & 0 & 0 \\ 0 & 0 & 0 & 0 & 0 \\ 0 & 0 & 0 & 0 & 0 \\ 0 & 0 & 0 & 0 & 0 \end{bmatrix} & \begin{bmatrix} 0 & 0 & 0 & 0 \\ 0 & 0 & 0 & 0 \\ 0 & 0 & 0 & 0 \\ 0 & 0 & 0 & 0 \end{bmatrix} \end{bmatrix}. \quad (4.50)$$

Both the  $\mathbf{L}$  and the  $\mathbf{F}$  matrix are built as composition of sparse matrices, which allows the implementation of high order  $P_N$  approximation characteristic matrices. Obviously, their dimensions depend upon both the  $N$  order of approximation received as input by the code, and on the mesh size chosen for the spatial discretization. Even though the sparse nature of the matrices created allows large matrix dimensions, the aim of computing the eigenvalues for the neutron transport equation approximated in high orders of  $P_N$  forces to a compromise between the accuracy in the spatial discretization and the dimension of the matrices characteristic of the generalized eigenvalue problem of which the eigenvalues and eigenvectors have to be computed. Then, starting from the  $P_1$  characteristic matrices, the global matrices of higher order of  $P_N$  approximation are built by means of hemming of the  $P_1$  global matrices, as described in the successive section.

#### 4.4.2 $P_N$ global matrices automation

This section is devoted to briefly outline the logical path followed in the automation for the computation of eigenvalues and eigenvectors characteristic of neutron transport equation in the simplified model presented in previous sections and developed in arbitrarily high orders of the  $P_N$  approximation. Once the order  $N$  of the  $P_N$  approximation is given as input to the code specific of the eigenproblem desired, the implementation of the global left- and right-hand matrix of the problem starts. Firstly, a matrix containing the characteristic coefficients of the  $P_N$  system of equations for the one-dimensional model is created in order to collect the values of the coefficients which will be recalled later in the creation of the global matrix. As a way of example, the development of the code for the  $k$  eigenvalue problem in  $P_2$  approximation is reported.

Table 4.1: Coefficients matrix created by the implemented code referred to the system of differential equations of  $P_2$  approximation in  $k$  eigenvalue

	LHS		RHS		
	$\frac{m}{2m+1}$	$\Sigma$	$\frac{m+1}{2m+1}$	$\nu\Sigma_f\delta_{m0}$	$\Sigma_s\delta_{m0}$
<b>Eq.1</b> ( $m = 0$ )	0	$\Sigma$	1	$\nu\Sigma_f$	$\Sigma_s$
<b>Eq.2</b> ( $m = 1$ )	$\frac{1}{3}$	$\Sigma$	$\frac{2}{3}$	0	0
<b>Eq.3</b> ( $m = 2$ )	$\frac{2}{5}$	$\Sigma$	0	0	0

Referring to the equation for the moments in the  $k$ -eigenvalue (3.67), the  $P_2$  characteristic system of differential equations consists in:

$$\Sigma_a \phi_0 + \frac{d\phi_1}{dx} = \frac{1}{k} \nu \Sigma_f \phi_0 \quad (4.51)$$

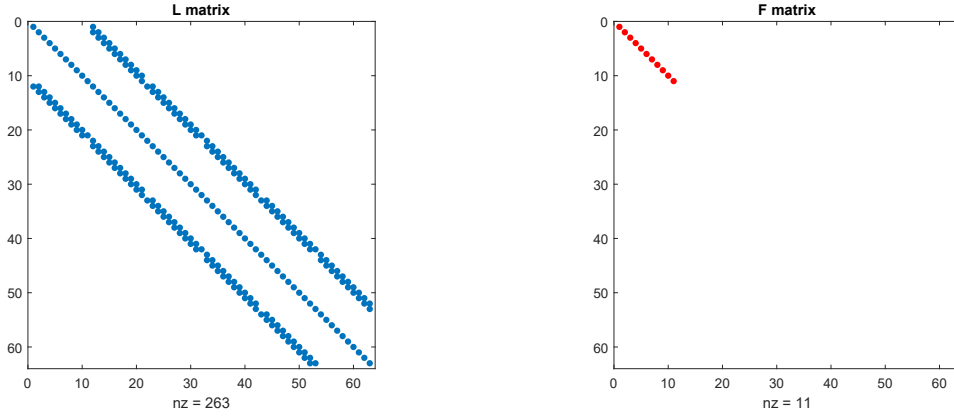
$$\frac{1}{3} \frac{d\phi_0}{dx} + \Sigma \phi_1 + \frac{2}{3} \frac{d\phi_2}{dx} = 0 \quad (4.52)$$

$$\frac{2}{5} \frac{d\phi_1}{dx} + \Sigma \phi_2 = 0 \quad (4.53)$$

where the terms are disposed in such a way that the moments of the angular flux appear in ascending order of indexes in each equation. Hence, a coefficient matrix is created in order to store the coefficients of each term in the respective equation of the system, starting from the general expression of the coefficients as function of the order of the equation, explicitly visible in the moments equation (3.67). Specifically, for the  $P_2$  case the matrix structure is shown in Table 4.1.

Then, the creation of the global left-hand matrix, which in the  $k$ -eigenvalue case comprises the discretization of the leakage operator, and of the right-hand matrix, characterized by the fission operator instead, is performed by hemming the  $P_1$  characteristic global matrices with as many additional sub-matrices as needed to accomplish the complete discretization of the  $P_N$  system terms missing. Observing that the  $P_1$  matrices structure is common to the ones of any higher  $P_N$  approximation indeed, the sub-matrices necessary to a comprehensive description of the differential equations discretization of both the odd and even higher order approximations are added to the  $P_1$  nucleus by means of its hemming with square diagonal and rectangular tridiagonal sub-matrices, whose associated coefficients are the ones stored in the coefficient matrix presented above (see Table 4.1), and that correspond to the operators discretization required by the specific approximation. Thus, the global left-hand and right-hand matrices characteristic of the generalized eigenvalue problem which has to be solved, are built as block sparse matrices for both the case of odd- and even-order  $P_N$  approximations.

The sparsity pattern of the resulting matrices is then reported in figure 4.3, referring to  $P_5$  approximation in the  $k$ -eigenvalue formulation.



(a) Leakage operator matrix.

(b) Fission operator matrix.

Figure 4.3: Sparsity patterns of the global left-hand (a) and right-hand matrix (b) of the generalized eigenvalue problem in  $k$  eigenvalue with  $P_5$  approximation.

#### 4.4.3 Boundary conditions evaluation and imposition

Together with the  $P_N$  approximation order  $N$  required by the user, the implemented code receives as input also the type of boundary conditions desired to solve the linear system of equations. Both Mark and Marshak boundary conditions can be provided to imposed vacuum boundary conditions.

While in the generation of the problem global matrices, the distinction between odd- and even-orders of the  $P_N$  approximation does not imply substantial differences in the code implementation, the numerical computation and imposition of boundary conditions have required a more delicate development. Indeed, from the theoretical standpoint, the significant difference affecting the even-order approximations with respect to the odd ones, consists in the fact that they do not represent a more accurate approximation in refers to the preceding odd-order  $P_N$ . As instance, considering the  $P_1$  approximation which corresponds to the diffusion approximation, the  $P_2$  approximation still corresponds to a diffusion model, meaning that the degree of accuracy of  $P_2$  approximation is not higher than that of  $P_1$ . In order to increment the model accuracy is necessary to develop the successive odd-order  $P_N$  approximation, in this case  $P_3$  approximation. Hence, even-order  $P_N$  approximations do not give additional information in refers to the neutron angular distribution and this condition is reflected in the discussion about  $P_N$  boundary conditions [8].

Indeed, both odd- and even-order  $P_N$  approximations requires  $N + 1$  boundary conditions to result in a well-posed problem. In case of Mark boundary conditions (3.52), the  $N + 1$  conditions are computed starting from the  $N + 1$  roots of the Legendre polynomial of order  $N + 1$ , which range symmetrically from  $-1 \leq \mu \leq 1$ . The difference between the two types of approximation order arises in the fact that even-order approximation boundary

conditions comprise the root  $\mu = 0$ , where  $\mu$  represents the cosine of the angle formed by the neutron motion direction and the  $x$ -axis. However, neutrons traveling along the direction individuated by the  $\mu = 0$  never meet the configuration boundary and, as a consequence, they do not provide further information about the neutron angular distribution solution of the problem. An analogous aspect may be also referred to Marshak boundary conditions.

In the implemented code both Mark and Marshak boundary conditions are evaluated by means of the Symbolic Math Toolbox provided by MATLAB. A preliminary developed function starts computing the coefficients of the angular flux moments involved by the  $P_N$  approximation required, directly derived from the relations stated by Mark and Marshak conditions. Then, these coefficients are manipulated in order to derive the proper equations to be substitute in the original linear system of equations corresponding to the spatial discretization of the  $P_N$  approximation desired.

As yet reported for the generation of the left- and right-hand matrix of the generalized  $k$ -eigenvalue problem, a draft of the numerical process developed for the implementation of the boundary conditions in the  $P_2$  approximation is here reported. The general principles upon which the imposition of conditions is based is yet reported in Sect. 4.3.

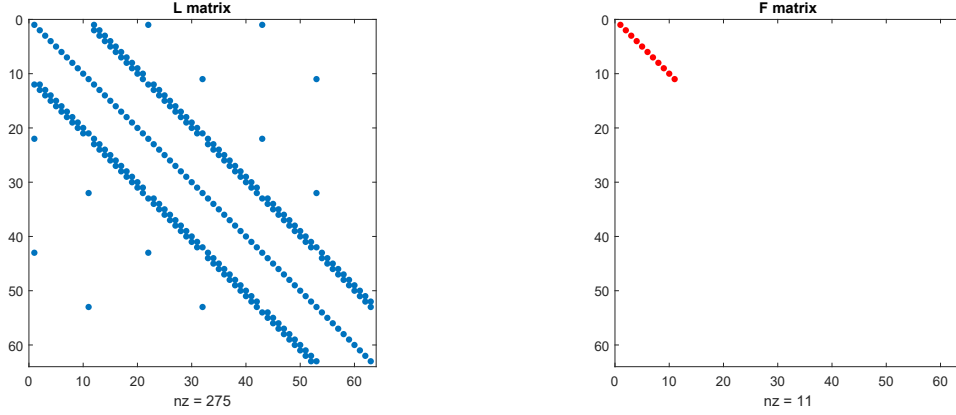
Thus, in case of Mark conditions, the  $N + 1$  roots of the Legendre polynomial of order  $N + 1$  are computed in order to evaluate the angular moments coefficients referred to the  $P_2$  approximation expression of the angular flux evaluated at the boundaries for the prescribed directions. Being  $N$  even in the case considered, the direction corresponding to  $\mu = 0$  is let apart and only the positive and negative cosine values estimated are taken into consideration for the substitution in the boundary conditions expressions. The relations which are referred to in this particular case are:

$$\begin{aligned}\phi(0, \mu_1) &\approx \frac{1}{2}P_0(\mu_1)\phi_0(0) + \frac{3}{2}P_1(\mu_1)\phi_1(0) + \frac{5}{2}P_2(\mu_1)\phi_2(0) = 0 && \text{with } \mu_1 > 0 \\ \phi(a, \mu_2) &\approx \frac{1}{2}P_0(\mu_2)\phi_0(a) + \frac{3}{2}P_1(\mu_2)\phi_1(a) + \frac{5}{2}P_2(\mu_2)\phi_2(a) = 0 && \text{with } \mu_2 < 0.\end{aligned}\tag{4.54}$$

These equations, in relation to the notation exploited in the spatial discretization for numerical computation, may be rewritten as:

$$\begin{aligned}\frac{1}{2}P_0(\mu_1)\phi_1^0 + \frac{3}{2}P_1(\mu_1)\phi_1^1 + \frac{5}{2}P_2(\mu_1)\phi_1^2 &= 0 && \text{with } x_1 = 0 \\ \frac{1}{2}P_0(\mu_2)\phi_{end}^0 + \frac{3}{2}P_1(\mu_2)\phi_{end}^1 + \frac{5}{2}P_2(\mu_2)\phi_{end}^2 &= 0 && \text{with } x_{end} = a\end{aligned}\tag{4.55}$$

from which the symbolic expressions for the unknowns  $\phi_1^1$  and  $\phi_{end}^1$  are derived as function of the remaining angular moments evaluated at  $x_1 = 0$  and  $x_{end} = a$  respectively.



(a) Leakage operator matrix.

(b) Fission operator matrix.

Figure 4.4: Sparsity patterns of the global left-hand (a) and right-hand matrix (b) of the generalized eigenvalue problem in  $k$  eigenvalue with  $P_5$  approximation and boundary conditions imposed.

In case of Marshak's boundary conditions instead, the equations for  $\phi_1^1$  and  $\phi_{end}^1$  are derived from the integral relations:

$$\begin{aligned} \int_0^1 d\mu \left( \frac{1}{2} P_0(\mu) \phi_0(0) + \frac{3}{2} P_1(\mu) \phi_1(0) + \frac{5}{2} P_2(\mu) \phi_2(0) \right) &= 0 \\ \int_{-1}^0 d\mu \left( \frac{1}{2} P_0(\mu) \phi_0(a) + \frac{3}{2} P_1(\mu) \phi_1(a) + \frac{5}{2} P_2(\mu) \phi_2(a) \right) &= 0. \end{aligned} \quad (4.56)$$

Then, the outcomes  $\phi_1^1$  and  $\phi_{end}^1$  are inserted in the corresponding equations of the original  $P_2$  approximation system of equations which, in the  $k$ -eigenvalue case, consist in:

$$\begin{aligned} \frac{\phi_{1+\frac{1}{2}}^1 - \phi_1^1}{\Delta x/2} + \Sigma_a \phi_1^0 &= \frac{1}{k} \nu \Sigma_f \phi_1^0 \\ \frac{\phi_{end}^1 - \phi_{end-\frac{1}{2}}^1}{\Delta x/2} + \Sigma_a \phi_{end}^0 &= \frac{1}{k} \nu \Sigma_f \phi_{end}^0. \end{aligned} \quad (4.57)$$

Lastly, the coefficients of each angular moment terms appearing in the symbolic expressions (4.57) are converted into double precision values and stored in a coefficients matrix characteristic of Mark or Marshak boundary coefficients.

The resulting values are then substituted in the properly corresponding positions of the left-hand matrix  $L$  by means of a recursive procedure. The same process is followed for  $P_N$  approximations of higher orders and in other eigenvalue types formulations of the neutron transport equation.

An example of the modified sparsity pattern due to the imposition of boundary conditions in  $P_5$  approximation, for the  $k$ -eigenvalue formulation is shown in Figure 4.4.

#### 4.4.4 Eigenvalues and eigenvectors calculation

The eigenvalues and eigenvectors computation is finally performed in the implemented code through the ARPACK package provided by MATLAB, specific for the solution of large scale eigenvalue problems [28]. This package is based on the Implicit Restarted Arnoldi Method (IRAM), an iterative method for the solution of eigenvalues and eigenvectors of large sparse matrices. Specifically, IRAM is the method upon which the MATLAB function *eigs* is implemented. This function is able to provide subset of eigenvalues and eigenvectors [29], starting from the matrix characteristic of both a standard or generalized eigenvalue problem. In the code implemented in the thesis, the problem has been considered in its generalized form in order to exploit the capability of the function *eigs* to choose the more suitable algorithm for the manipulation of the matrix according to their specific characteristics.

The default converge tolerance has been exploited in the computations, equal to  $10^{-14}$  and a subset of 20 eigenvalues and its associated eigenvectors has been required. The magnitude characteristic of the desired eigenvalues can be optionally specified, in particular the smallest or the largest magnitude, and the function can also provide the subset of the eigenvalues nearest to a given shift value. In the analyzed case the smallest magnitude eigenvalues are of interest and, according to the generalized eigenproblem formulation in case of  $k$ ,  $\gamma$  and  $\delta$  eigenvalues, the final results are obtained by the inversion of the outcomes returned by *eigs*.

Other possible options to the function regards the maximum number of iterations allowed to the algorithm and the maximum size of the Krylov subspace to be used. Experiments in the changing of these last two options have been performed during the code implementation without reporting substantial increments in the result accuracy, thus the default values have been left for the calculus. Nevertheless, accurate considerations about these aspects can be found in [27].

As regards the eigenvectors evaluated by the ARPACK package, a remark should be pointed for the case considered. The code implementation presented in the thesis exploited instead a staggered grid for the spatial discretization of the differential equations modeled. As a consequence, due to the spatial discretization setting, the solution vectors associated to odd-order angular flux moments present a length diminished of a unit with respect to the one characteristic of even-order moments. Thus, to perform the reconstruction of the angular flux based on the relation for this quantity peculiar of the  $P_N$  approximation, an interpolation process to extent the even-order discrete moments at the query points is foreseen in the implementation.

# Chapter 5

## Numerical results

In order to test the reliability of the numerical results provided by the implemented code, comparisons to benchmark criticality results for the case of the  $k$ ,  $\gamma$  and  $\alpha$  eigenvalue have been performed, together with appropriate grid independence studies, necessary because of the spatial discretization involved by the model considered. Due to a lack of both reference numerical results and theoretical information concerning the  $\delta$  eigenvalue, only a preliminary study has been conducted for this type of eigenvalue.

Once that an acceptable quality of the numerical results obtained has been verified, considerations about the different results obtained with even-order  $P_N$  approximations with respect to those deriving by odd-order approximations are reported. Furthermore, comparison concerning the use of Mark boundary conditions rather than Marshak type conditions are performed for the each eigenvalue type calculations. Indeed, a quite different convergence trend to the reference value for increasing orders of the  $P_N$  approximation can be individuated looking to the results conducted on the fundamental eigenvalue specifically.

A convergence study of the method implemented by ARPACK package is beyond the scope of the present work and only a simple and intuitive verification on the obtained eigenvectors is reported.

Furthermore, for each eigenvalue type a study regarding the variation of the fundamental mode with respect to the slab thickness and the critical parameter is conducted, except for the case of  $\delta$  eigenvalue which, as yet mentioned, has implied difficulties in the interpretation.

### 5.1 Grid independence study

Grid independence studies are common numerical practices performed in order to ensure that the chosen mesh resolution is sufficiently refined in such a way that the solution obtained is independent of it. Thus, the residual error between the solution obtained with the most refined mesh and the ones outcome of calculations with coarser meshes, has been investigated

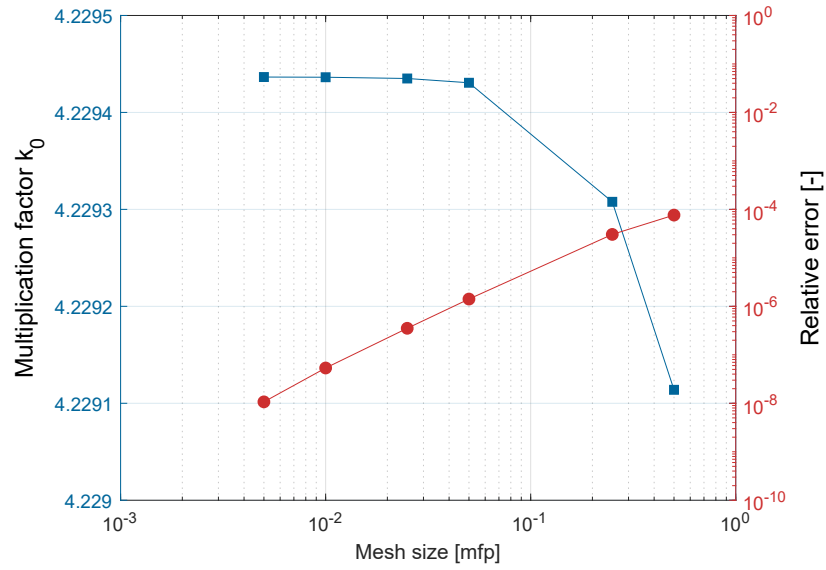


Figure 5.1: Grid independence study on the fundamental multiplication factor  $k_0$  for a multiplying slab of thickness 8 mfp, with  $P_5$  and Marshak boundary conditions.

as function of the mesh size.

Furthermore, being aim of the present work the computation of not only the eigenvalue type fundamental mode but also some higher-modes, a particular attention has been posed on the accuracy of the results obtained for the fundamental eigenvalue about grid independence study, since ARPACK algorithm for the eigenvalues and eigenvectors calculation converged first on this value. As a consequence, assuming a worst convergence on higher-modes, a particularly fine mesh size has been used in order to prevent from excessive numerical error affecting higher-modes solution.

For sake of brevity, the grid independence study performed for the  $k$  eigenvalue and the  $\alpha$  eigenvalue only are reported. An exactly analogous investigation has been conducted for the other eigenvalue types. The analysis has been performed considering a slab of thickness equal to 8 mean free paths (mfp) developing the  $P_5$  approximation with Marshak boundary conditions. The nuclear data set exploited is reported in Table 5.1.

Hence, as shown in Figures 5.1-5.2, a decreasing mesh size leads to decreasing error in the evaluation of the fundamental eigenvalue, as expected. The relative error, reported on the right y-axis of each figure, has been considered as the residual between the eigenvalue computed with the current mesh size and the one obtained with the most refined mesh. In order to be conservative for the reasons mentioned above, a mesh size equal to 0.005 mfp has been adopted in the model implementation, corresponding to a relative error of an order of magnitude with ranges from  $10^{-8}$  and  $10^{-7}$  for each eigenvalue type.

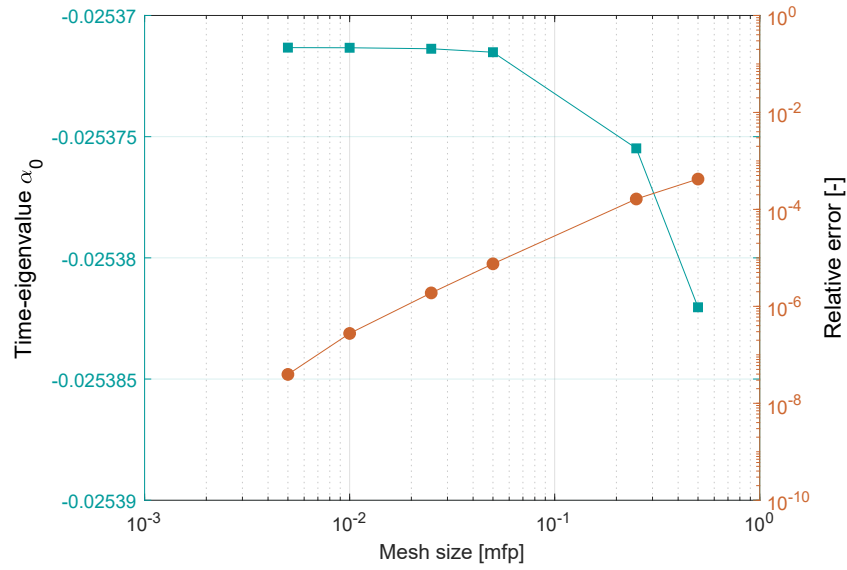


Figure 5.2: Grid independence study on the fundamental time eigenvalue  $\alpha_0$  with  $P_5$  and Marshak boundary conditions.

Table 5.1: Nuclear data adopted in grid independence study and in benchmark assessments.

Parameter		Value
Total cross-section [ $\text{cm}^{-1}$ ]	$\Sigma_t$	1.0
Scattering cross-section [ $\text{cm}^{-1}$ ]	$\Sigma_s$	0.8
Absorption cross-section [ $\text{cm}^{-1}$ ]	$\Sigma_a$	0.2
Production cross-section [ $\text{cm}^{-1}$ ]	$\nu\Sigma_f$	1.0

## 5.2 Comparison to benchmark criticality results

A comparison to available benchmark values of the results obtained in the evaluation of the fundamental and higher-modes for the case of the  $k$  and the  $\gamma$  eigenvalue of the neutron transport equation by R. S. Modak in [30], are performed. Specifically, Modak results are referred to the first six even modes of the  $k$  and the  $c$  eigenvalue for the mono-energetic model of a homogeneous one-dimensional slab and sphere. The results presented by Modak are, in turn, the outcomes of a comparison with those found by Dahl and Sjöstrand in [31].

As concerned the cases of interest for the present thesis, the reference values are evaluated with the application of the standard  $S_n$  method, with Gauss-Legendre quadrature sets for the directions representation. Vacuum boundary conditions have been imposed. Two different slab thicknesses are analyzed, 1 mfp and 8 mfp respectively, with isotropic scattering. The nuclear data adopted by Modak in its study are summarized in Table 5.1.

The eigenvalues presented by Modak are evaluated, for both the case of 1 mfp and 8 mfp slab dimension, with 100 meshes in the most accurate computation. For the thinner slab, 256

directions have been used, whereas for the 8 mfp slab calculations have been performed with 64 directions only.

Furthermore, in the reference work the  $k$ -eigenvalues have been obtained by the computation with the  $S_n$  method and then converted into the corresponding  $c$ -eigenvalues through the relation, valid in case of isotropic scattering:

$$c = \frac{\Sigma_s + \nu\Sigma_f/k}{\Sigma_t} \quad (5.1)$$

also presented in [32] in which the direct relations between the three main neutron transport eigenvalues  $k$ ,  $\alpha$  and  $c$  are reported.

In the present thesis a slightly different discussion has been made as regards the  $c$ -eigenvalue. As mentioned in Sect. 2.3 of Ch. 2, the  $c$  eigenvalue corresponds to the physical meaning of the mean number of secondary neutrons per collision. Thus, in its eigenvalue connotation, it indicates the average number of secondaries per collision needed to accomplish a steady-state neutron population distribution [32]. In the present work instead, the  $\gamma$  eigenvalue is investigated, intended as the effective multiplication factor per collision with the same physical and mathematical approach adopted in the discussion for the effective multiplication factor per fission  $k$ .

Hence, as done by Modak, which has correlated the numerically obtained  $k$ -eigenvalues with the  $c$ -eigenvalues presented by Dahl et al. in [31] evaluated through a semi-analytical method, the  $\gamma$ -eigenvalues outcome of the implemented code are related to the reference results through:

$$c = \frac{(\Sigma_s + \nu\Sigma_f)/\gamma}{\Sigma_t}. \quad (5.2)$$

## **k-eigenvalue assessments**

First, the fundamental multiplication factor  $k_0$  obtained with increasing orders of the  $P_N$  approximation is compared with the value obtained by Modak with  $S_{64}$  in the case of 1 mfp slab and with  $S_{256}$  for that of 8 mfp thickness. Vacuum boundary conditions are considered in all the studies presented which have been exploited as benchmark. A similar comparison has been conducted also in [33] and the reported results have been taken as a further benchmark concerning the lower-orders of  $P_N$  approximations used with respect to the  $S_n$  approximations exploited by Modak. Specifically, fundamental multiplication factor evaluated in [33] with  $S_4$ ,  $S_8$ ,  $S_{16}$  and  $S_{32}$  have been compared with the outcomes obtained with the corresponding  $P_N$  approximations by the code presented in the thesis. Mark boundary conditions has been considered fro the implemented results. The possibility of such a comparison has been considered since an equivalence between  $P_{N-1}$  and  $S_N$  approximation with even  $N$  has been demonstrated in literature. Nuclear data adopted are the same as those reported in 5.1.

Table 5.2: Fundamental multiplication factor  $k_0$  convergence to benchmark value at increasing order of  $P_N$  approximation with Mark boundary conditions. Reference values by Modak are evaluated with  $S_{256}$  in case of 1 mfp slab, and with  $S_{64}$  for the 8 mfp thick slab, both with vacuum boundary conditions. Reference values denoted as  $k_{0,BARC}$  have been evaluated with  $S_4, S_8, S_{16}$  and  $S_{32}$  respectively.

$P_N$	1 mfp		8 mfp	
	$k_{0,Modak} = 1.2264$		$k_{0,Modak} = 4.2300$	
	$k_0$	$k_{0,BARC}$	$k_0$	$k_{0,BARC}$
$P_3$	1.129077	1.129075	4.225109	4.225105
$P_7$	1.209379	1.209376	4.229069	4.229065
$P_{15}$	1.223481	1.223479	4.229844	4.229840
$P_{31}$	1.225737	1.225737	4.230024	4.230020

Table 5.3: Fundamental multiplication factor  $k_0$  convergence to benchmark value at increasing order of  $P_N$  approximation with Marshak BCs. Reference values by Modak are evaluated with  $S_{256}$  in case of 1 mfp slab, and with  $S_{64}$  for the 8 mfp thick slab, both with vacuum boundary conditions. Reference values denoted as  $k_{0,BARC}$  have been evaluated with  $S_4, S_8, S_{16}$  and  $S_{32}$  respectively.

$P_N$	1 mfp		8 mfp	
	$k_{0,Modak} = 1.2264$		$k_{0,Modak} = 4.2300$	
	$k_0$	$k_{0,BARC}$	$k_0$	$k_{0,BARC}$
$P_3$	1.171867	1.129075	4.228452	4.225105
$P_7$	1.219462	1.209376	4.229725	4.229065
$P_{15}$	1.225369	1.223479	4.229992	4.229840
$P_{31}$	1.226151	1.225737	4.230058	4.230020

The comparison outcomes are reported in Table 5.2. As shown in the table, the results obtained by the presented method agree well with the ones reported in [33], denoted as  $k_{0,BARC}$ . Specifically, in both the cases of 1 mfp and 8 mfp slab thickness, an agreement up to five decimal places is reported. Increasing the order of the  $P_N$  approximations, the fundamental  $k$ -eigenvalue found approaches better the reference result by Modak, even though, in the thinner slab case the evaluation still appears rough at the  $P_{31}$  approximation. It is indeed accurate up to two decimal places only with respect to the reference.

The convergence to the benchmark value is faster for the case of thicker slab which, at  $P_{31}$  approximation shows an agreement to 4 decimals. The better convergence, at the same order of  $P_N$  approximation, of the thicker slab with respect to the thinner one, may be related to the weaker impact of the leakages in larger systems.

An additional analysis performed with respect to the study conducted in [33] and in [30] regards the imposition of Marshak boundary conditions. The same procedure adopted to find the fundamental eigenvalue in case of  $P_N$  approximations with Mark boundary conditions, is exploited with the imposition of Marshak type conditions and the results are reported in Table 5.3.

Table 5.4: Even higher-order  $k$ -eigenvalues convergence to benchmark values at increasing orders of  $P_N$  approximation with Mark boundary conditions, for mesh size of 0.005 mfp. Benchmark values have been obtained with  $S_{64}$ , 100 meshes and vacuum boundary condition.

8 mfp					
$k$ -mode	$P_3$	$P_7$	$P_{15}$	$P_{31}$	Modak (1995)
$k_0$	4.2251089	4.2290691	4.2298438	4.2300236	4.2300510
$k_2$	2.0187740	2.0394894	2.0413997	2.0417997	2.041626
$k_4$	1.0812013	1.1355216	1.1384141	1.1387900	1.13835
$k_6$	0.6633973	0.7496759	0.7563779	0.7567577	0.75610
$k_8$	0.4424235	0.5448455	0.5586462	0.5591481	0.5583
$k_{10}$	0.3127659	0.4177842	0.4401845	0.4410772	0.440

For all the approximations considered, the fundamental eigenvalues found with Marshak boundary conditions are higher with respect to the ones obtained with Mark boundary conditions, and to the results reported in [33] denoted as  $k_{0,BARC}$ . The quite great enhancement is particularly visible in the case of the 1 mfp slab which gains a decimal in accuracy at the  $P_{31}$  approximation. Considering that in terms of implementation efforts, Marshak boundary conditions are comparable to Mark type conditions, the accuracy gained with the former conditions is quite attractive, especially in case of low-order approximations which present a rough accuracy.

Then, higher-order  $k$ -eigenvalues results are compared. In this case only references by Modak [30], referred to  $S_{64}$ , are considered. Table 5.4 shows the numerical results obtained for the first 6 even order  $k$ -eigenvalues for the mono-energetic slab with isotropic scattering, at increasing odd-orders  $P_N$  approximation. The slab thickness analyzed is the thicker one (8 mfp), and Mark boundary conditions have been imposed.

Although an accuracy improvement, talking about criticality calculations, is desirable, the results obtained for both the fundamental and higher-order  $k$ -eigenvalues can be considered as verified, taking into account the different method used for the angular approximation. The best agreement is shown by the highest order  $P_N$  approximation, as expected. Starting from an accuracy up to 4 decimals at the fundamental mode, it worsens in higher-modes evaluation reaching only two decimal figures of accuracy at the tenth mode, with respect to results provided by Modak [30]. It is highlighted that the accuracy discussed is referred to the results taken as benchmark, and is not an absolute accuracy of the computed results obtained with the code implemented for the present thesis.

In order to verify the associated eigenvectors solution founded by ARPACK package, a simple verification is made evaluating:

$$\mathbf{L}\varphi_n - \frac{1}{k_n}\mathbf{F}\varphi_n = 0 \quad \text{with } n=0,2,\dots,10. \quad (5.3)$$

Table 5.5: Higher-mode  $k$ -eigenvalues and eigenvectors verification computed with increasing order of  $P_N$  approximations and Mark boundary conditions for the case of 8 mfp slab thickness.

$k$ -mode	$P_3$		$P_7$	
	$ k_n - k_{n,ref} $	$ \mathbf{L}\varphi_n - \lambda_n\mathbf{F}\varphi_n $	$ k_n - k_{n,ref} $	$ \mathbf{L}\varphi_n - \lambda_n\mathbf{F}\varphi_n $
$k_0$	$4.9420 \cdot 10^{-3}$	$1.166 \cdot 10^{-13}$	$1.8668 \cdot 10^{-3}$	$8.116 \cdot 10^{-14}$
$k_2$	$2.2859 \cdot 10^{-2}$	$3.628 \cdot 10^{-14}$	$5.0124 \cdot 10^{-3}$	$1.536 \cdot 10^{-13}$
$k_4$	$5.7148 \cdot 10^{-2}$	$2.845 \cdot 10^{-14}$	$1.0724 \cdot 10^{-2}$	$8.110 \cdot 10^{-14}$
$k_6$	$9.2702 \cdot 10^{-2}$	$2.151 \cdot 10^{-14}$	$2.4038 \cdot 10^{-2}$	$5.760 \cdot 10^{-14}$
$k_8$	$1.1587 \cdot 10^{-1}$	$1.613 \cdot 10^{-14}$	$4.0373 \cdot 10^{-2}$	$2.725 \cdot 10^{-14}$
$k_{10}$	$1.2723 \cdot 10^{-1}$	$5.898 \cdot 10^{-15}$	$5.4845 \cdot 10^{-2}$	$1.784 \cdot 10^{-14}$

Taking into consideration the error due to the use of floating-point computations, the result of such a relation must approach the null vector. Table 5.5 reports the difference in absolute value of the  $n$ th-mode of  $k$ -eigenvalues with respect to the Modak benchmark values, and the first element of the numerical solution vector corresponding to the verification for the eigenvectors expressed by relation (5.3). Such a verification is well satisfied.

### $\gamma$ - eigenvalues assessments

The benchmark tests conducted for the  $k$  eigenvalue case is here presented for the  $\gamma$  eigenvalue results. In order to compare the values obtained by the implemented code with the ones provided by Modak in [30] referred to the  $c$  eigenvalue, the expression (5.2) is exploited. Nuclear data (Table 5.1) and methodologies are the ones reported in the previous section. The reference  $c_0$  in case of thinner slab dimension, 1 mfp, is evaluated with  $S_{256}$  and 100 meshes. In case of thicker slab, benchmark result refers to  $S_{64}$  and 100 meshes.

Table 5.6 shows the fundamental  $c$  eigenvalue, denoted as  $c_0$ , evaluated for two slab thicknesses with increasing orders of  $P_N$  approximation, with the imposition of Mark and Marshak boundary conditions respectively.

The trend yet outlined for the  $k$ -eigenvalues calculations can be individuated again for the  $c$  eigenvalue case, corresponding to the  $\gamma$  eigenvalues computations implemented in the thesis, although a difference arises in terms of magnitude of variations individuated. Indeed, still a convergence to an accuracy up to 3 decimal places is obtained with respect to the reference value by means of  $P_{31}$  approximation, but the fundamental mode evaluated with lower-orders of  $P_N$  approximation are better than the corresponding fundamental  $k$ -eigenvalues presented in the previous paragraph. The  $c_0$  value evaluated with  $P_3$  shows an accuracy up to the first decimal which is not reached in the case of  $k_0$ , for the same set of nuclear data.

Furthermore, Marshak boundary conditions still indicate a faster convergence to the reference value with respect to Mark type, but with a lower impact in terms of result significant

Table 5.6: Convergence of  $c_0$  eigenvalue to benchmark values at increasing orders of  $P_N$  approximation with Mark and Marshak boundary conditions. Benchmark values by Modak [30] refer to 100 meshes and  $S_{256}$  for 1 mfp slab, while  $S_{64}$  in case of 8 mfp slab.

$P_N$	1 mfp		8 mfp	
	$c_{0,Modak} = 1.61537$		$c_{0,Modak} = 1.03640$	
	Mark	Marshak	Mark	Marshak
$P_3$	1.685679	1.653339	1.036680	1.036493
$P_7$	1.621573	1.620033	1.036458	1.036422
$P_{15}$	1.617339	1.616080	1.036415	1.036407
$P_{31}$	1.615835	1.615559	1.036405	1.036403

digits. In the case of slab thickness equal to 8 mfp, the fundamental mode presents an accuracy of 4 decimals yet with  $P_3$  approximation and Marshak boundary conditions, reaching the fifth decimal with  $P_{15}$ . Once again, a faster convergence is expected in slab characterized by thicker thickness due to the reduced leakage of neutrons from the boundary.

In the case of slab of 8 mfp thick, with Mark boundary conditions imposed, the convergence at increasing orders of accuracy of the  $P_N$  approximation, as regards higher-mode eigenvalues, is shown in Table 5.7. As expected, the accuracy increases at increasing orders of  $P_N$  approximations, and higher-modes accuracy is worst than that of the fundamental eigenvalue. A better convergence can be reached by both further refining the spatial mesh or with higher  $P_N$  approximations. However, being the model analyzed a first-order model, a finer mesh implies larger dimensions of the problem matrices and higher computational costs to the eigenvalue solver. A compromise between problem dimensions and computational costs requirement, specially in the perspective of the application of such a model to multigroup problems in two- or three-dimensional configurations, is required.

Nevertheless, a quite good accuracy is accomplished yet with  $P_{15}$  approximation. The fundamental mode presents a four decimal places accuracy with respect to the reference value. Looking at higher-modes, the last three even-modes,  $c_6$ ,  $c_8$  and  $c_{10}$ , show an inverse trend in the convergence behavior at increasing orders of  $P_N$  approximation. Indeed, values at  $P_{15}$  result nearer, in terms of relative distance, to the reference values found by Modak. This unexpected behavior may be related to the increment of the dimensions of the sparse matrices input of the eigenvalue solver which increase the difficult the algorithm convergence. Since an accurate analysis of the algorithm implemented by ARPACK is not treated in this master thesis, and the *eigs* function provided in MATLAB has been used as a black box eigenvalue solver, only qualitatively comments on the evaluated values can be drafted. Conversely, this trend may be also related merely to the different angular approximation method exploited in the implemented code,  $P_N$ , and the one used in reference studies,  $S_n$ .

Table 5.7: Even higher-order  $c$ -eigenvalues convergence to benchmark values at increasing orders of  $P_N$  approximation with Mark boundary conditions. Benchmark values by Modak [30] refer to 100 meshes and  $S_{256}$  for 1 mfp slab, while  $S_{64}$  in case of 8 mfp slab.

8 mfp					
$c$ -mode	$P_3$	$P_7$	$P_{15}$	$P_{31}$	Modak (1995)
$c_0$	1.0366802	1.0364586	1.0364153	1.0364052	1.0364038
$c_2$	1.2953501	1.2903187	1.2898599	1.2897640	1.289806
$c_4$	1.7248971	1.6806525	1.6784150	1.6781250	1.678464
$c_6$	2.3073922	2.1339097	2.1220904	2.1214269	2.12257
$c_8$	3.0602775	2.6353826	2.5900417	2.5884349	2.5914
$c_{10}$	3.997279	3.1935801	3.0717744	3.0671765	3.072

Table 5.8: Nuclear data adopted in benchmark assessments for  $\alpha$ -eigenvalue case.

Parameter	Value	
Total cross-section [ $\text{cm}^{-1}$ ]	$\Sigma_t$	1.0
Scattering cross-section [ $\text{cm}^{-1}$ ]	$\Sigma_s$	1.0
Neutron velocity [ $\text{cm/s}$ ]	$v$	1.0
Slab thickness range [mfp]	a	1-10

## $\alpha$ -eigenvalues assessments

In the  $\alpha$ -eigenvalue case, benchmark tests have been performed with comparisons analogous to those conducted in [27], [32] and [34] with respect to the accurate results provided by Dahl et al. [35] for different homogeneous slab thicknesses.

In [27], prompt  $\alpha$  eigenvalues are calculated with a least-squared functional together with spatial finite elements and the spherical harmonics method to treat the angular discretization. In order to compare the obtained results with those previously found by Dahl et al. [35] with semi-analytical methods, a homogeneous, mono-energetic, purely scattering slab is considered. The presented results concern the dominant  $\alpha$  eigenvalues for mono-energetic slabs with size ranging from 1 to 25 mfp. In the present thesis, smaller slab dimensions have been considered and the range of investigation was limited to thickness equal to 10 mfp. The  $\alpha$ -eigenvalues are provided in a dimensionless version obtained as  $\alpha/v\Sigma_s$ , where  $v$  is the neutron velocity.

Nuclear data exploited in the benchmark tests for  $\alpha$ -eigenvalues computations are summarized in Table 5.8.

A comparison with both results provided in [27] and [34] has been performed but, for sake of brevity, only some of the obtained results are reported in this section. Specifically, Table 5.9 shows the dimensionless  $\alpha$ -eigenvalues obtained by the implemented code with  $P_{15}$  and  $P_{31}$  increasing slab thicknesses, ranging from 1 mfp to 10 mfp, with the application of

Table 5.9: Dimensionless  $\alpha$ -eigenvalue fundamental and higher-modes convergence with respect to results by Dhal et al with semi-analytical methods.  $P_N$  refers to Marshak boundary conditions imposition.

a	$\alpha$ -mode	$P_{15}$	$P_{31}$	Dhal et al. (1983)
1	$\alpha_0$	$-6.11749 \cdot 10^{-1}$	$-6.08609 \cdot 10^{-1}$	$-6.08072 \cdot 10^{-1}$
2	$\alpha_0$	$-2.96981 \cdot 10^{-1}$	$-2.96799 \cdot 10^{-1}$	$-2.96728 \cdot 10^{-1}$
	$\alpha_0$	$-8.11127 \cdot 10^{-2}$	$-8.10983 \cdot 10^{-2}$	$-8.10933 \cdot 10^{-2}$
5	$\alpha_1$	$-3.41391 \cdot 10^{-1}$	$-3.41259 \cdot 10^{-1}$	$-3.41216 \cdot 10^{-1}$
	$\alpha_2$	$-8.39057 \cdot 10^{-1*}$	$-8.41633 \cdot 10^{-1}$	$-8.34837 \cdot 10^{-1}$
	$\alpha_0$	$-2.53530 \cdot 10^{-2}$	$-2.53508 \cdot 10^{-2}$	$-2.53520 \cdot 10^{-2}$
	$\alpha_1$	$-1.02993 \cdot 10^{-1}$	$-1.02982 \cdot 10^{-1}$	$-1.02978 \cdot 10^{-1}$
10	$\alpha_2$	$-2.37991 \cdot 10^{-1}$	$-2.37954 \cdot 10^{-1}$	$-2.37942 \cdot 10^{-1}$
	$\alpha_3$	$-4.40001 \cdot 10^{-1}$	$-4.39858 \cdot 10^{-1}$	$-4.39814 \cdot 10^{-1}$
	$\alpha_4$	$-7.33540 \cdot 10^{-1}$	$-7.24568 \cdot 10^{-1}$	$-7.24185 \cdot 10^{-1}$

Marshak boundary conditions. The results by Dahl et al. [35] are reported for the comparison. As can be seen by Table 5.9, only the real eigenvalues outcomes of the application of IRAM are listed, except for the second-order mode in case of 5 mfp thickness which has presented a small imaginary part at  $P_{15}$ , indicated with an asterisk in the table.

As concern the accuracy, the same trends highlighted in [27] can be observed in the reported values. In particular, values accurate up to three decimal places are found with  $P_{31}$  approximation and Marshak boundary conditions. As a difference with respect to the  $k$ -eigenvalue case, higher-modes do not present worsen accuracy when founded. Lathouwers [27] relates the improvement to a sufficiently fine mesh, previously justified also by the dedicated grid independence study reported in Sect 5.1. As a consequence, the discriminating factor in the accuracy issue, for the case of  $\alpha$  eigenvalue, consists in the order of the  $P_N$  approximation adopted for the computation.

Lastly, Table 5.10 reports the results of the particular case of slab thickness equal to 5 mfp in comparison to those founded by Lathouwersin [27] at the same  $P_N$  approximations exploited. The occurrence of a small imaginary part as concern the second-order modes evaluated with  $P_{15}$  is experienced also in that case. As the  $P_N$  approximation is increased in accuracy, the corresponding eigenvalue is founded as real.

In conclusion, as regards the  $\alpha$ -eigenvalue case, even though results present an evident lower accuracy with respect to those previously computed by Dahl et al. [35], five decimals accurate, they show the same accuracy level reached by several comparable studies. An analogous consideration can be argued also for the previously presented eigenvalue types.

Table 5.10: Comparison of dimensionless  $\alpha$ -eigenvalue higher-modes obtained for a 5 mfp thick slab with respect to the reference values provided by Lathouwers [27], both obtained with  $P_N$  approximation.

5 mfp				
$\alpha$ -mode	$P_{15}$		$P_{31}$	
	Lathouwers (2003)		Lathouwers (2003)	
$\alpha_0$	$-8.11127 \cdot 10^{-2}$	$-8.12167 \cdot 10^{-2}$	$-8.10983 \cdot 10^{-2}$	$-8.12030 \cdot 10^{-2}$
$\alpha_1$	$-3.41391 \cdot 10^{-1}$	$-3.41493 \cdot 10^{-1}$	$-3.41259 \cdot 10^{-1}$	$-3.41379 \cdot 10^{-1}$
$\alpha_2$	$-8.39057 \cdot 10^{-1*}$	$-8.39587 \cdot 10^{-1*}$	$-8.41633 \cdot 10^{-1}$	$-8.38878 \cdot 10^{-1}$

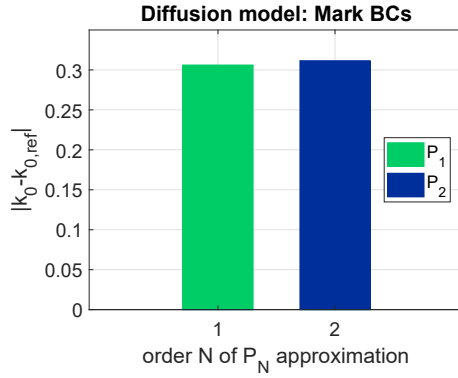
### 5.3 Odd- and even-order $P_N$ approximations comparison

The implementation of a numerical code able to automatize the solution of the different neutron transport eigenproblems with the application of the  $P_N$  approximation in its most general case, has given the possibility of a comparison between odd-orders and even-orders of the angular approximation. As yet mentioned, even-orders  $P_N$  do not represent an increment in the accuracy order of the approximation with respect to the odd-order ones. The  $P_1$  approximation, which corresponds to the diffusion approximation, is first-order accurate. The  $P_2$  approximation still consists in diffusion and the order of accuracy is the same of  $P_1$ . Hence, to obtain a second-order accurate  $P_N$  approximation, one has to consider  $P_3$  approximation [5],[8].

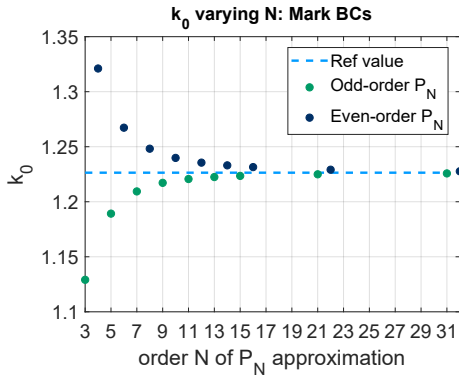
Nevertheless, as briefly shown in Sect. 4.2 discussing the  $P_N$  approximation spatial discretization scheme,  $P_2$  still leads to a diffusion model characterized by a second-order differential equation, but with a different diffusion coefficient with respect to that of the  $P_1$  approximation. Therefore, the influence of the difference in the coefficients of even-order  $P_N$  approximations has been investigated, in the present work, through the comparison of the neutron transport eigenproblems solutions developed by means of increasing orders of the  $P_N$  approximation, both odd and even, with the imposition of Mark and Marshak boundary conditions.

#### 5.3.1 Fundamental eigenvalue convergence

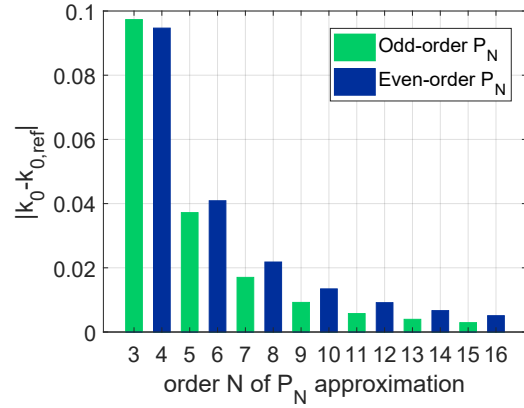
This section is devoted to the presentation of the results obtained in the implementation of both odd- and even-order of  $P_N$  approximations for the neutron transport equation in its eigenvalue forms. The fundamental eigenvalue of the different eigenvalue-spectra, computed by means of IRAM implemented by the ARPACK package in MATLAB for increasing orders of  $P_N$  approximation, is investigated in its convergence behavior to a reference values, as function of the order of the angular expansion.



(a) Diffusion absolute error.



(b)  $k_0$ .



(c)  $P_N$  absolute error.

Figure 5.3: Fundamental multiplication factor convergence at increasing orders of  $P_N$  approximation with imposition of Mark boundary conditions for the case of 1 mfp slab. The associated relative error with respect to the reference value, 1.2264, is reported for  $P_1$  and  $P_2$  in (a), and for higher-order  $P_N$  in (c). In (b),  $k_0$  convergence trends are reported for  $P_N$  ranging from  $P_3$  to  $P_{32}$ .

The obtained numerical results are first reported for the case of the  $k$  eigenvalue, both for Mark and Marshak boundary conditions, and then, the other eigenvalue-types results follow with an analogous presentation.

## k-eigenvalue

First, the fundamental multiplication factor, evaluated with respect to the benchmark value for a multiplying homogeneous slab reactor exploited in the benchmark assessments based upon the results provided by Modak in [30] for a 1 mfp thick slab, are reported for increasing orders of  $P_N$  approximation, ranges from  $P_1$  to  $P_{32}$ , with Mark boundary conditions imposed.

The material properties used for the computation are summarized in Table 5.1, previously reported. The slab thickness chosen is equal to 1 mfp, the most critical in terms of convergence velocity with respect to the two slab thicknesses investigated in the benchmark tests for  $k$

eigenvalue.

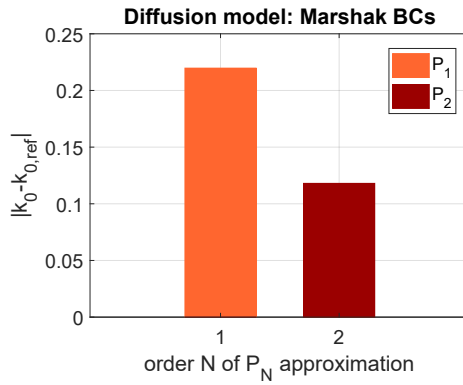
In the top graphic of Figure 5.3, the absolute error between the computed fundamental  $k$  eigenvalue and the reference value equal to 1.2264 is reported for the case of  $P_1$  and  $P_2$  approximation. As shown in figure, the  $P_1$  approximation is slightly more accurate than  $P_2$ . As shown by the figure, a convergence to the reference value, in the case considered equal to 1.2264, is confirmed for increasing order of  $P_N$  approximations.

Then, as regards higher-order approximations, a similar asymptotically convergence behavior may be traced for both odd-order and even-order  $P_N$ , as shown in the left bottom part of Figure 5.3. Specifically, while odd-order  $P_N$  approach the benchmark value from lower estimates, even-order  $P_N$  approach it from higher ones. In general, as yet mentioned in the comments to benchmark results, a significantly slow convergence may be noted in the case of  $k$  eigenvalue, with particularly rough estimations of the fundamental multiplication factor at low-order  $P_N$  approximation. As a consequence, in order to reach an acceptable accuracy in the results, especially high-order of  $P_N$  must be employed. Nevertheless, this discussion is made only in reference to the available benchmark result obtained with a  $S_{256}$  approximation.

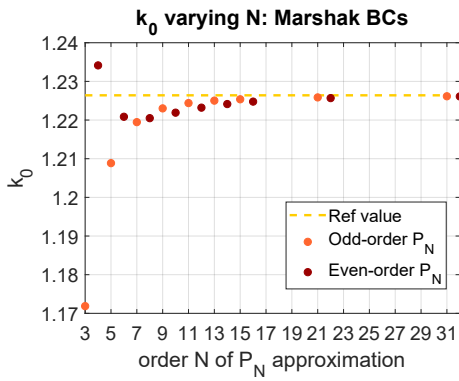
Considering the quite wide variation presented by the fundamental multiplication factor results evaluated with  $P_3$  and  $P_4$  approximation, a reasons of the great distance may be related to the superficial use of the eigensolver exploited for the eigenvalue evaluation in the implemented code. In recent years several studies and research efforts have been dedicated to the investigation of the different algorithms for the solution of eigenvalue problems and diverse strategies have been individuated to obtain a better convergence of results for each algorithm, based upon the specific eigenproblem treated. These strategies are out of the scope of the present thesis, but they are individuated as a possible future field of investigation related both to this specific thesis work, and more in general for criticality calculations in neutron transport.

Then, the distance between the computed fundamental multiplication eigenvalue  $k_0$  and the reference value by Modak [30] in absolute value at a fixed orders of  $P_N$ , is graphically displayed on the right of the bottom part of Figure 5.4. A quite surprising result is obtained in case of  $P_4$  approximation, the corresponding  $k_0$  computed is nearer to the reference value with respect to the estimate given by  $P_3$  approximation. However, if one looks to the percentage improvement, it consists in 0.2%, representing only a slight enhancement. Starting from  $P_5$  instead, odd-order  $P_N$  approximations reclaim their role of more accurate approximations, with an average distance in the result evaluation, from the corresponding even-order approximations, equal to 0.3%.

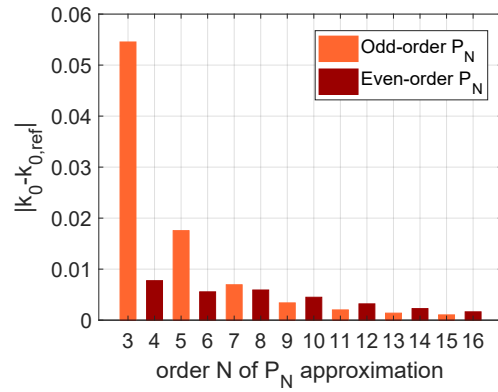
A similar result to that found for  $P_4$  has been obtained for lower-order of  $P_N$  approximations, specifically  $P_1$  and  $P_2$ , in an application of the spherical harmonics method to Marshak wave problem with Marshak boundary conditions, both for time-dependent [36] and steady-state



(a) Diffusion absolute error.



(b)  $k_0$ .



(c)  $P_N$  absolute error.

Figure 5.4: Fundamental multiplication factor convergence at increasing orders of  $P_N$  approximation with imposition of Marshak boundary conditions for the case of 1 mfp slab. The associated relative error with respect to the reference value, 1.2264, is reported for  $P_1$  and  $P_2$  in (a), and for higher-order  $P_N$  in (c). In (b)  $k_0$  convergence trends are reported for  $P_N$  ranging from  $P_3$  to  $P_{32}$ .

case [37].

Then, the same procedure adopted for the study of the convergence behavior of the fundamental multiplication factor  $k_0$  for increasing orders of  $P_N$  has been then conducted in the case of Marshak boundary conditions imposition. Some evident differences with respect to the case of Mark boundary conditions can be individuated looking to Figure .5.4.

The same range of variation of the order of  $P_N$  approximation is reported for Marshak boundary conditions case. As shown in figure, different convergence behaviors can be traced in the case of odd-order and even-order  $P_N$ . Indeed, while the odd-order  $P_N$  with Marshak conditions follow the same asymptotically type trend to the reference value yet individuated in case of Mark boundary conditions, a substantial difference is represented by the case of even-order  $P_N$ . Indeed, while  $k_0$  evaluated with  $P_4$  show the same approach to the reference value displayed for Mark boundary conditions case, a smaller value with respect to reference

is computed with  $P_6$  and  $P_7$ . From  $P_8$ , the approaching trend aligns with the one presented by odd-order  $P_N$ .

Looking then to the figures showing the associated absolute error, on the top and bottom right side of Figure 5.4, a trend similar to that individuated for  $P_4$  with Mark boundary conditions, can be individuated for  $P_2$ ,  $P_4$ ,  $P_6$  and  $P_8$  approximation in this case. However, while in case of Mark condition the improvement revealed by  $P_4$  with respect to  $P_3$  presents a small magnitude, in this case  $P_2$  shows a quite great enhancement in  $k_0$  evaluation and  $P_4$  with Marshak boundary conditions leads to an accuracy up to the first decimal place not reached by  $P_3$ . The faster convergence is visible also for  $P_6$  and  $P_7$ , but with reduced extents. From  $P_9$ , odd-order approximations converge better than even-order one.

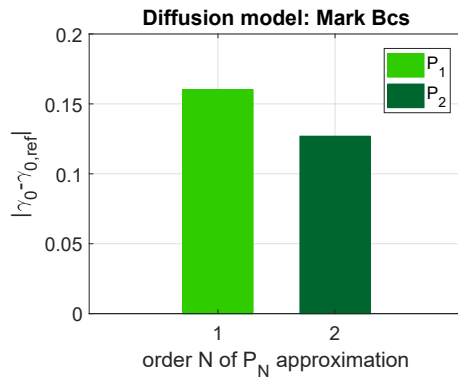
### $\gamma$ eigenvalue

The discussion about the results obtained in the case of  $\gamma$  eigenvalue are analogous to those obtained in the  $k$  eigenvalue case, as expected since the similar nature of the two multiplicative eigenvalues of the neutron transport equation. The study has been conducted applying the same procedure adopted for the previously presented eigenvalue-type. The reference value for the fundamental multiplication factor per collision  $\gamma_0$  used is the one exploited in the benchmark test reported in Sect. 5.2. In the benchmark assessments, the results referred to the  $\gamma$  eigenvalue have been reported as the corresponding  $c$ -eigenvalues. In this section, the  $\gamma$  eigenvalue in the form originally considered in the thesis is presented.

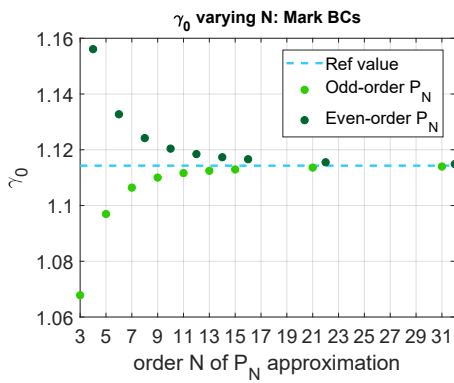
Figure 5.5 shows the convergence to the reference value equal to 1.1143 for a multiplying homogeneous slab of 1 mfp thickness computed for increasing orders of the angular approximation, with Mark boundary conditions. The corresponding absolute distance between the computed  $\gamma_0$  and the benchmark value is reported.

Then, in the Figure. 5.6, the values obtained with Marshak boundary conditions are graphically displayed.

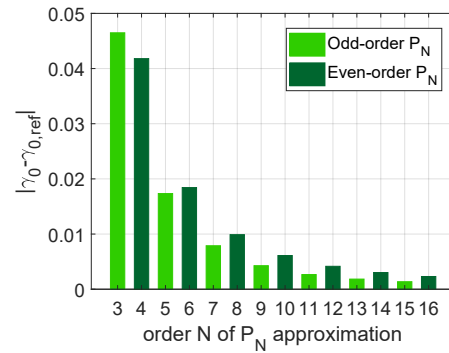
As for the case of the effective multiplication factor per fission, the same trends of convergence both with Mark and Marshak boundary conditions. However, a difference arises in the variation range with respect to the reference value for low-order  $P_N$ , which is more narrow than the one recorded in the  $k$  eigenvalue case. As a consequence, a faster convergence for increasing orders of  $P_N$  is noted. In particular, for  $N = 4$  and Marshak boundary conditions, a result accurate to two decimals place is obtained. Another remarkable difference is related to lower even-order approximations which present better convergence with respect to the corresponding odd-order  $P_N$ . Specifically, in case of Mark boundary conditions, both  $P_2$  and  $P_4$  present a slightly better convergence with respect to  $P_1$  and  $P_3$ , respectively. In case of Marshak type conditions, the better convergence is extended to  $P_8$ .



(a) Diffusion absolute error.

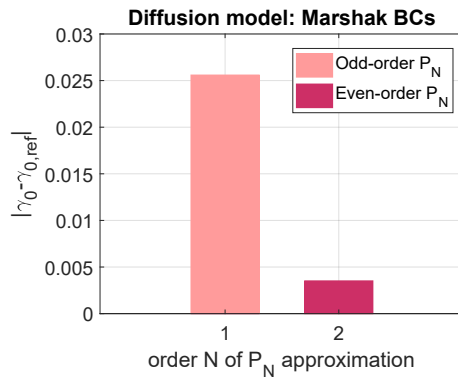


(b)  $\gamma_0$ .

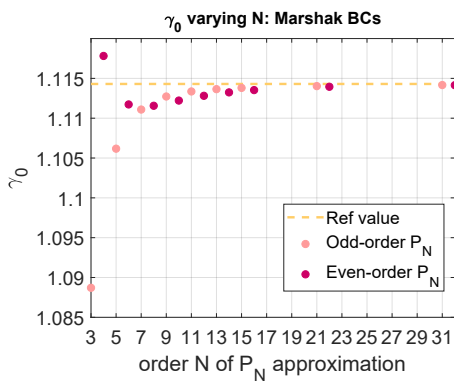


(c)  $P_N$  absolute error.

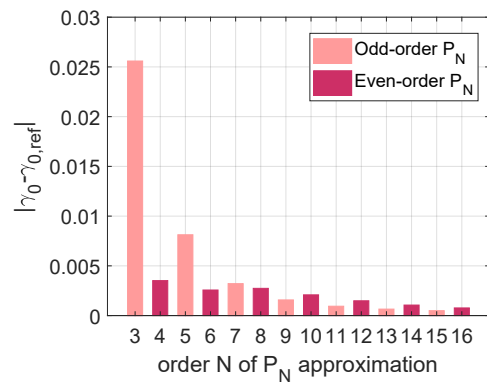
Figure 5.5: Fundamental multiplication factor per collision convergence at increasing orders of  $P_N$  approximation with imposition of Mark boundary conditions for the case of 1 mfp slab. The associated relative error with respect to the reference value, 1.1143, is reported for  $P_1$  and  $P_2$  in (a), and for higher-order  $P_N$  in (c). In (b)  $\gamma_0$  convergence trends are reported for  $P_N$  ranging from  $P_3$  to  $P_{32}$ .



(a) Diffusion absolute error.



(b)  $\gamma_0$ .



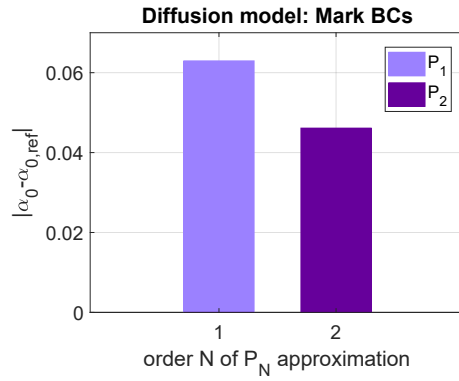
(c)  $P_N$  absolute error.

Figure 5.6: Fundamental multiplication factor per collision convergence at increasing orders of  $P_N$  approximation with imposition of Marshak boundary conditions for the case of 1 mfp slab. The associated relative error with respect to the reference value, 1.1143, is reported for  $P_1$  and  $P_2$  in (a), and for higher-order  $P_N$  in (c). In (b)  $\gamma_0$  convergence trends are reported for  $P_N$  ranging from  $P_3$  to  $P_{32}$ .

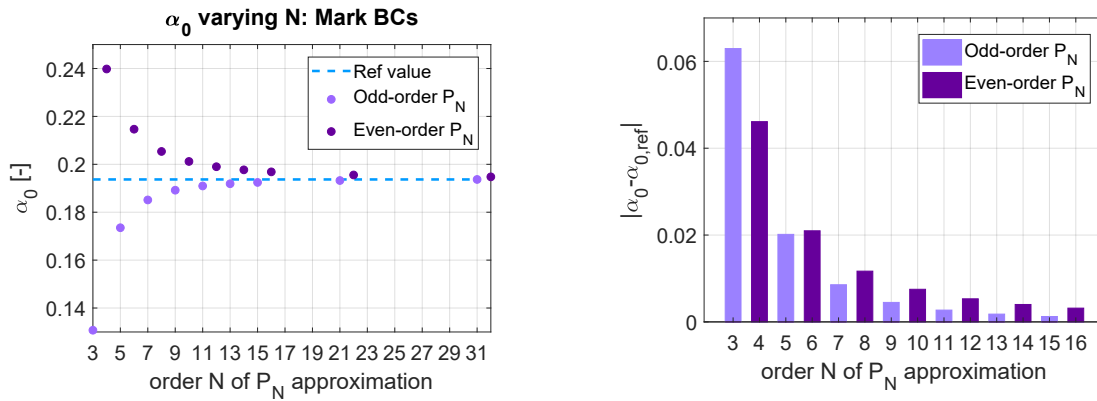
## $\alpha$ eigenvalue

For sake of brevity, as done for  $\gamma$  eigenvalue, only the differences arising with respect to the  $k$  or  $\gamma$  eigenvalue case results are discussed.

For the  $\alpha$  eigenvalue, in order to be consistent with the system characteristics adopted in the previous eigenvalue-type calculations, a difference set of nuclear data has been adopted for the convergence study with respect to those exploited in benchmark section. The homogeneous and multiplying slab of thickness equal to 1 mfp is considered. The values of the cross-sections characteristic of the problem analyzed are reported in Table 5.1. As reference value, the fundamental time eigenvalue computed with  $P_{41}$ ,  $\alpha_0 = 0.19368$ , is used. The dimensionless version of  $\alpha_0$ , evaluated as  $\alpha_0/v\Sigma_t$ , is considered.



(a) Diffusion absolute error.



(b)  $\alpha_0$ .

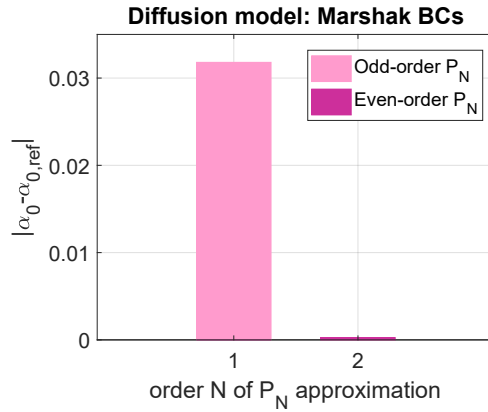
(c)  $P_N$  absolute error.

Figure 5.7: Dimensionless fundamental time eigenvalue convergence at increasing orders of  $P_N$  approximation with imposition of Mark boundary conditions for the case of 1 mfp slab. The associated relative error with respect to the reference value,  $\alpha_0 = 0.19368$ , is reported for  $P_1$  and  $P_2$  in (a), and for higher-order  $P_N$  in (c). In (b)  $\alpha_0$  convergence trends are reported for  $P_N$  ranging from  $P_3$  to  $P_{32}$ .

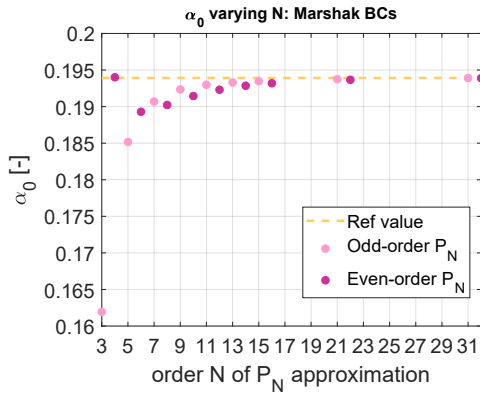
Figure 5.7 displays the convergence behavior for increasing orders of  $P_N$  with Mark boundary conditions imposed, of the fundamental time eigenvalue and the corresponding

error, at fixed  $P_N$ , with respect to the reference value of  $\alpha_0$ . In this case, as for  $\gamma$  eigenvalue,  $P_2$  and  $P_4$  approximations show a better convergence with respect to  $P_1$  and  $P_2$ .

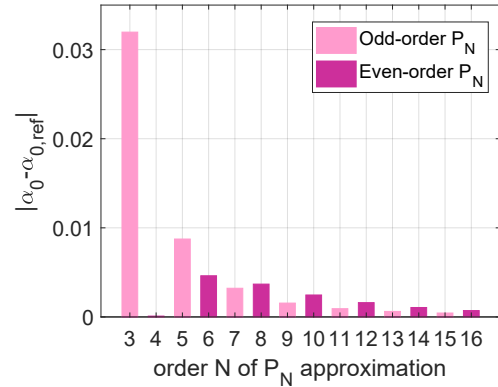
The results obtained with Marshak boundary conditions are shown in Figure 5.8. The same behavior observed in the previous eigenvalue-types may be individuated also in this case, with the better convergence referring to even-order  $P_N$  yet meet for  $\gamma_0$ . Specifically, the  $\alpha_0$  obtained with  $P_2$ ,  $P_4$  and  $P_6$  shows a better accuracy in comparison to  $P_1$ ,  $P_3$  and  $P_5$ , respectively.



(a) Diffusion absolute error.



(b)  $\alpha_0$ .



(c)  $P_N$  absolute error.

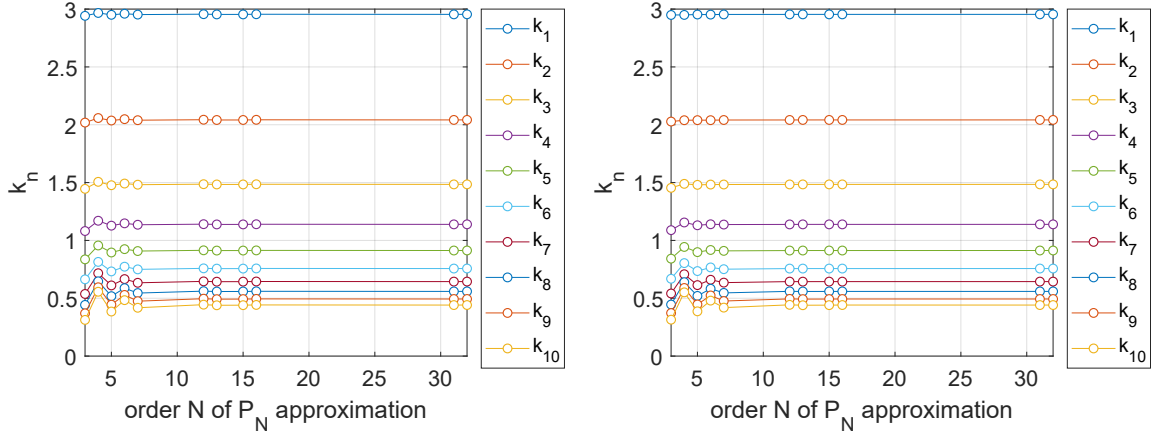
Figure 5.8: Dimensionless fundamental time eigenvalue convergence at increasing orders of  $P_N$  approximation with imposition of Marshak boundary conditions for the case of 1 mfp slab. The associated relative error with respect to the reference value,  $\alpha_0 = 0.19368$ , is reported for  $P_1$  and  $P_2$  in (a), and for higher-order  $P_N$  in (c). In (b)  $\alpha_0$  convergence trends are reported for  $P_N$  ranging from  $P_3$  to  $P_{32}$ .

### 5.3.2 Higher-order modes convergence

The graphical representation of a portion of the eigenvalue spectrum computed at increasing orders of  $P_N$  approximation is reported in this section. For each eigenvalue type, the ten

Table 5.11: Nuclear data adopted in higher-order modes computations for  $k$  and  $\gamma$  eigenvalue case.

Parameter		Value
Total cross-section [ $\text{cm}^{-1}$ ]	$\Sigma_t$	1.0
Scattering cross-section [ $\text{cm}^{-1}$ ]	$\Sigma_s$	0.8
Production cross-section [ $\text{cm}^{-1}$ ]	$\nu\Sigma_f$	1.0
Slab thickness [mfp]	$a$	8



(a) Mark boundary conditions.

(b) Marshak boundary conditions.

Figure 5.9: Convergence of the first ten higher-orders of the  $k$  eigenvalue at increasing orders of  $P_N$  approximation, evaluated with Mark (a) and Marshak (b) boundary conditions for 8 mfp slab.

first higher-order modes are presented in order to analyze the nature of the spectrum. In the implemented code, 20 eigenvalues have been required to the eigensolver.

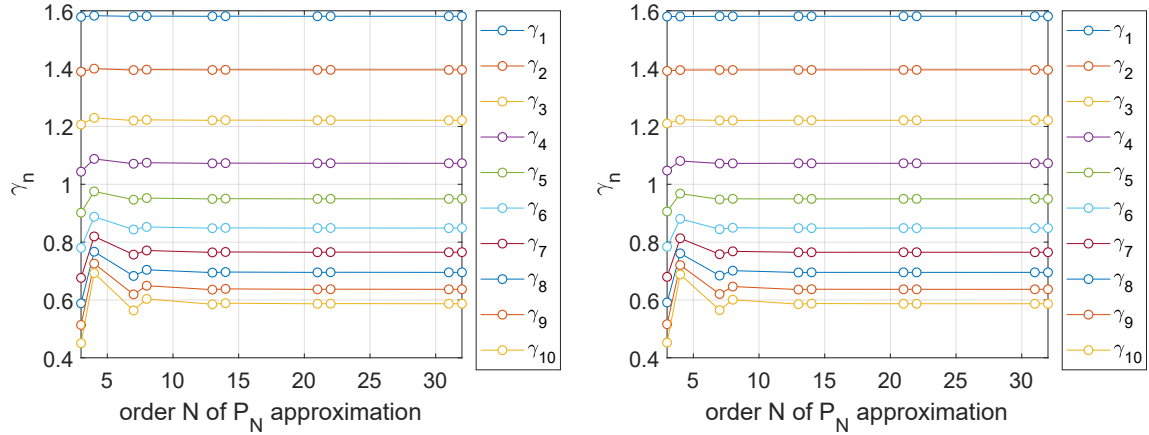
The nuclear data set of the case for which results are presented is reported in Table 5.11, referred to  $k$  and  $\gamma$  eigenvalue.

### k eigenvalue

For the case of a mono-energetic slab with isotropic scattering, all the computed discrete eigenvalues, result of the  $k$  eigenvalue problem develop with  $P_N$ , are real. Figure 5.9 shows the first part of the partial spectrum required to the eigensolver. The fundamental eigenvalue  $k_0$  is not reported. In figure, the different higher-order eigenvalues computed at increasing orders of  $P_N$  approximation are presented for the case of Mark and Marshak boundary conditions. As regards boundary conditions, Marshak boundary conditions generally work better at lower-orders of  $P_N$ , then Mark boundary conditions present a faster convergence.

As the mode order increases, a more evident oscillation in convergence occurs and higher-orders of  $P_N$  are needed to achieve a reasonable accuracy, proof of the incremented difficult of the eigensolver in their computation.

## $\gamma$ eigenvalue



(a) Mark boundary conditions.

(b) Marshak boundary conditions.

Figure 5.10: Convergence of the first ten higher-order of the  $\gamma$  eigenvalue at increasing orders of  $P_N$  approximation, evaluated with Mark (a) and Marshak (b) boundary conditions for 8 mfp slab.

Results analogous to those found in the  $k$  eigenvalue case are obtained also for the  $\gamma$  eigenvalue. The partial discrete spectrum computed consists in all real and positive eigenvalues. The same convergence trends described for the previous eigenvalue-type may be observed in Figure 5.10, which reports the convergence at increasing orders of  $P_N$  approximation of the first ten higher-modes, both for Mark and Marshak boundary conditions.

## $\alpha$ eigenvalue

The partial  $\alpha$  eigenvalue spectrum is reported for the case yet exploited in the benchmark tests, in order to have a further validation in the investigation. The nuclear data used in the higher-modes computation are reported in Table 5.12.

First, the  $\alpha$  eigenvalue higher-modes obtained with the implemented code have proved to be both real and complex values, for any of the  $P_N$  approximation developed. The fundamental mode  $\alpha_0$ , individuated as the one with the smallest real part in modulus, has been found always as a real value. As known from theory [20], the nature of the  $\alpha$  eigenvalue

Table 5.12: Nuclear data adopted in higher-order modes computations for  $\alpha$  eigenvalue case.

Parameter		Value
Total cross-section [ $\text{cm}^{-1}$ ]	$\Sigma_t$	1.0
Scattering cross-section [ $\text{cm}^{-1}$ ]	$\Sigma_s$	0.8
Neutron velocity [ $\text{cm/s}$ ]	$v$	1.0
Slab thickness [mfp]	$a$	5

spectrum consists in a discrete part and in a continuous portion. In case of slab geometry, real discrete eigenvalues can be found only below the Corngold limit [32], which is equal to the product  $\Sigma_t v$ , with  $v$  neutron velocity, changed in sign. In this case it corresponds to -1 [27]. Eigenvalues with an algebraically larger real part constitute the continuous part of the spectrum.

Figure. 5.11 graphically displays the 20 eigenvalues outcome of the implemented code in graphics having the real axis as abscissa and imaginary axis as the ordinate one. A progress in the order of  $P_N$  approximation is considered.

In this case a great difference in what is computed by odd-order and even-order  $P_N$  may be noted. While with odd-order  $P_N$  few real eigenvalues and many complex values are obtained, in case of even-order  $P_N$  only real values are computed. Between real results, higher-modes are individuated as the real values which follow the fundamental one, obtained for any low-order  $P_N$ . In general, yet in case of odd-order  $P_N$ , a substantial increment in the computational time required by the ARPACK subroutine for the computation is observed, with respect to the previous eigenvalue-types. The increase becomes even more evident for even-order  $P_N$  in comparison to odd-order approximation.

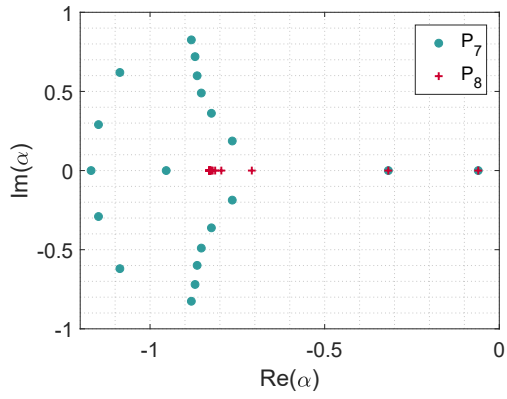
Specifically, at  $P_7$ , only two out of the twenty required eigenvalues are found as real. The corresponding even-order  $P_N$ ,  $P_8$ , converges instead to sixty out of twenty eigenvalues. The algorithm fails in the convergence in four cases out of twenty required solutions indeed. From  $P_8$  on, as regards even-order  $P_N$ , an increasing number of the required solutions do not arrive at convergence and the computational time continues to increase. Furthermore, at  $P_{42}$  a pair of complex values are obtained, warning of the increased difficult in the numerical convergence of the results.

Incrementing the odd-order of  $P_N$  leads, as expected, to an higher number of modes found as real. The more abundant complex obtained values move closer to the Corngold limit and no values of the continuous spectrum are found.

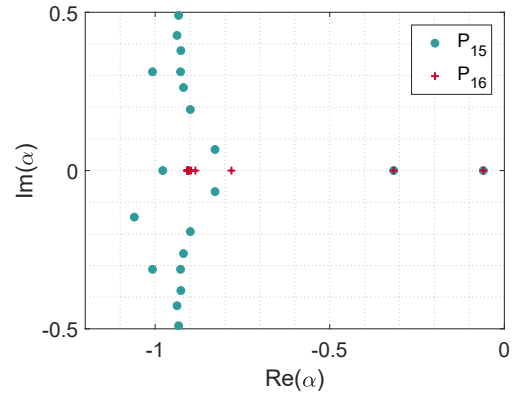
The reasons of such a different behavior observed in the eigenvalues computation with odd- or even-order  $P_N$  approximations is not clear and quite surprising. Surely, this can represents an interesting starting point for future researches. In particular, a theoretic study concerning the spectrum of the matrices obtained by the implementation of the  $P_N$  approximation for neutron transport generalized eigenvalue problems are needed to a further investigation in these numerical results.

### **$\delta$ eigenvalue**

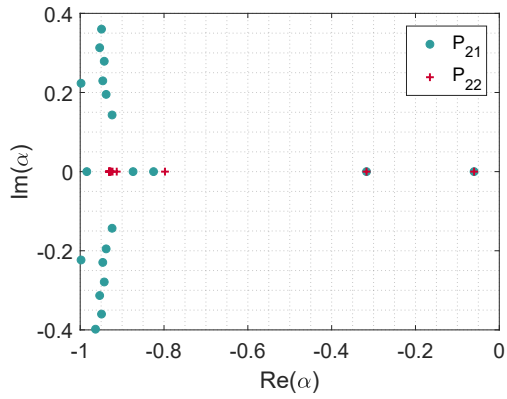
The  $\delta$  eigenvalue, which has been left from discussion until now because of the lack of information about, is here considered. Calculations have been performed with the data setting used by Modak in [30], referred to a mono-energetic, homogeneous, multiplying slab. Once



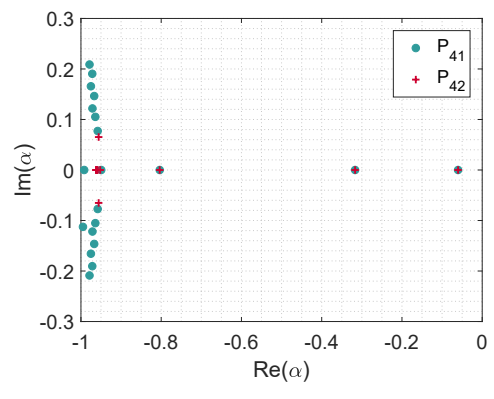
(a)  $P_7 - P_8$ .



(b)  $P_{15} - P_{16}$ .



(c)  $P_{21} - P_{22}$ .



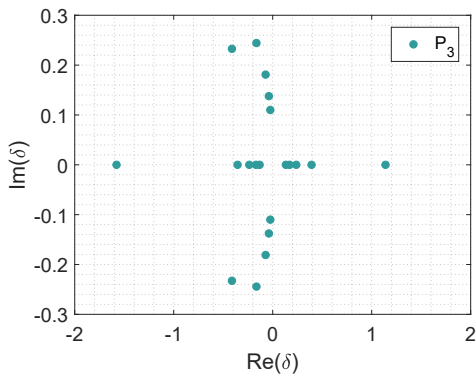
(d)  $P_{41} - P_{42}$ .

Figure 5.11: Dimensionless time eigenvalue partial discrete spectrum computed at increasing orders of  $P_N$  approximation, both odd and even, with imposition of Mark boundary conditions for the case of a mono-energetic purely scattering slab of 5 mfp thickness.

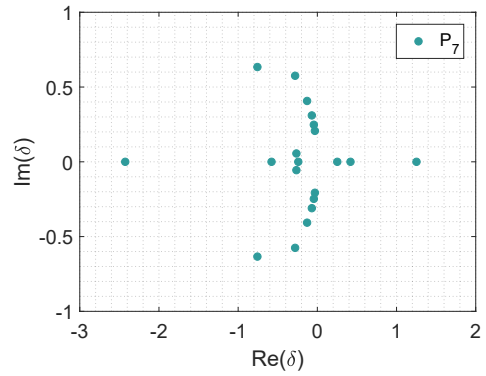
again, data are summarized in Table 5.1. Results are reported for the case of a 1 mfp thick slab, for increasing orders of  $P_N$  approximation with Mark boundary conditions applied.

First of all, due to the formulation of the generalized  $\delta$  eigenvalue problem developed, presented in Sect. 2.4, the implementation of the even-order  $P_N$  leads to singular matrices in its discretized version. As a consequence, the eigenproblem in this formulation can not be solved and only odd-order  $P_N$  have been considered.

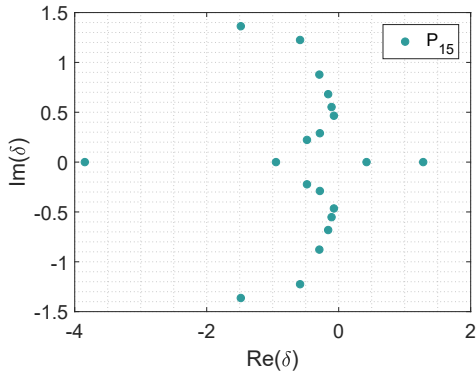
In the following analysis, the fundamental effective density factor  $\delta_0$  is treated as part of the discrete spectrum obtained.



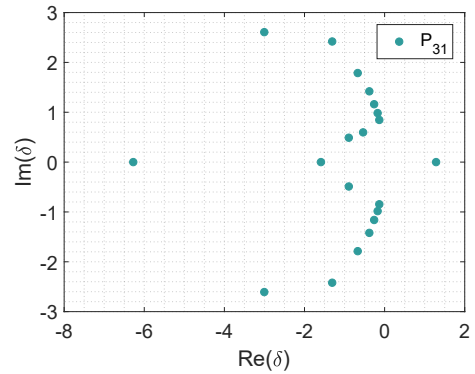
(a)  $P_3$  approximation.



(b)  $P_7$  approximation.



(c)  $P_{15}$  approximation.



(d)  $P_{31}$  approximation.

Figure 5.12: Density factor,  $\delta$ , partial discrete spectrum computed at increasing orders of  $P_N$  approximation, with imposition of Mark boundary conditions for a multiplying slab of 1 mfp thickness.

Figure 5.12 shows the graphical representation of 20 discrete eigenvalues outcome of the IRAM computation, for different odd-orders of  $P_N$  approximation. Similarities with the case of the  $\alpha$  eigenvalue computations are found. Indeed, also in case of  $\delta$  eigenvalue, few real eigenvalues and many complex ones are obtained. Nevertheless, a difference arises in the convergence behavior at increasing orders of  $P_N$ . Indeed, while in case of  $\alpha$  eigenvalue for

Table 5.13: Nuclear data adopted in eigenvectors calculations for  $k$  eigenvalue.

Parameter		Value
Total cross-section [ $\text{cm}^{-1}$ ]	$\Sigma_t$	1.0
Scattering cross-section [ $\text{cm}^{-1}$ ]	$\Sigma_s$	0.9
Fission cross-section [ $\text{cm}^{-1}$ ]	$\Sigma_f$	0.1
Average number of fission neutrons [-]	$\nu$	1.2
Slab thickness [mfp]	a	5

odd-order approximations some of the eigenvalues previously founded as complex, appearing combined with the complex conjugate, coalesce in their real part, leaving apart the small imaginary component, in case of  $\delta$  eigenvalue the behavior is the one observed for even-order  $P_N$  in the  $\alpha$  eigenvalue case. This means that at increasing odd  $N$ , the number of real eigenvalues founded by the eigensolver algorithm decreases.

At  $P_{31}$ , only 3 out of the 20 required modes are found as real, which indicate a particularly slow convergence. Furthermore, the eigenvector associated to the eigenvalues found not converge to the expected solution, appearing as a parabola with upward concavity.

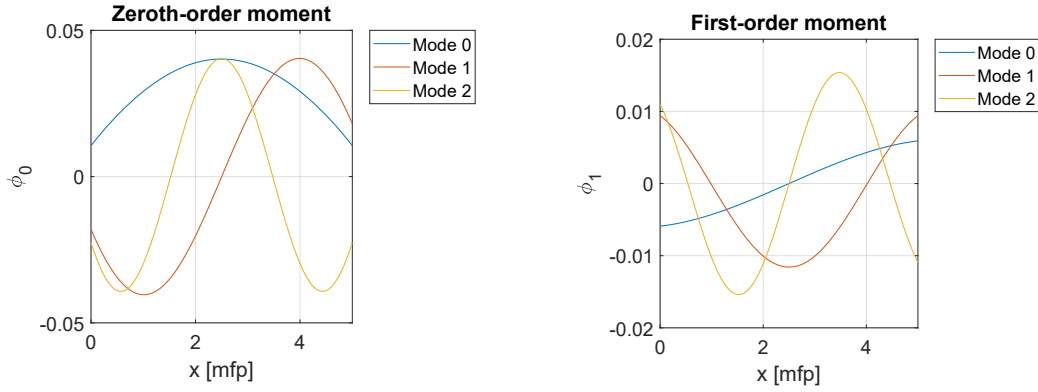
### 5.3.3 Associated eigenvectors

By way of example, the first three harmonics of the zeroth-order moment  $\phi_0$  and the first-order moment  $\phi_1$ , for the  $k$  eigenvalue case, are reported. Analogous results are obtained for the  $\gamma$  and  $\alpha$  eigenvalue, while the  $\delta$  eigenvalue case is left for future investigation due to lack of both theoretic and numerical information.

Results are presented in relation to the computed eigenvectors with  $P_3$  approximation and Mark boundary conditions. The characteristics of the system adopted for the evaluation are given in Table 5.13.

The MATLAB function *eigs* returns the eigenvectors associated to each eigenvalue required in a matrix whose columns are the respective eigenvectors. A normalization of the type  $\varphi_n/\text{norm}(\varphi_n)$  has been considered, where  $n$  indicates the specific mode. Since odd-order moments solution vector present a reduced length with respect to even-order ones, due to the use of a staggered grid in the problem spatial discretization, appropriate interpolation procedures have been performed.

Figure 5.13 shows on the left the zeroth-order moment  $\phi_0$  associated to the first three  $k$  eigenvalue modes. As expected from theory, the fundamental mode, denoted as *mode 0*, is the only solution with a constant sign over all the spatial domain. This is the only mode with a physical meaning and it is associated to the neutron total flux  $\Phi$ . Higher-order modes present oscillations of increasing frequency, with no meaning from the physical standpoint.



(a)  $\phi_0$  harmonics.

(b)  $\phi_1$  harmonics.

Figure 5.13: First three harmonics of the zeroth-order moment  $\phi_0$  evaluated for  $k$  eigenvalue problem with  $P_3$ , Mark boundary conditions in case of 5 mfp slab.

On the right of Figure 5.13, the first three harmonics of the first-order moment  $\phi_1$  are shown instead. As for  $\phi_0$ , the fundamental mode is the unique to which a physical meaning is associated, denoting the neutron current  $J$

Figure fig:angular flux show the angular flux as function of both the spatial and the angular variable. The flux has been obtained through a reconstruction performed on the fundamental solution eigenvector whose components were the discrete moments of the angular flux, based on the angular flux expression peculiar of the  $P_N$  approximation.

Some slightly negative values are assumed by the angular flux as function of the space coordinate at the slab boundaries for directions identified by  $\mu = -0.5$  and  $\mu = 0.5$ . A brief investigation is made in relation to the second-order partial derivative of the angular flux with respect to the  $x$  variable. Starting from the one-dimensional mono-energetic steady-state neutron transport equation for an homogeneous medium:

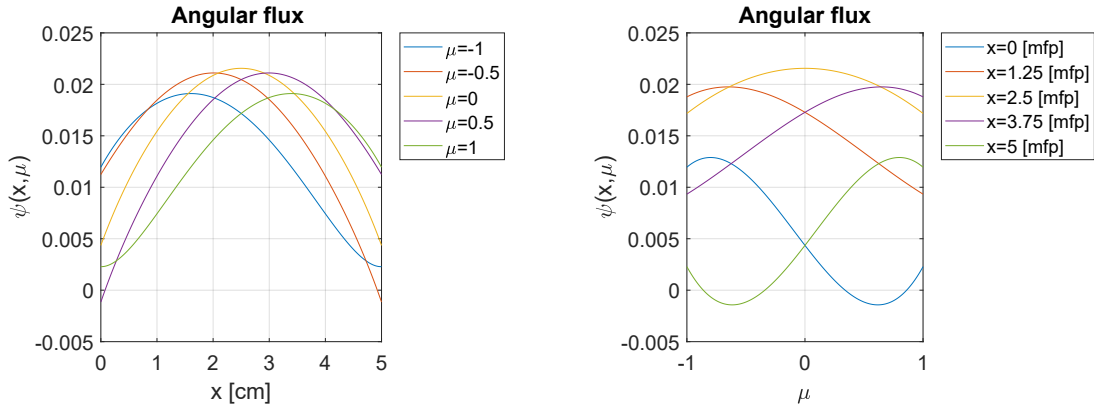
$$\mu \frac{\partial \varphi(x, \mu)}{\partial x} + \Sigma_t \varphi(x, \mu) = \frac{c}{2} \Phi(x) \quad (5.4)$$

an expression for the second-derivative of the angular flux with respect to  $x$  is derived yielding, with  $\Sigma_t = 1 \text{cm}^{-1}$ :

$$\frac{\partial^2 \varphi(x, \mu)}{\partial^2 x} = \frac{1}{\mu^2} \varphi(x, \mu) - \frac{c}{2\mu} \Phi(x) + \frac{c}{2\mu} \frac{d\Phi(x)}{dx}. \quad (5.5)$$

Hence, negative values of the angular flux are assumed as a possible outcomes.

Finally, a comparison of the total flux obtained with increasing orders of  $P_N$  approximation, both odd- and even-orders, for the system characterized by the data summarized in Table 5.13, are shown in Figure 5.15. The overall total flux solution is reported on the top, whereas two



(a) Angular flux for fixed positions.

(b) Angular flux for fixed directions.

Figure 5.14: Angular flux evaluated for  $k$  eigenvalue problem with  $P_3$ , Marshak boundary conditions in case of 5 mfp slab. On the left, the angular flux as function of  $x$ -coordinate for fixed directions is reported, while on the right the angular flux function of the direction variable for fixed  $x$ -coordinate can be observed.

details are visible in the lower part of the figure set. For odd-order  $P_N$ , as the order increases, smaller values of the total flux are founded at the center of the slab. The trend is instead inverted in case of even-order  $P_N$ . An exactly inverted behavior for both odd- and even-order  $P_N$  is observed in proximity of the right-hand side boundary.

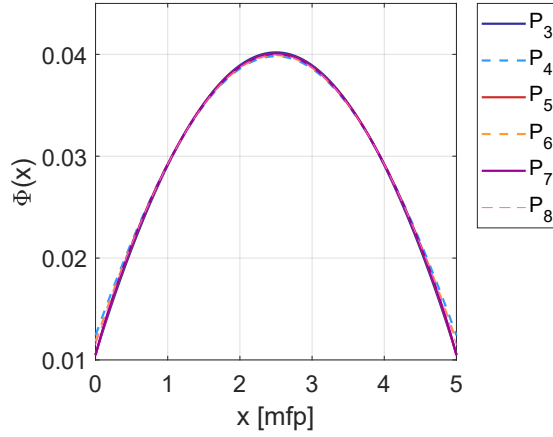
For sake of brevity, the similar results obtained in case of  $\gamma$  and  $\alpha$  eigenvalue are not reported.

### 5.3.4 Parametric studies

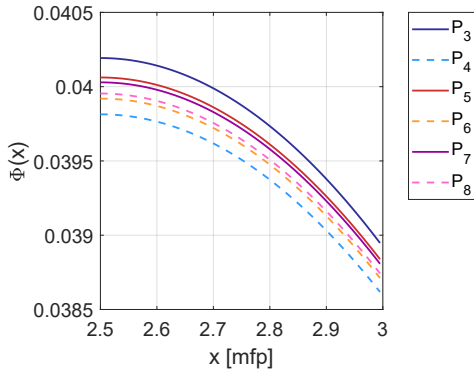
#### slab dimension dependency

Two different parametric studies have been conducted in order to investigate the behavior of each eigenvalue type with respect to the system dimensions and its characteristic critical parameter. The studies concern the  $k$ ,  $\gamma$  and  $\alpha$  eigenvalue. First, the fundamental mode of each analyzed eigenvalue type has been studied as function of increasing slab thicknesses. For both the case of  $k$  and  $\gamma$  eigenvalue, a slab size ranging from 5 to 30 mfp has been considered. In case of  $\alpha$  eigenvalue instead, the higher value of thickness range has been limited to 10 mfp, due to the higher computational costs required by this type of eigenvalue. A  $P_7$  approximation with Marshak boundary conditions has been adopted in the model implementation for the calculations. The nuclear data exploited in the evaluation are summarized in Table 5.14.

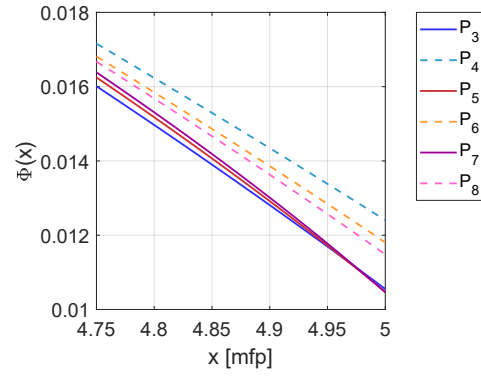
Figure 5.17 show the results for the eigenvalues fundamental modes as function of the thickness range investigated. For all the three different eigenvalue types, an increase in the system dimension returns an incremented fundamental mode. The increase is higher at lower dimensions while in the right part of the thicknesses range, for analogous relative slab



(a) Overall solution.



(b) Slab central portion.

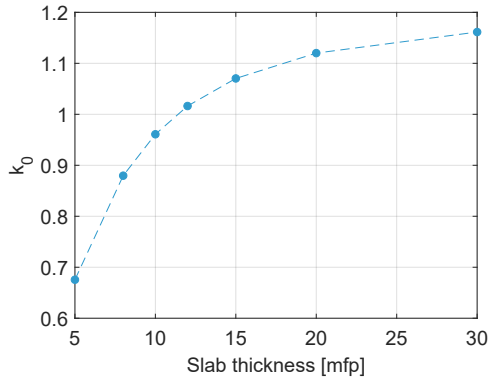


(c) Slab right-hand boundary.

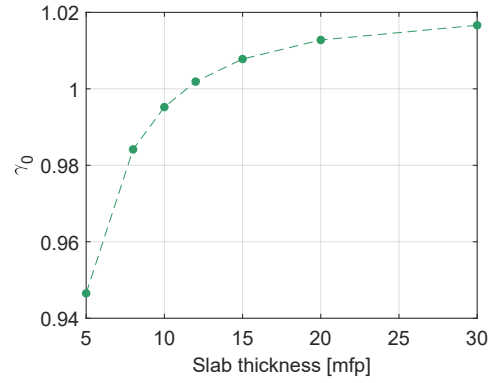
Figure 5.15: The zeroth-order moment associated to the fundamental mode, meaning the total flu  $\Phi$ , at increasing orders of  $P_N$  approximation with Mark boundary conditions for a 5 mfp slab domain. The overall solution is reported on the top (a), while two details are reported in the lower part (b), (c).

Table 5.14: Nuclear data adopted in parametric studies.

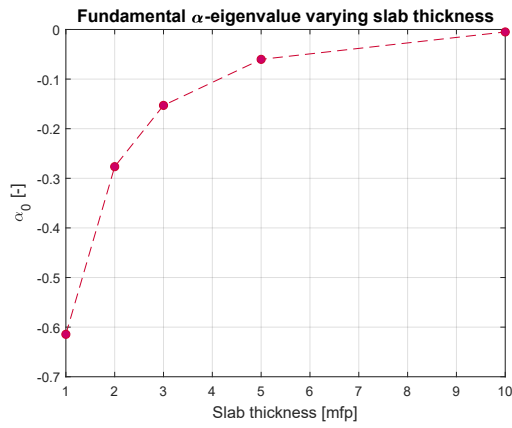
Parameter		Value
Total cross-section [ $\text{cm}^{-1}$ ]	$\Sigma_t$	1.0
Scattering cross-section [ $\text{cm}^{-1}$ ]	$\Sigma_s$	0.9
Absorption cross-section [ $\text{cm}^{-1}$ ]	$\Sigma_a$	0.1
Production cross-section [ $\text{cm}^{-1}$ ]	$\nu\Sigma_f$	1.2



(a)  $k$  eigenvalue



(b)  $\gamma$  eigenvalue

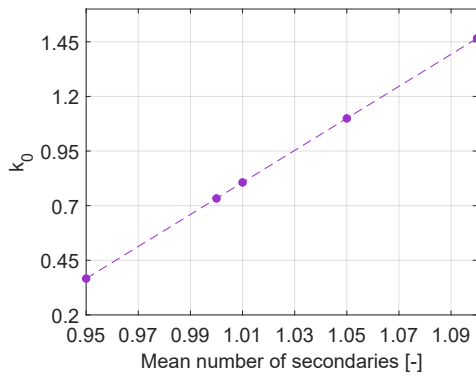


(c)  $\alpha$  eigenvalue

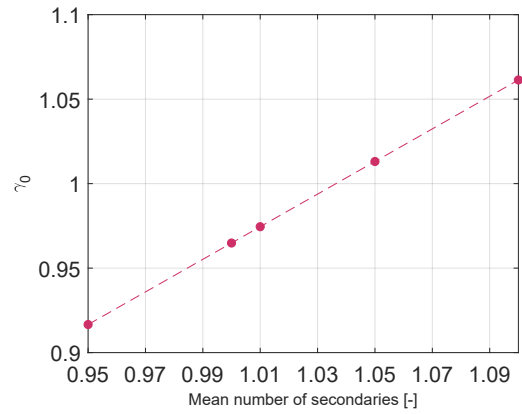
Figure 5.16: Fundamental multiplication factor per fission  $k_0$ , per collision  $\gamma_0$  and time eigenvalue  $\alpha_0$ , as function of the slab thickness, evaluated with  $P_7$  and Marshak boundary conditions.

variations, lower increment in the fundamental eigenvalue are observed. The  $k$  eigenvalue show the slower convergence. Such results are related to the lower impact of the neutrons leakages out of the slab boundaries, in thicker systems, combined with an increased in the multiplying material.

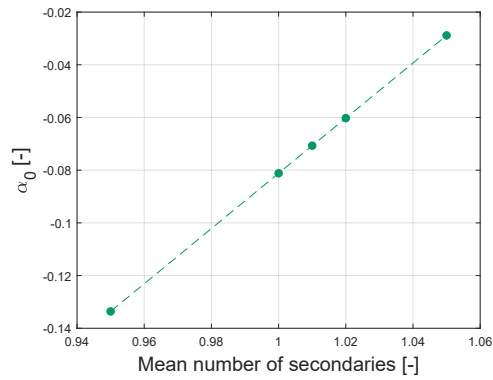
Finally, at fixed system size,  $P_N$  approximation and boundary conditions, the critical parameter  $c$  is varied in order to investigate the system response. The variation has been performed through the modification of the average number of neutrons per fission event. In case of  $k$  and  $\gamma$  eigenvalue, a slab thickness of 8 mfp is adopted, while in case of  $\alpha$  computations referred to a 5 mfp thick slab. Linear proportionality between the increase in the critical parameter and the increment in the computed fundamental eigenvalue can be observed for each eigenvalue type.



(a)  $k$  eigenvalue.



(b)  $\gamma$  eigenvalue.



(c)  $\alpha$  eigenvalue.

Figure 5.17: Fundamental multiplication factor per fission  $k_0$ , per collision  $\gamma_0$  and time eigenvalue  $\alpha_0$ , as function of the critical parameter  $c$ , evaluated with  $P_7$  and Marshak boundary conditions.

# Chapter 6

## Conclusions

The drive for this thesis has been the interest in the investigation of the different eigenvalue formulations of neutron transport equation in a mono-energetic, one-dimensional model. After a brief presentation of the integro-differential version of the neutron transport equation, both in general and one-dimensional geometry, in chapter 1, the criticality problem for the neutron transport has been outlined in chapter 2. Specifically, the four different eigenvalue formulations, related to the  $k$ ,  $\gamma$ ,  $\alpha$  and  $\delta$  eigenvalue have been presented, with the associated physical interpretation. While the effective multiplication factor per fission  $k$ , together with the time eigenvalue  $\alpha$ , boast a large number of dedicated studies, fewer works are reserved for the  $\gamma$  eigenvalue, and almost none are devoted to the  $\delta$  eigenvalue, which remains the more obscure eigenvalue type.

Then, the spherical harmonics method, the angular approximation selected in the present work, is outlined for both general and one-dimensional spatial configuration in chapter 3, where the neutron transport eigenvalue formulations, the solution of which are object of the entire work, are presented. The majority of the studies dedicated to criticality calculations, have been found related to the application of the Discrete Ordinates, the  $S_n$  method, for the angular representation of the neutron angular flux. As a consequence, a lack of results obtained by means of the  $P_N$  method, as concern criticality computations, has been observed.

Chapter 4 has been devoted to the presentation of the matrix formulations outcomes of the spatial discretization of the generalized eigenvalue problems in  $P_N$  approximation, which have been solved through the implementation of a numerical code, specific for the solution of arbitrarily high-orders of  $P_N$  approximation. The code, which has been implemented in MATLAB environment, has been developed with a modular structure where each module is dedicated to the solution of one of the four eigenvalue types considered. Both Mark and Marshak boundary condition have been implemented. The automation to arbitrarily high-orders of  $P_N$ , both odd- and even-orders, has given the possibility of a comparison of both the calculation performances in relation to the  $P_N$  order nature, and to the specific eigenvalue

type considered.

The comparison with the available benchmark numerical results, presented in the first sections of chapter 5, shows a well agreement between the eigenvalues computed by the implemented code and those reported in the reference studies. This result is also related to the efficacy of the eigensolver exploited in the implemented code, the Implicit Restarted Arnoldi Method implemented in the ARPACK package. For the case of a homogeneous, mono-energetic slab, no benchmark numerical results have been found for the case of the  $\delta$  eigenvalue. As a consequence, only a preliminary study has been conducted for this eigenvalue types.

The fundamental and some higher-modes convergence at increasing orders of  $P_N$  approximation have been investigated for each eigenvalue type, both with Mark and Marshak boundary conditions. The main result which can be highlighted in relation to the  $P_N$  approximation order, is that the generally stated superiority in accuracy of the odd-order  $P_N$  with respect to the even-order  $P_N$ , for low-orders of approximation, specially with Marshak boundary conditions, is not always verified in the cases considered in the present work. Specifically, as regards the fundamental mode convergence, with the  $k$  eigenvalue  $P_4$  shows a better convergence with respect to  $P_3$  for Mark boundary conditions, and with Marshak boundary conditions the improvement extends even from  $P_2$ , to  $P_8$ . Similar results are obtained for  $\alpha$  and  $\gamma$  eigenvalue, which in addition to the  $k$  eigenvalue, shows a better convergence also with  $P_2$  and Mark boundary conditions, with respect to  $P_1$ . Then, it is generally found that Marshak boundary conditions works better than Mark type conditions at lower-orders of  $P_N$  approximation, while the trend is inverted at high-order  $P_N$ .

Furthermore, a small portion of the discrete spectrum of each eigenvalue type has been computed with the implemented code, showing some unexpected results as concerns the convergence at increasing orders of  $P_N$  approximation. Specifically, for the  $\alpha$  eigenvalue an inverted convergence behavior of numerical outcomes obtained with odd- and even-order  $P_N$  is observed.

Thus, these results suggest that a deeper investigation in the study of even-order  $P_N$  approximations with respect to the odd-order ones, may represent an interesting field for future researches, as regards solutions of the neutron transport equation in angular approximations.

Then, some results concerning the eigenvectors outcomes of the implemented code are reported for the  $k$  eigenvalue case. The first three harmonics for both the zeroth-order and the first-order angular flux moment are reported. Specific for the case of the zeroth-order moment a brief description of the influence on the solution of the order of the  $P_N$  exploited, is given. Then, the angular flux as function of the spatial coordinate at fixed directions, is shown for the case of  $P_3$  approximation with Mark boundary conditions in the  $k$  eigenvalue case. For the same set of model conditions, the angular flux as function of the angular variable at

fixed slab locations has been also reported.

Finally, two parametric studies have been conducted as a further investigation of criticality results, for the case of  $k$ ,  $\gamma$  and  $\alpha$  eigenvalue. In these analysis, the variation of the slab dimensions and of the critical parameter have been taken into account.

Hence, a systematic presentation of criticality numerical results obtained with odd- and even-orders  $P_N$  approximation, have been performed in the present work for the  $k$ ,  $\gamma$ ,  $\alpha$  and  $\delta$  eigenvalue. Lack of information both from the theoretical and numerical standpoint concerning the  $\delta$  eigenvalue, has forced to qualitative discussion about the obtained results for this eigenvalue. Furthermore, in the most diffused criticality studies, the Discrete Ordinates method is exploited as angular approximation, and the contribution represented by the present work may be inserted in an initial fulfillment of a systematic work performed for the  $P_N$  approximation. Finally, interesting results have been observed in relation to even-order  $P_N$  approximations, which are generally discarded in transport models implementation, applied to criticality results, suggesting an interesting field for future investigation.

# Bibliography

- [1] International Energy Agency, *World Energy Outlook 2015*. 2015.
- [2] International Atomic Energy Agency, *Nuclear power and sustainable development*. 2016.
- [3] Cacuci D. G., Ronen Y., Shayer Z., Wagschal J. J. and Yeivin, Y., “Eigenvalue-Dependent Neutron Energy Spectra: Definitions, Analyses, and Applications,” *Nuclear Science and Engineering*, vol. 81, pp. 432–442, 1982.
- [4] Wu Y., *Fusion Neutronics*, ch. Neutron Transport Theory and Simulation. Springer Singapore, 2017.
- [5] Bell G. I. and Glasstone S., *Nuclear Reactor Theory*. New York: Van Nostrand Reinhold Co., 1970.
- [6] Davison B. and Sykes J. B., *Neutron Transport Theory*. Oxford: Clarendon Press, 1957.
- [7] Hanus M., *Mathematical Modeling of Neutron Transport*. PhD thesis, University of West Bohemia, 2014.
- [8] Meghreblian R. V. and Holmes D. K., *Reactor Analysis*. New York: McGraw-Hill,, 1960.
- [9] Duderstadt J. J. and Martin W. R., *Transport Theory*. New York: John Wiley & Sons, 1979.
- [10] Montagnini B., “Appunti del corso di fisica dei reattori nucleari.” Lecture Notes.
- [11] Lamarsh J. R., *Introduction to Nuclear Reactor Theory*. Addison-Wesley Pub. Co., 1966.
- [12] Lewis E. E., *Fundamentals of Nuclear Reactor Physics*. Amsterdam: Elsevier/Academic Press, 2008.
- [13] Duderstadt J. J. and Hamilton L. J., *Nuclear Reactor Analysis*. Wiley, 1976.

- [14] Zweifel P. F., *Reactor Physics*. New York: McGraw-Hil, 1973.
- [15] Ronen Y., Shvarts, D. and Wagschal J. J., “A Comparison of Some Eigenvalues in Reactor Theory,” *Nuclear Science and Engineering*, vol. 60, pp. 97–101, 1976.
- [16] Quarteroni A., Saleri F. and Gervasio P., *Scientific computing with MATLAB and Octave*. New York: Springer, 2013.
- [17] Velarde G., Ahnert C. and Aragonès J. M., “Analysis of the Eigenvalue Equations in  $k$ ,  $\lambda$ ,  $\gamma$ , and  $\alpha$  Applied to Some Fast- and Thermal-Neutron Systems,” *Nuclear Science and Engineering*, vol. 66, pp. 284–294, 1978.
- [18] Hébert A., “Applied Reactor Physics,” 2009. Presses internationales Polytechnique.
- [19] Protopopescu V., “Eigenvalue Problems for the Boltzmann Operator in Various Formulations,” *Advance in nuclear science and technology*, vol. 15, pp. 1–45, 1982.
- [20] Sahni D. C., Garis N. S. and Sjöstrand N. G., “Spectrum of one-speed Neutron transport operator with reflective boundary conditions in slab geometry,” *Transport Theory and Statistical Physics*, vol. 24, pp. 629–656, 1995.
- [21] Verdù G., Ginestar D., Roman J. and Vidal V., “3D Alpha Modes of a Nuclear Power Reactor,” *Journal of Nuclear Science and Technology*, vol. 47, no. 5, pp. 501–514, 2010.
- [22] Sanchez R., Tomatis D., Zmijarevic I. and Gyu Joo H., “Analysis of alpha modes in multigroup diffusion,” *Nuclear Engineering and Technology*, vol. 49, no. 6, pp. 1259 – 1268, 2017. Special Issue on International Conference on Mathematics and Computational Methods Applied to Nuclear Science and Engineering 2017 (M&C 2017).
- [23] Sahni D. C., “Some new results pertaining to criticality and time eigenvalue of one-speed neutron transport equation,” *Progress in Nuclear Energy*, vol. 30, no. 3, pp. 305 – 320, 1997.
- [24] Sahni D. C. and Sjöstrand N. G., “Criticality and time eigenvalues in one-speed neutron transport,” *Progress in Nuclear Energy*, vol. 23, no. 3, pp. 241 – 289, 1990.
- [25] Abramowitz M. and Stegun I. A., *Handbook of Mathematical Functions (with Formulas, Graphs, and Mathematical Tables)*. New York: Wiley, 1972.
- [26] G. K.A.I.L. and S. Anjana, “Modeling of planar plasma diode,” *International Letters of Chemistry, Physics and Astronomy*, vol. 8, pp. 220–242, 09 2013.

- [27] Lathouwers D., “Iterative Computation of Time-eigenvalues of the Neutron Transport Equation,” *Annals of Nuclear Energy*, vol. 30, pp. 1793–1806, 2003.
- [28] Lehoucq R. B., Sorensen D. C. and Yang C., “ARPACK USERS GUIDE: Solution of Large Scale Eigenvalue Problems by Implicitly Restarted Arnoldi Methods.,” 1997.
- [29] “MATLAB,” 2017. version 9.3.0.
- [30] Modak R. S., Sahni D. C. and Paranjape S. D., “Evaluation of Higher K-Eigenvalue of Neutron Transport Equation by Sn Method,” *Annals of Nuclear Energy*, vol. 22, no. 6, pp. 359 – 366, 1995.
- [31] Dahl E. B. and Sjöstrand N. G., “Eigenvalue Spectrum of Multiplying Slabs and Spheres for Monoenergetic Neutrons with Anisotropic Scattering,” *Nuclear Science and Engineering*, vol. 69, no. 1, pp. 114–125, 1979.
- [32] Modak R. S. and Gupta A., “A Simple Scheme for the Direct Evaluation of the Time-Eigenvalues of Neutron Transport Equation,” *Annals of Nuclear Energy*, vol. 30, pp. 211–222, 2003.
- [33] Deo K., Krishnani P. D. and Modak R. S., “Development of one-dimensional neutron transport theory code based on method of characteristics,” tech. rep., Bhabha Atomic Research Centre, Mumbai, 2014.
- [34] Betzler B. R., *Calculating alpha eigenvalues and eigenfunctions with a Markov Transition Rate Matrix Monte Carlo method*. PhD thesis, University of Michigan, 2014.
- [35] Dahl E. B., Protopopescu V. and Sjöstrand N. G., “On the relation between decay constants and critical parameters in monoenergetic neutron transport,” *Nuclear Science and Engineering*, vol. 83, pp. 374–379, 1983.
- [36] S. I.R. and P. G.C., “Boundary conditions for differential approximations,” *Journal of Quantitative Spectroscopy and Radiative Transfer*, vol. 25, no. 4, pp. 325 – 337, 1981.
- [37] G. C. Pomraning, “Radiative transfer via spherical harmonics,” *Transport Theory and Statistical Physics*, vol. 8, no. 2, pp. 67–97, 1979.
- [38] Filippone W. L. and Conversano R., “Ordinary and generalized eigenvectors of low-order SN diamond difference transport operators,” *Nuclear Science and Engineering*, vol. 83, pp. 75–89, 1983.
- [39] Lewis E. E. and Miller W. F., *Computational Methods of Neutron Transport*. La Grange Park: American Nuclear Society, 1993.

- [40] Warsa J.S., Waering T.A., Morel J.E., McGhee J.M. and Lehoucq R.B., “Krylov subspace iterations for the calculation of k-eigenvalues with SN transport codes,” *Proceedings of Nuclear Mathematical and Computational Sciences*, vol. 83, pp. 75–89, 2003.
- [41] Barbarino A., *Numerical Methods for Neutron Transport Calculations of Nuclear Reactors*. PhD thesis, Politecnico di Torino, 2014.